SANDIA REPORT

SAND2014-1897
Unlimited Release
Printed March 2014

Compaction Behavior of Surrogate Degraded Emplaced WIPP Waste

Scott T. Broome, David R. Bronowski, S. James Kuthakun, Courtney G. Herrick, and Tom W. Pfeifle

Prepared by
Sandia National Laboratories
Albuquerque, New Mexico 87185 and Livermore, California 94550

Sandia National Laboratories is a multi-program laboratory managed and operated by Sandia Corporation, a wholly owned subsidiary of Lockheed Martin Corporation, for the U.S. Department of Energy's National Nuclear Security Administration under contract DE-AC04-94AL85000.

Issued by Sandia National Laboratories, operated for the United States Department of Energy by Sandia Corporation.

Available to DOE and DOE contractors from
U.S. Department of Energy
Office of Scientific and Technical Information
P.O. Box 62
Oak Ridge, TN 37831

Telephone: (865) 576-8401
Facsimile: (865) 576-5728
E-Mail: reports@adonis.osti.gov
Online ordering: http://www.osti.gov/bridge

Available to the public from
U.S. Department of Commerce
National Technical Information Service
5285 Port Royal Rd.
Springfield, VA 22161

Telephone: (800) 553-6847
Facsimile: (703) 605-6900
E-Mail: orders@ntis.fedworld.gov
Online order: http://www.ntis.gov/help/ordermethods.asp?loc=7-4-0#online

SAND2014-1897
Unlimited Release
March 2014

Compaction Behavior of Surrogate Degraded Emplaced WIPP Waste

Scott T. Broome, David R. Bronowski, S. James Kuthakun, and Tom W. Pfeifle
Geomechanics Department
Courtney G. Herrick
Performance Assessment and Decision Analysis Department
Sandia National Laboratories
P.O. Box 5800
Albuquerque, New Mexico 87185

Abstract

The present study results are focused on laboratory testing of surrogate waste materials. The surrogate wastes correspond to a conservative estimate of degraded Waste Isolation Pilot Plant (WIPP) containers and TRU waste materials at the end of the 10,000 year regulatory period. Testing consists of hydrostatic, triaxial, and uniaxial strain tests performed on surrogate waste recipes that were previously developed by Hansen et al. (1997). These recipes can be divided into materials that simulate 50% and 100% degraded waste by weight. The percent degradation indicates the anticipated amount of iron corrosion, as well as the decomposition of cellulosics, plastics, and rubbers (CPR). Axial, lateral, and volumetric strain and axial, lateral, and pore stress measurements were made. Two unique testing techniques were developed during the course of the experimental program. The first involves the use of dilatometry to measure sample volumetric strain under a hydrostatic condition. Bulk moduli of the samples measured using this technique were consistent with those measured using more conventional methods. The second technique involved performing triaxial tests under lateral strain control. By limiting the lateral strain to zero by controlling the applied confining pressure while loading the specimen axially in compression, one can maintain a right-circular cylindrical geometry even under large deformations. This technique is preferred over standard triaxial testing methods which result in inhomogeneous deformation or "barreling". Manifestations of the inhomogeneous deformation included non-uniform stress states, as well as unrealistic Poisson's ratios (> 0.5) or those that vary significantly along the length of the specimen. Zero lateral strain controlled tests yield a more uniform stress state, and admissible and uniform values of Poisson's ratio.

ACKNOWLEDGMENTS

The authors would like to Dwayne Kicker, Shelly Nielsen, and Sean Dunagan for their reviews of this report.

This research is funded by WIPP programs administered by the Office of Environmental Management (EM) of the U.S Department of Energy.

CONTENTS

FIGURES

TABLES

NOMENCLATURE

Cal Lab	SNL Primary Standards Calibration Laboratory
CPR	Cellulosics, plastics, and rubbers
DAS	Data Acquisition System
DOE	U.S. Department of Energy
DOE/CBFO	U.S. Department of Energy/Carlsbad Field Office
DRZ	Disturbed Rock Zone
EPA	U.S. Environmental Protection Agency
ES&H	Environmental Safety and Health
FEA	Finite Element Analysis
I/D	Intensifier/Dilatometer
I/O	Input/Output
ID	Inside Diameter
kip	1000 pounds-force, from combination of "kilo" and "pound"
ksi	kip per square inch (1000 psi)
LVDT	Linear Variable Differential Transformer
MgO	Magnesium Oxide
NP	(SNL WIPP) Nuclear Waste Management Procedure
NQ	non-QA
OD	Outside Diameter
PA	Performance Assessment
PHS	Primary Hazard Screening
PI	SNL/DWMP Principal Investigator or Designee
POP	Pipe Overpack
ν	Poisson's Ratio
PSL	Primary Standards Laboratory
QA	Quality Assurance
QAPD	QA Program Document
Records Center	SNL/DWMP Records Center
SAF	Soils and Foams Model
SN	Scientific Notebook
SNL	Sandia National Laboratories
SNL-GL	Sandia National Laboratories-Geomechanics Laboratory
SNL/DWMP	Sandia National Laboratories/Defense Waste Management Programs
SP	(SNL WIPP) Activity/Project Specific Procedure
TP	Test Plan
u/r	unload/reload
U.S.	United States
TRU	Transuranic
TWD	Technical Work Document
WC	Weidlinger Cap Model
WIPP	Waste Isolation Pilot Plant
Work Control	WIPP Work Control Process

1. INTRODUCTION

1.1. Background and Motivation

The Waste Isolation Pilot Plant (WIPP) is a United States (U.S.) Department of Energy (DOE) mined, underground repository, certified by the U.S. Environmental Protection Agency (EPA), and designed for the safe management, storage, and disposal of transuranic (TRU) radioactive waste resulting from United States defense programs. The wastes are emplaced in panels excavated at a depth of 655 m (2,150 ft) in the Permian Salado Formation. Following emplacement of waste and the MgO engineered barrier material, the panels will be isolated from the operational mine using an approved closure system. The repository is linked to the surface by four shafts that ultimately will be decommissioned and sealed.

Performance Assessment (PA) modeling of WIPP performance requires full and accurate understanding of coupled mechanical, hydrological, and geochemical processes and how they evolve through time. The overarching objective of this report focuses on room closure modeling, specifically the compaction behavior of waste and the constitutive relations to model this behavior. A principal goal of this study is make use of an improved waste constitutive model parameterized to a well-designed data set.

The specific objective of this report is to document hydrostatic, triaxial, and uniaxial strain loading tests conducted on surrogate degraded waste as data required to develop a better constitutive model for WIPP waste behavior. Previous work (Hansen et al., 1997) was performed on different recipes of surrogate material for the WIPP PA Spallings model parameter evaluation, but these experiments did not provide data needed to correlate volume change to other test parameters. Hansen et al. (1997) also performed triaxial tests on surrogate degraded waste mixtures, but only a limited number of confining pressures were used. A larger range of confining pressures is needed to assist in the modeling efforts for the long term effects of WIPP room closure characteristics.

The test plan (Broome and Costin, 2010) governing the experimental program described herein calls for testing both fresh and surrogate degraded waste forms to capture the full evolutionary behavior of the waste as it is expected to degrade with time. Testing was terminated after completion of the surrogate degraded waste experiments as part of programmatic cuts enacted by the DOE Carlsbad Field Office (DOE/CBFO). Further testing on surrogate fresh waste is required to capture the full range of WIPP waste compaction behavior before a new model can be implemented in WIPP Performance Assessment. The compaction behavior of surrogate fresh waste is needed to describe the anticipated behavior of WIPP waste during early times of the repository when room closure, waste compaction, and chemical changes are occurring at their fastest rates. Hydrostatic, triaxial, and uniaxial compaction tests on surrogate fresh waste are planned to begin in calendar year 2014.

2. MATERIAL AND SAMPLE PREPARATION

2.1 Material Preparation

Two unique recipes were used for all samples within this report; 1) a recipe representing a waste state where 50% degradation has occurred and 2) a recipe representing a waste state where 100% degradation has occurred (Hansen et al., 1997). The percent degradation indicates the anticipated amount of iron and the amount of cellulosics, plastics, and rubbers (CPR) that are anticipated to be degraded by weight. A description of the constituents for both the 50% and 100% degraded mixtures is presented in Table 1.

Table 1. Ingredient description for 50% and 100% degraded surrogate waste mixtures from Hansen et al. (1997).

Mass (kg) and percent by weight of materials in test specimens				
Material	Case 1 (50% degraded)		Case 2 (100% degraded)	
Iron, not corroded	1.9	18.3%	0	0.0%
Corroded iron and other metals	4.6	44.4%	7.3	67.0%
Glass	1.0	9.6%	1.0	9.2%
Cellulosics + plastics + rubber	0.7	6.8%	0	0.0%
Solidification cements	1.2	11.6%	1.2	11.0%
Soil	0.5	4.8%	0.5	4.6%
MgO backfill	0	0.0%	0	0.0%
Salt precipitate, corrosion-induced	0.47	4.5%	0.90	8.3%
Salt precipitate, MgO-induced	0	0.0%	0	0.0%
Total batch size	10.37	100.0%	10.9	100.0%

Details of each material category (50% case)	
Iron, not corroded:	9.14% Steel 1 to 2mm thick, ~10 to 20mm squares.
	9.14% Alloys 1-2 mm thick, ~10 to 20mm squares. Also misc small hardware, screws etc
Corroded iron and other metals:	44.4% Iron Oxide pass No. 18 (1mm or 0.0394") sieve
Glass:	9.6% 2 to 3 mm thick and pass 3/8" (9.5mm) sieve
Cellulosics:	0.675% paper (6 to 8 mm squares or ~2 inch long strips).
	0.675% cotton (thin strands ~1" long or snipped cotton balls)
	0.675% sawdust (as received)
	0.675% peat (as received)
Plastics:	0.675% Poly sheet (~12 mm max dimension) (half may be degraded plastic if available)
	0.675% Poly bottle (~8 to 12 mm max dimension) (half may be degraded plastic if available)
	0.675% Shredded plastic grocery bags
Rubber:	0.675% Gloves ~8 to 12 mm maximum size.
	0.675% Rubber bands (6 to 8mm maximum size)
	0.675% O-rings (6 to 8mm maximum size)
Solidification cements:	5.786% Sheetrock, pass 3/8" (9.5mm) sieve.
	5.786% Concrete, pass 3/8" (9.5mm) sieve.
Soil:	4.8% typical soil (outside geomechanics lab) pass 3/8" (9.5mm) sieve.
Salt:	4.5% From WIPP. Pass 3/8" (9.5mm) sieve.
Saturation water:	Brine made from tap water and crushed WIPP salt.

Percentages of each constituent in each recipe were taken directly from Hansen et al. (1997). Most of the details of the constituents in Table 1 are relatively simple to obtain and reproduce. The constituent iron oxide is the exception.

Iron oxide in the form of goethite was collected locally at an outcrop at an elevation of 5760 ft and located at the following UTM coordinates: 13S 363409E 387186N. Figure 1 shows a picture of the outcrop where the goethite was sorted and collected by hand. The material was then crushed in one of the loading frames in the SNL-GL so that it passed a No. 18 sieve.

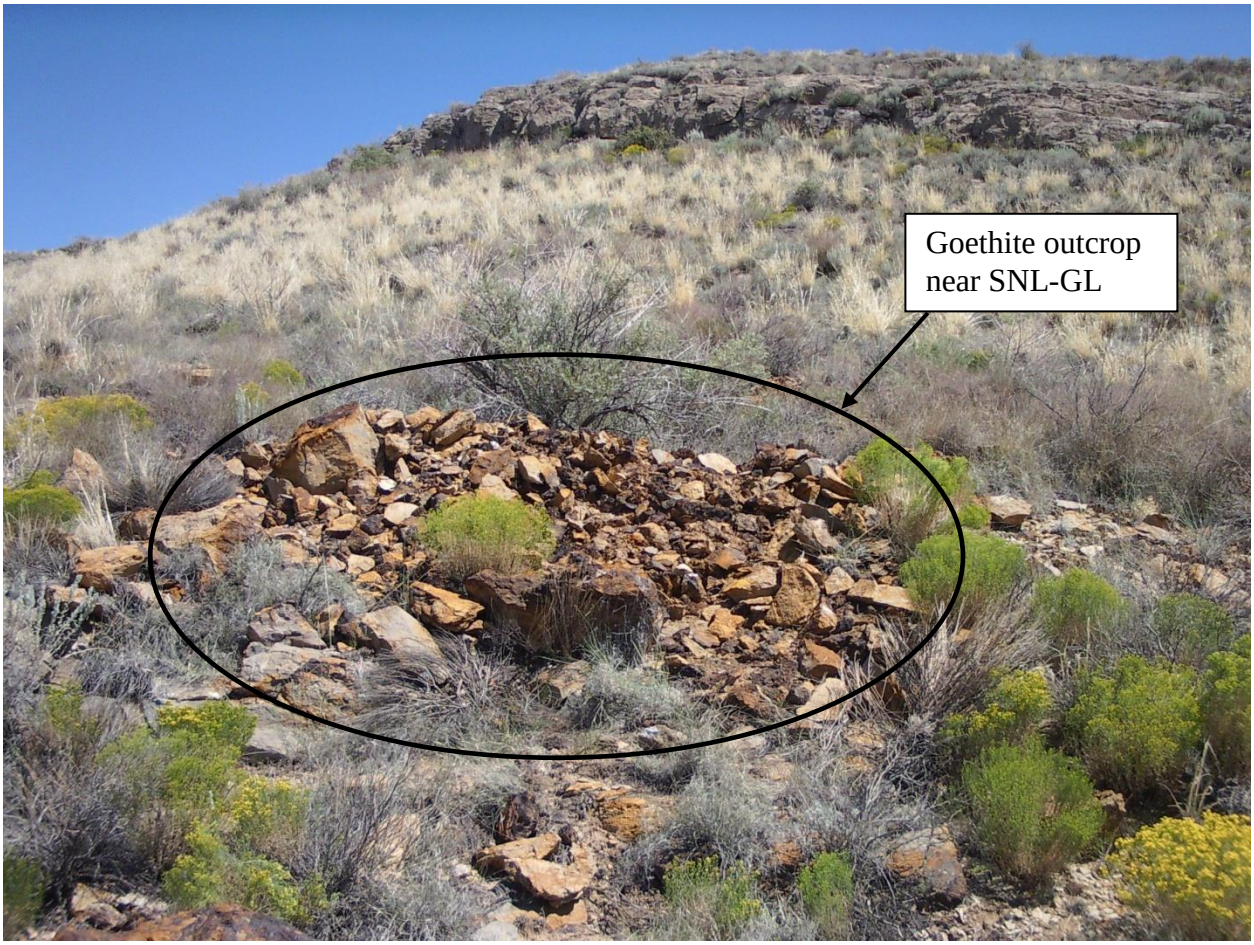

Figure 1. Goethite outcrop for iron oxide constituent in all samples.

2.2 Sample Preparation

Once the constituents were prepared as described in Table 1, they were combined into a bowl and saturated with brine. The brine was prepared by mixing crushed WIPP salt with tap water at room temperature until the crushed WIPP salt no longer dissolved; crushed WIPP salt was left in the container while the brine was used. Figure 2 shows a batch of 100% degraded material ready for insertion into a sample mold. Preserved in the Sandia WIPP Records Center, constituents of each test specimen are fully documented in the Scientific Notebook (SN) (SNL 2010, SNL 2012).

Figure 2. Batch of 100% degraded material ready for insertion into a sample mold.

3. EXPERIMENTAL METHODS AND EQUIPMENT

3.1 Pre-test Specimen Assembly

3.1.1. Hydrostatic Tests

After the material was saturated and mixed in a bowl, it was put into a cylinder of known volume (1641 cc). Leftover material was discarded. By subtracting the weight of the empty 'volume standard', the weight of the material in the 'volume standard' was then calculated and a pre-test density determined by dividing material weight by the volume. Figure 3 shows a saturated 50% recipe contained within the 'volume standard'. A repeatable sample volume was important for hydrostatic testing because of the utilization of dilatometry to measure volumetric strain. Section 3.4 describes in detail the experimental method employed to accurately record volumetric strain during a test.

A section of gum rubber tubing of nominal 4" inside diameter and 1/8" wall thickness was attached to the unvented specimen end cap using tie wire. A stiff plastic shell was placed around the outside diameter of the gum rubber. The purpose of the shell was to keep the specimen in a shape that approximated a right circular cylinder. The material (1641 cc) was then put into a gum rubber jacket and the other end cap inserted until brine was detected from the vent port. A felt metal filter was used on the vented end cap. The vented end cap was made so that multiple ports connected to the main external drain port prevented clogging during sample deformation. Figure 4 shows a sample ready for hydrostatic testing and details the components of the assembly.

Figure 3. Saturated 50 % recipe contained within the 'volume standard' ready for insertion into gum rubber jacket assembly.

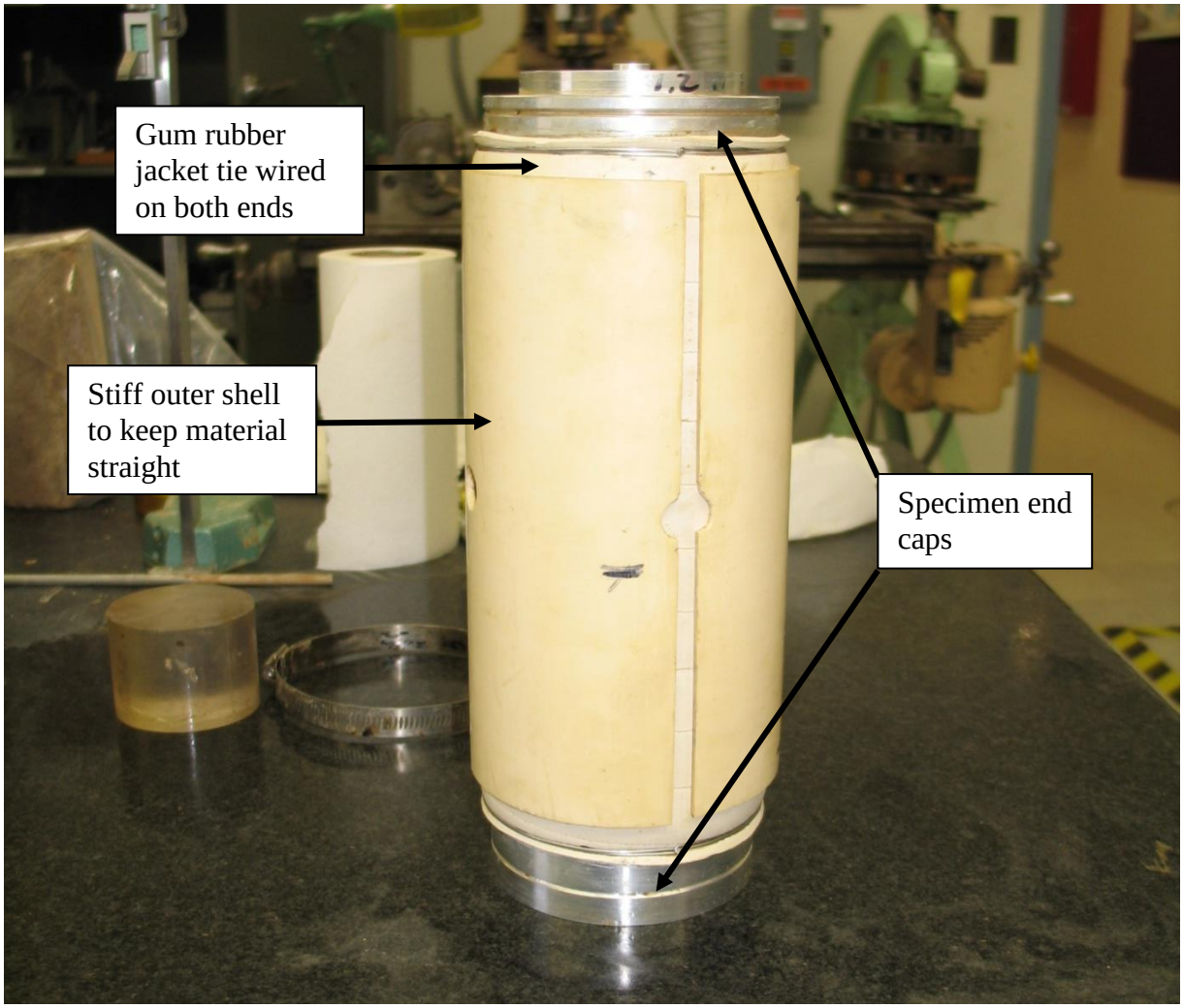

Figure 4. Sample ready for hydrostatic testing and details the components of the assembly.

3.1.2 Triaxial and Uniaxial Strain Tests

Originally, triaxial tests were to be the same specimens used in the hydrostatic tests. The material deforms irregularly during hydrostatic compaction such that the volume of the triaxial sample would not be known by conventional dimensional methods. In addition, upon depressurization, the gum rubber jacket wrinkles and does not facilitate a mounting point for radial measurements. It was decided to pre-compact the material in a split die to 80% of the target confining pressure as illustrated in Figure 5. The die compaction forms the material into a fairly uniform right circular cylinder and allows the use of heat shrink tubing as the jacketing material. During die compaction, the sample is drained from both the top and bottom, and brine was observed along the seam of the die. After die compaction, the sample is unloaded down to approximately 40 pounds of force (180 N). The small load is left on the material to ensure alignment of the sample stack while the heat shrink jacket is shrunk onto the sample and end caps. Initially, only one jacket was used but after multiple jacket leaks (at confining pressures of 5 MPa and above), all 50% degraded material samples received two heat shrink jackets, while 100% degraded samples always were tested with one jacket.

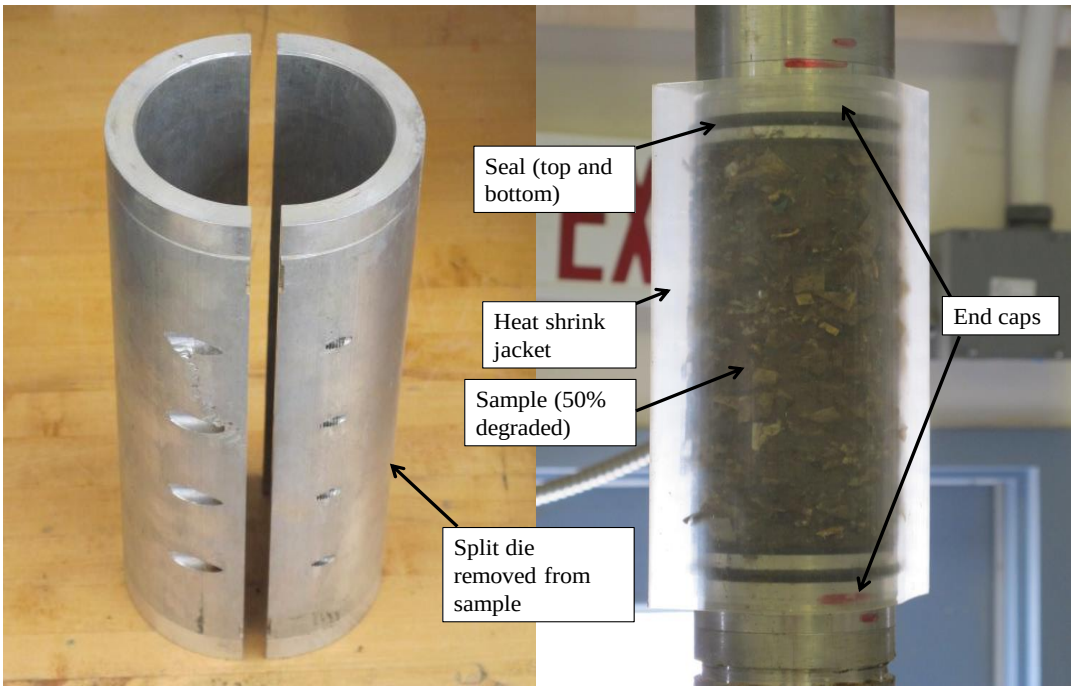

Figure 5. Split die shown along with die compacted 50% degraded material prior to application of a heat shrink jacket.

A triaxial sample, mounted on the pressure vessel base and ready for testing, is shown in Figure 6. The sample is drained from both the top and bottom end caps. The top end cap has a port on the side. This port is connected to the vessel base with a flexible tube. The bottom end cap is ported in the center and connects to the vessel base with a sealed nipple.

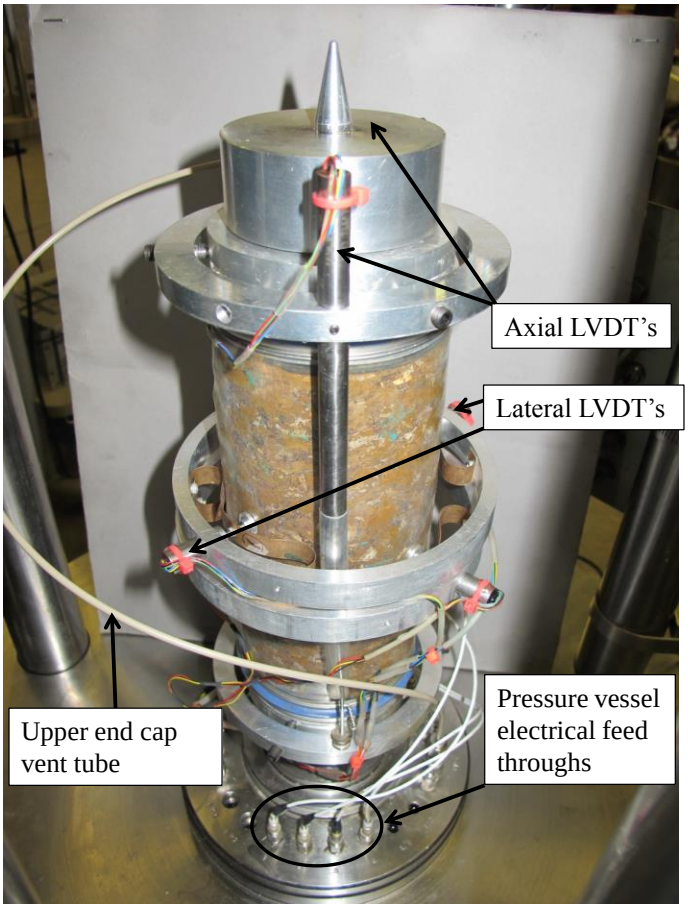

Figure 6. A triaxial sample (50% degraded material) mounted on the pressure vessel base and ready for testing.

3.2 Test Systems

Three computer-controlled servohydraulic test systems, all manufactured by MTS Systems Corporation (MTS), were used in the testing of the 50% and 100% degraded sample. The systems were selected primarily to match capabilities to the load and confining pressure requirements specified in the test matrix. As shown in Table 2, the primary differences among the test systems were the maximum axial loads and confining pressures that could be applied during a test.

Table 2. Test System Capabilities and Utilization

Test System	Axial Force Range MN (kip)	Confining Pressure Range MPa (ksi)	Utilization
0.1 MN	0 – 0.1 (0 – 22)	NA (NA)	Frame served as a hydrostatic I/D run in parallel with 1.0 MN system.
1.0 MN	0 – 1 (0 – 220)	0 – 100 (0 – 15)	All samples tested with a 100 MPa pressure vessel.
1.0 MN AT	0 – 1 (0 – 220)	NA (NA)	Die compaction of triaxial and uniaxial strain samples.

3.2.1 MTS 0.1 MN Test System

Hydrostatic tests were performed using a MTS 0.1 MN test system. This system comprises a standard two-column load frame, MTS FlexTest™ digital controller, and desktop PC. The system served solely as an intensifier/dilatometer (I/D) (see Figure 7) that ran in parallel with the dedicated I/D mounted near the 1.0 MN frame.

The standard MTS two-column load frame is equipped with a movable crosshead to accommodate different specimen/equipment geometries as shown in Figure 7. A hydraulic actuator located in the base of the frame is capable of applying axial force over a range of 0 to 0.1 MN (0 to 22 kips) in both tension and compression. Force is measured by an electronic load cell mounted on the crosshead, while the relative displacement of the load actuator is determined from a linear variable differential transformer (LVDT) mounted internal to the actuator housing.

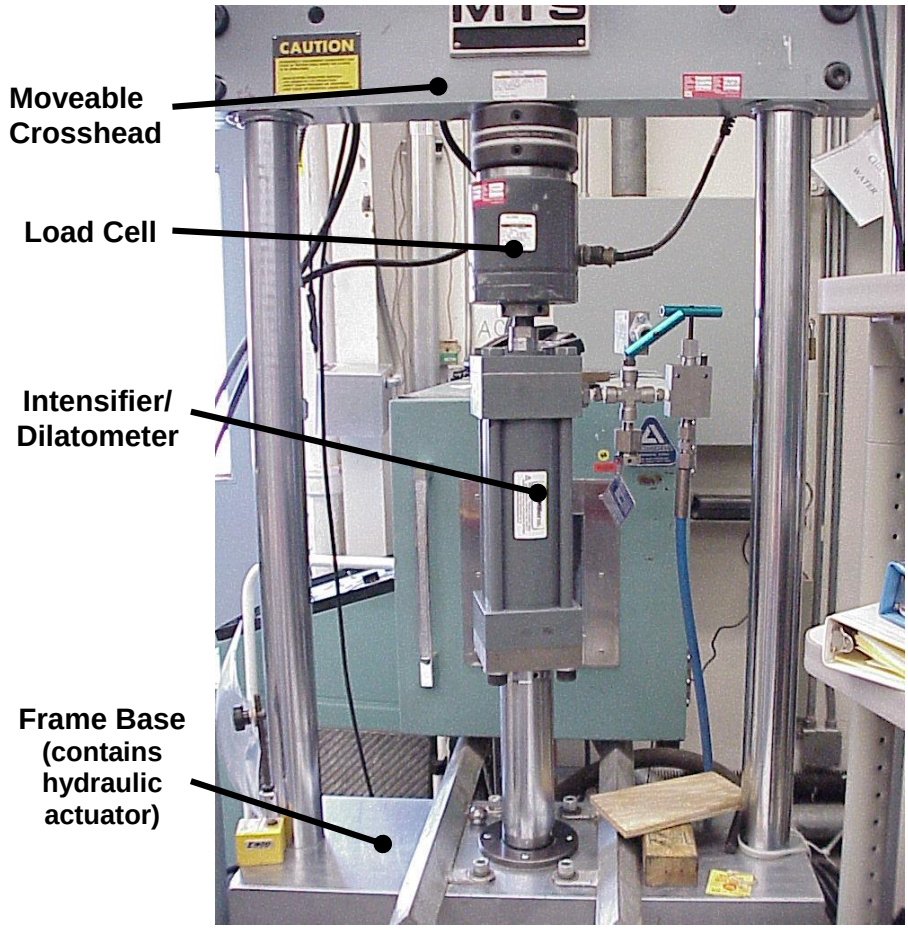

Figure 7. MTS 0.1 MN Test System used as an I/D for hydrostatic testing.

The FlexTest™ controller provides digital servocontrol, function generation, transducer conditioning, data acquisition, hydraulic control, and digital input/output (I/O) for the 0.1 MN test system. Load (axial tension or compression) control is provided through a closed-loop electro-hydraulic system that drives a servovalve based on the magnitude of an electrical "error" signal defined as the difference between a generated command signal and a feedback signal. The servovalve opens and closes in proportion to the error signal allowing more or less hydraulic fluid to enter the load actuator, which in turn accelerates or decelerates the relative displacement of the actuator. The command signal produced by the function generator is programmed by the user and can take the form of a ramp, any of several wave forms (sine, triangular, square), or a user-defined wave form. The feedback signal is the output of an electronic transducer used to monitor test response such as a load cell or LVDT. The FlexTest™ system allows for changes in the command signal form and switching among various feedback signals (known as mode switching) during testing. In the case of the hydrostatic tests, the user-specified command signal was a ramp and the feedback transducer used was the load cell (converted to pressure based on piston area of the I/D).

The desktop PC provides user interface with the controller through 100 Mbit/sec ethernet connections and is equipped with a Microsoft® Windows XP multi-tasking operating system and

MTS Model 793 TestStar IIm software. The TestStar software allows the user to configure test system control (command signal and feedback mode), set up channels for data acquisition, acquire and store data (in ASCII, Lotus, or Excel formats), and plot X-Y data in real-time.

3.2.2 MTS 1 MN Test System

The hydrostatic, triaxial, and uniaxial strain tests were performed using the MTS 1 MN test system. This system comprises a standard four-column load frame, SBEL pressure vessel, MTS FlexTest™ digital controller, and desktop PC.

Except for its four-column design and greater force capacity, the 1 MN test system (Figure 8) is very similar to the 0.1 MN system in that it is equipped with a movable crosshead, a base-mounted hydraulic load actuator (0 to 1 MN or 0 to 220 kips) with LVDT, and a crosshead-mounted load cell. In contrast to the 0.1 MN system, the 1 MN test system integrates a 100 MPa (15,000 psi) pressure vessel and pressure intensifier to allow testing under confining pressure.

The pressure vessel (Figure 9) is a hardened-steel thick-walled hollow cylinder with inside and outside diameters of 178 mm (7 inches) and 229 mm (9 inches), respectively, and an overall length of 311 mm (12.25 inches). It is fitted with o-ring sealed top and bottom closure plates that are secured to the vessel with eight 43 mm (1.7-inch) diameter threaded tie rods. The top closure plate contains a through-going 54 mm (2.125 inch) concentric hole to accommodate a steel push rod that transmits axial load from the actuator/test frame to the top end cap of the specimen assembly (Figure 9) during testing. The top and bottom closure plates also contain feed-throughs used to connect the cable leads of the specimen-mounted electronic instrumentation (e.g., displacement transducers) with the FlexTest controller. The intensifier that services the pressure vessel is designed as a double-bore linear piston to step hydraulic line pressures of 20 MPa (3,000 psi) in the larger bore to test pressures of 200 MPa (30,000 psi) in the smaller bore through the mechanical advantage provided by the ratio of the two bore areas. An LVDT tracks the relative position of the piston during operation. High-pressure steel tubing connects the high-pressure bore of the intensifier to the pressure vessel.

The digital controller and desktop PC are essentially identical to those used for the 0.1 MN system. However, the 1 MN system has a second servovalve and controls used to drive the pressure intensifier. For the degraded waste testing, the feedback signal for this second servovalve was radial displacement for the uniaxial strain tests and confining pressure for the triaxial and hydrostatic tests. Data was collected as voltages through a data acquisition system (DAS) and converted to engineering units post testing. The DAS was certified for use by WIPP QA program. Operation of the servovalves was accomplished using the TestStar software loaded on the desktop PC. This software was also used for reference during the test; important parameters were converted to engineering units for real time test monitoring.

3.2.3 MTS 1 MN AT Test System

The triaxial and uniaxial strain tests were die compacted (see Section 3.1.2) to create a nearly uniform right circular cylinder in the MTS 1 MN AT test system. This system comprises a two-column load frame, MTS FlexTest™ digital controller, and desktop PC.

Except for its greater force capacity, the 1 MN AT test system (Figure 10) is very similar to the 0.1 MN system in that it is equipped with a movable crosshead, a base-mounted hydraulic load actuator (0 to 1 MN or 0 to 220 kips) with LVDT, and a crosshead-mounted load cell. In contrast to the 0.1 MN system, the 1 MN AT test system integrates a rotational component with a torque cell for torsion applications. The rotary component was deactivated for all tests presented in this report.

The digital controller and desktop PC are essentially identical to those used for the 0.1 MN system. However, the 1 MN AT test system has a second servovalve and controls used to drive a pressure intensifier. The pressure intensifier on the 1 MN AT test system was not used for testing in this report. Data was collected as voltages through a data acquisition system (DAS) and converted to engineering units post test. The DAS was certified for use by WIPP QA program and is the same DAS used on the 1 MN test system. Operation of the servovalves was accomplished using the TestStar software loaded on the desktop PC. This software was also used for reference during the test; important parameters were converted to engineering units for real time test monitoring.

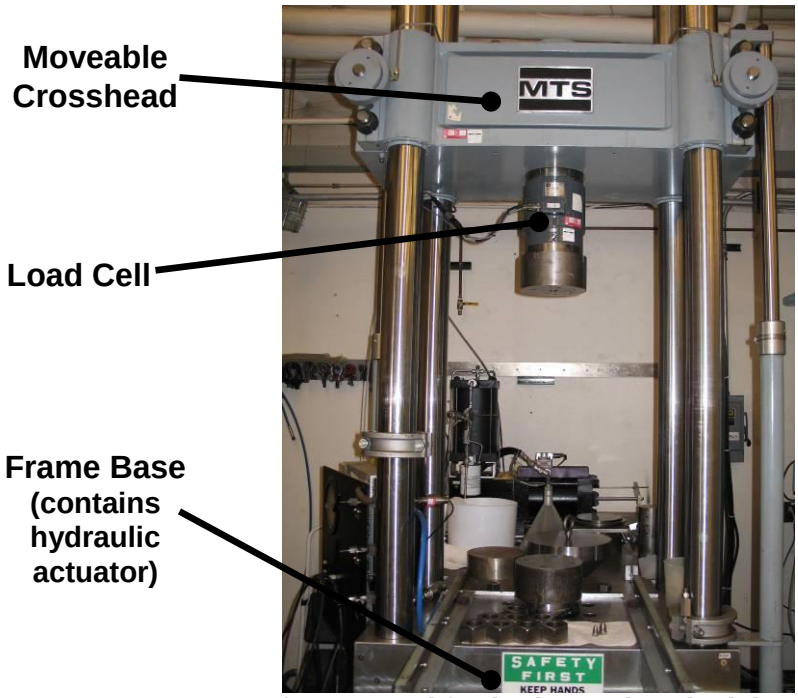

Figure 8. MTS 1 MN test frame used for hydrostatic, triaxial, and uniaxial strain testing.

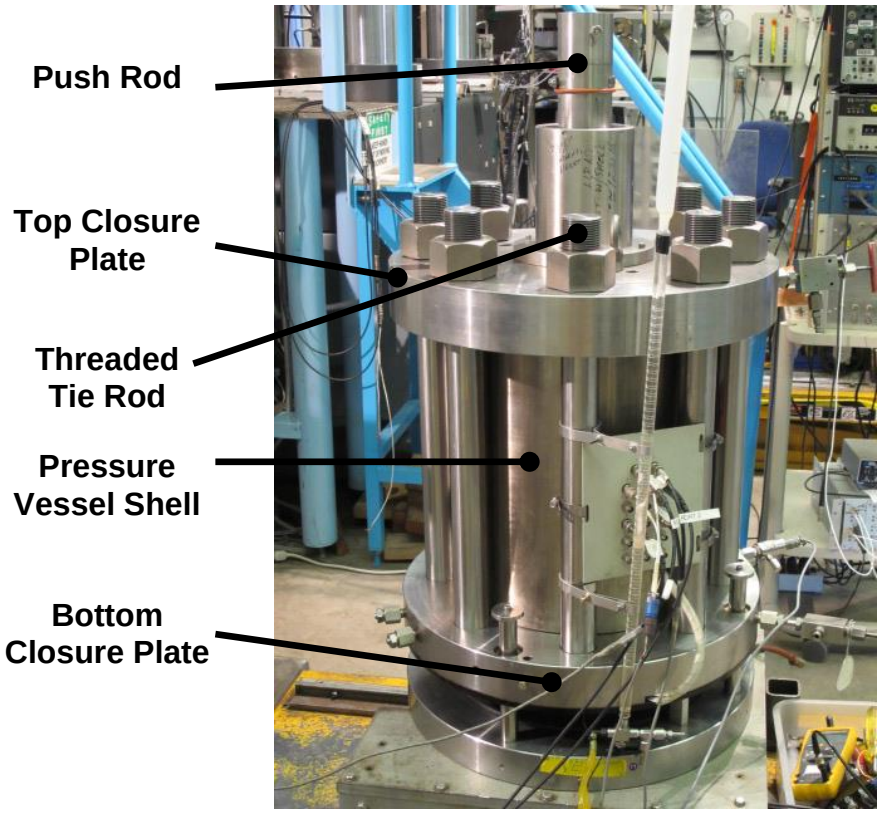

Figure 9. SBEL 100 MPa pressure vessel used with 1 MN test system.

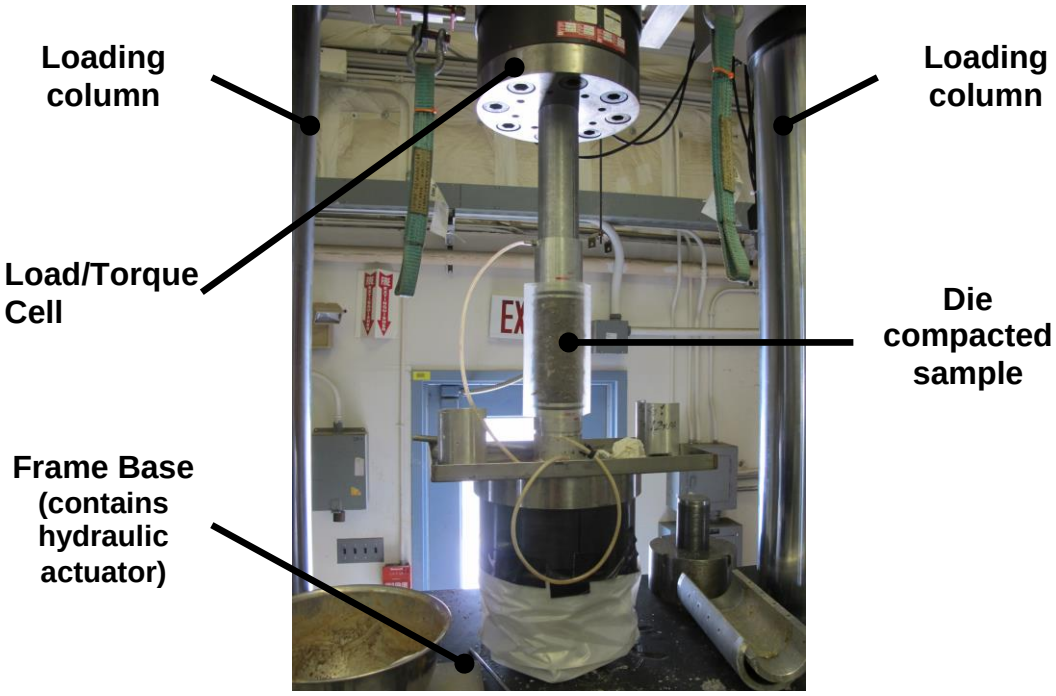

Figure 10. MTS 1 MN AT test frame used for triaxial and uniaxial strain specimen preparation.

3.3 Instrumentation and Calibration

The instrumentation used with each test system is summarized in Table 3. The instrumentation consisted of electronic transducers for measuring force, pressure, and displacement (axial, radial, I/D, and actuator). Elapsed time in seconds was recorded for each logged data point using the internal clock of the data acquisition system.

3.3.1 Axial Force

Total axial force was measured by load cells mounted on the moveable crossheads of each frame. A secondary load cell was used inside the pressure vessel on the 1 MN system. For confined tests conducted in the 1 MN system, the total force measured by the external load cell included a contribution of force required to react against the confining pressure from the steel push rod that transmitted load from the test frame to the specimen. Because small loads were expected on specimens with low confining pressures, an internal load cell was utilized in tandem with the external load cell on the 1 MN system. The external axial specimen force on the 1 MN system was calculated during data reduction as the total measured force reduced by the product of the confining pressure and the area of the push rod. Changes in specimen diameter were also accounted for in the calculated specimen force using the outputs of the radial displacement transducers to update specimen diameter.

3.3.2 Pressure

For tests conducted in the 1 MN systems, vessel pressure was measured using a pressure transducer located in the high-pressure line leading from the pressure intensifier to the pressure vessel. The length of pressure line between the pressure transducer and the pressure vessel was 1.2 m (3.9 ft). Pressure losses in the line over these lengths are negligible.

3.3.3 Deformation

Triaxial and uniaxial strain specimen deformation (axial and radial) was determined using LVDT's mounted directly on the test specimens. LVDT's were selected based on anticipated deformation magnitudes and physical space limitations within the pressure vessels. Axial and radial displacements were measured and strains were calculated from the measured displacements using appropriate gage lengths.

Table 3. Test System Instrumentation

Measurement	Type	Make / SN	Calibrated Range
MTS 0.1 MN Test System			
Axial force	Load cell	MTS 661.21A-03 / 3266	0 – 0.1 MN
Actuator displacement	LVDT	MTS / 971	±100 mm
MTS 1 MN Test System			
Axial external force	Load cell	MTS 661.31A-02 / 211	±900 KN
Axial Internal force	Load cell	Honeywell 060-G731-01/967275	0–133 KN
Axial Internal force	Load cell	Honeywell 060-1588-01/1306086	0-222 KN
Confining Pressure	Pressure transducer	BLH GP-3000/53554	0 – 21 MPa
Axial displacement	LVDT	Schaevitz 1000-MHR / 339 & 1795	±25.4 mm
Radial displacement	LVDT	Schaevitz 100-MHR / 1123 & 45957	±3.6 mm
Radial displacement	LVDT	Schaevitz 100-MHR/ 3244 & 19166	±3.6 mm
Actuator displacement	LVDT	MTS / 124	±100 mm
Pore pressure	Pressure transducer	Precise Sensors, Inc. / 22801	0 – 7 MPa
Dilatometer	LVDT	Milwaukee / HBD-42 1277218	±154 ml
MTS 1 MN AT Test System			
Axial force	Load cell	MTS 662.10A-10 / 2814	±900 KN
Actuator displacement	LVDT	MTS / 0219-0001	±100 mm

As shown in Figure 11a on a 100% degraded waste sample, axial displacement was measured using a pair of diametrically-opposed LVDTs mounted between two rings that were attached to the upper and lower metal end caps with set screws. The gage lengths for this configuration were the overall lengths of the individual test specimens. The LVDTs for radial displacement were mounted near specimen mid-height in two metal rings that were held in place with spring pressure as shown in Figure 11b. Using this configuration, two spring-loaded LVDTs were clamped in the ring with the cores extending out to a contact pad. The contact pad was machined with a radius that matched the radius of the sample. The second ring was rotated 90^{o} from the first so as to measure radial displacements across a diameter orthogonal to the first. The gage lengths for these two sets of measurements were the original diameters of each test specimen.

Hydrostatic sample deformation was measured by the displacement of the intensifiers/dilatometers on the 0.1 MN and 1.0 MN systems. On the 0.1 MN system, the displacement of the frame actuator was calibrated to the volume of fluid expelled from the dilatometer (mL/V). A similar process was used for the dilatometer on the 1.0 MN system except that the dilatometer displacement used a LVDT mounted to the side of the dilatometer. Section 3.4.1 discusses in detail the use of dilatometry to measure volumetric strain on the hydrostatic compression samples.

3.3.4 Calibrations

All instrumentation was calibrated against standards traceable to the U.S. National Institute of Standards and Technology (NIST). Crosshead-mounted load cells and actuator LVDTs were calibrated by MTS using NIST traceable transfer standards. These vendor-supplied calibrations were certified by the SNL Primary Standards Laboratory (PSL). Pressure transducers were calibrated directly by the SNL PSL. Specimen-mounted LVDTs, the internal force load cell, and intensifiers/dilatometers were calibrated by SNL-GL staff using transfer standards certified by the SNL PSL.

All calibrations were performed with the instruments installed in their normal operating configuration. Thus, the calibrations accounted not only for errors in the transducers themselves but also for errors and/or noise attributed to cabling, signal conditioning, and data acquisition loggers. Calibration records for all transducers are maintained in the Measurement and Test Equipment binder for this project and will be retained in the WIPP Records Center.

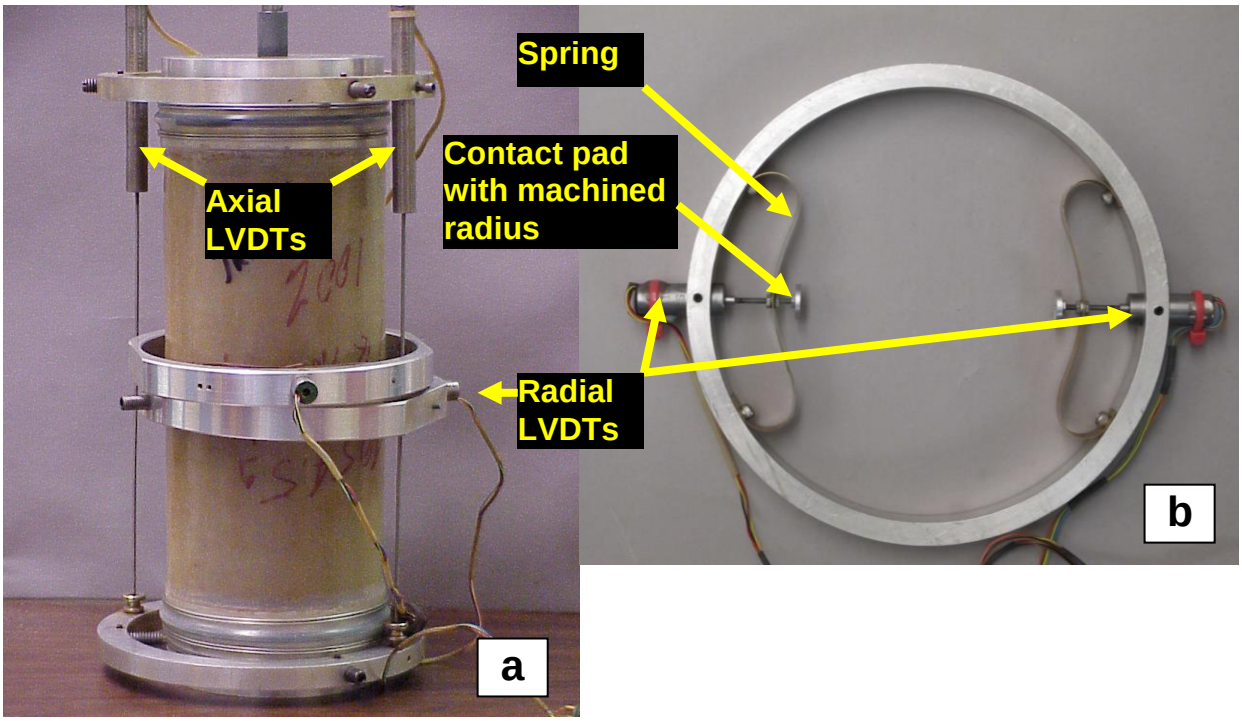

Figure 11. Typical instrumented test specimen used in the 1 MN test systems: (a) Axial and radial deformations measured using LVDTs mounted in rings and (b) detail of radial deformation ring.

3.4 Test Methods

3.4.1 Hydrostatic Compression

Hydrostatic compression testing utilized dilatometry to measure volumetric strain of the sample. In simple terms the process works in the following manner:

- A known volume of test material is placed in a length of rubber tubing
- The tubing ends are plugged using end caps
- The assembly is placed in a pressure vessel and the vessel filled with confining fluid
- The vessel is plumbed to an I/D
- The I/D system produces pressure in the pressure vessel by displacing fluid
- The fluid displacement (volume) is measured
- As pressure compresses the sample material, additional fluid is required to maintain the desired pressure
- Fluid displacement relates to volumetric strain of the sample material

In practice there are several tasks that are critical to the overall process in order to produce reliable/accurate measurements. Fluid volume measured by the dilatometer is not a direct relationship to material compaction. This is due to the complexity of the total test system and

how it responds to pressure changes. Some significant considerations are: 1) the fluid itself is compressible, 2) the pressure vessel, test frame, and associated plumbing all strain under pressure and 3) the rubber jacket material compresses. It is not practical to attempt analytical corrections for each contributing component. Instead, total system response is measured by performing tests on a known volume of known material via a test billet. By this process, a system response baseline is produced which is subtracted from material test data.

In order for the above described process to be reliable, several points are critical: 1) the configuration under which the system response was measured must not change. This includes using the same (or identical) sample assembly hardware and the same initial volume of test material, 2) the same pressure vessel, dilatometers, and all plumbing components are used, and 3) consistent starting position of dilatometer and vessel pistons and proper system filling and purging of air. All items relate directly to assuring that the same amount of confining fluid is in the system for every test. A plastic stuffer was inserted into the pressure vessel to remove as much fluid as possible from the system. Using a stuffer makes the system stiffer and increases the accuracy of the volumetric strain data when factoring out the system response from the test data.

Every test must be performed at the same pressurization rate to minimize a difference in heating/cooling effects on the system response test and sample test. All testing used defined pressurization rates to assure that test time periods are consistent.

Hydrostatic tests are performed in two parts. The first part uses the entire system where the 0.1 MN frame is the driving I/D to compact the sample. The 0.1 MN dilatometer is then isolated (valve closed) and testing continues using the 1 MN dilatometer.

Preparation of the system for a test begins with closing the vessel and positioning it in the test frame. The vessel is then filled with confining fluid (tap water with anti-corrosive additive). Next, the system drain valve is opened and each I/D is operated to completely empty. Each system vent valve (one near each I/D and one at the top of the pressure vessel) is opened to purge each section of plumbing. Purging continues until no air bubbles are observed from the vent.

Testing begins by operating the 0.1 MN test frame in pressure control mode using programmed rates. Different pressurization rates are used throughout the test. Initially, the 0.1 MN I/D is driven to deliver confining fluid to produce a very slow but constant rate of pressure increase. The pressure rate is increased twice during this portion of the test. The initial slow rate(s) are to allow sufficient time for brine to be expelled from the sample via the vent port. The rates were also selected to approximate the shape of a time/pressurization curve if a constant volume displacement rate were used. While more complicated from a programming standpoint, the pressure rate method allows all samples, regardless of material stiffness, to be performed in the same period of time. Additionally, system response tests, which would pressurize quickly using a volume displacement rate, were also performed over the same time period by using this method.

Pressurization rates for the first part of the test (only using the 0.1 MN I/D) are:

- 30 Pa/sec from start of test to 0.1 MPa
- 100 Pa/sec from 0.1 MPa to 0.3 MPa
- 300 Pa/sec from 0.3 MPa to approximately 1.0 MPa

The first part of the test takes 2.13 hours to complete and is terminated (0.1 MN I/D valve closed) when either a fluid volume displacement of 400.0 ml is obtained or a pressure of 1 MPa is reached. If 1 MPa pressure is reached first, the 1 MN frame is operated to back out the vessel piston until the full 400.0 ml is delivered from the 0.1 MN I/D. If 400.0 ml of fluid volume displacement is reached first then the second part of the test begins using the 1 MN frame.

The second part of the test continues to pressurize the sample to the target pressure (usually 1 MPa) using only the 1 MN frame and I/D. This is performed by running the 1 MN I/D at a pressurization rate of 0.002 MPa/sec until the target pressure is obtained. The sample is then held at this pressure overnight.

After the overnight hold (~16 hours), an unload/reload pressurization cycle is performed using the 1 MN I/D to obtain bulk modulus data at 1 MPa. After the unload/reload loop is performed the pressure is raised to the next hydrostatic pressure level of 2 MPa at 0.002 MPa/sec. The sample is held at 2 MPa overnight and an unload/reload loop performed at 2 MPa the next morning. This process is repeated at 5 and 15 MPa. After the unload/reload loop at 15 MPa, the sample is unloaded completely and the test dissembled. Figure 12 shows a hydrostatic test after testing with the jacket still on the sample and with the jacket removed.

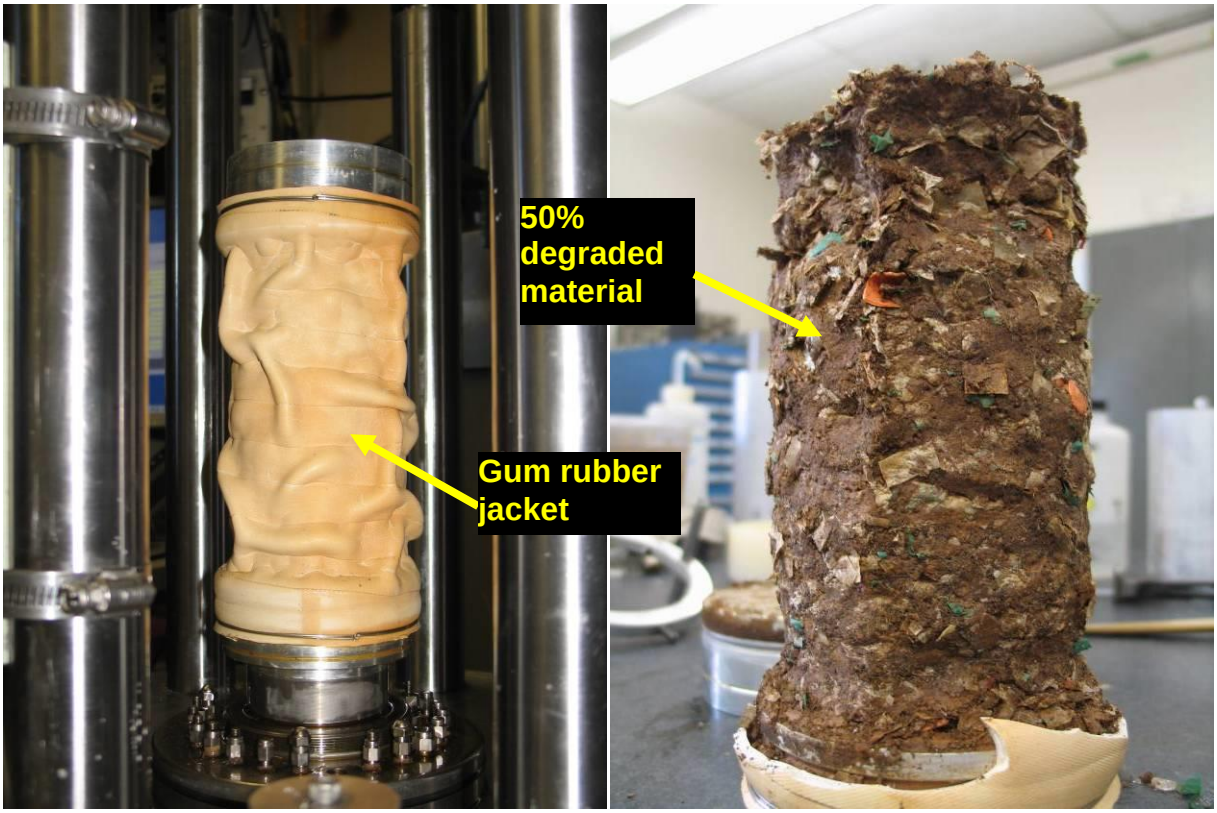

Figure 12. Typical hydrostatic test specimen (a) post test with vacuum applied to show compaction; note wrinkled gum rubber jacket (b) post test with jacket removed (50% degraded material).

After four hydrostatic tests were performed the test setup was modified to accommodate pore pressure readings. The decision to measure pore pressure arose from observed creep during the overnight pressure holds. Understanding whether the creep observed was based on pore pressure or material would help in the understanding of material behavior at these stress states. Additional discussion about material creep is found in Section 4.1 of this report.

The pore pressure measurements were made using a port added in the upper end cap that connected to a pressure vessel feed through via a flexible hose. A pressure transducer was added to the vessel port to monitor pressure. This pressure should represent the maximum material pore pressure as the measurement point is opposite the drained end of the sample.

3.4.2 Triaxial Compression

Figure 12 shows the irregular shape of material after hydrostatic testing. Because of this irregular shape, triaxial compression tests were not possible on post hydrostatic test material. A die compaction of both 50% and 100% surrogate degraded recipes was used to form right circular cylinders for jacketing and instrumentation for triaxial testing. Section 3.1.2 details the die compaction process performed on the 1 MN AT load frame.

After the material was die compacted to 80% of the target confining stress, a heat shrink jacket was shrunk on the sample with sealed aluminum end caps. Both end caps were vented and utilized a porous felt metal filter. Axial LVDT's were mounted on the end caps of the sample using aluminum rings with set screws to keep the rings from moving during testing. Radial LVDT's were mounted on either side of the sample center (see Figure 11). The sample was then mounted in the 100 MPa capacity pressure vessel and pressure was increased to the target confining pressure (1, 2, 5, or 15 MPa) at 0.002 MPa/sec. The sample was held at this confining pressure in a hydrostatic stress state overnight (approximately 16 hours).

The next day, an unload/reload loop was performed to obtain bulk modulus data. This is similar to the bulk modulus data obtained from hydrostatic testing with the exception of the way volume strain was measured. With the hydrostatic tests, volumetric strain was determined dilatometrically as discussed in Section 3.4.1. Volumetric strain for the triaxial tests was determined by combining the output from the sample mounted axial and radial LVDT's. It should be noted that while the triaxial test was held in a hydrostatic stress state overnight, the majority of compaction occurred in a one dimensional stress state (die compaction). These quantities will be discussed further in Section 4.

After the bulk modulus loop was performed, the actuator was advanced on the 1 MN test system until the piston made contact with the top of the sample. After contact was made the actuator continued to advance and applied a differential stress to the sample. Confining pressure was held constant for the remainder of the test using feedback control from the pressure sensor and the 1 MN test system I/D. Multiple unload/reload loops were performed to determine Young's modulus and Poisson's ratio as the sample deformed. Samples were typically deformed around 15 to 20% axial strain.

After a number of tests were performed it was discovered that Poisson's ratio (ν) increased as axial strain increased. Although triaxial samples were vented from both ends, there was concern that pore pressure was building up inside the sample and causing the unrealistically high ν values (above 0.5). Two samples were tested (one 50% and one 100% degraded recipes) using slower pressure and axial strain rates. The confining pressure rate was reduced by 80% to 0.0004 MPa/sec (previously 0.002 MPa/sec) and the axial displacement rate was reduced to 0.0000175 in/sec (previously 0.00035 in/sec). The slow axial strain rate is 20 times slower than previous tests. No noticeable change in sample behavior was observed.

Sample barreling was considered a possibility and investigated by mounting one radial LVDT ring at approximately 25% from the top of the sample and another at sample mid-height (as opposed to both radial LVDT's mounted near sample mid-height). Calculating ν from the LVDT at sample mid-height revealed similar high values (over 0.5) as seen before but using the other radial LVDT (25% from the top of the sample) gave values of nearly half of that from the mid-height radial LVDT. While the tests performed thus far provide good Young's modulus and axial deformation data useful for failure envelope modeling, a different approach was deemed necessary to understand lateral sample behavior. Testing a sample in a uniaxial strain configuration would allow determination of ν as a function of density. Uniaxial strain tests are discussed in the next section.

3.4.3 Uniaxial Strain

Six uniaxial strain tests were performed (three on each recipe). Uniaxial strain tests are prepared identically to triaxial compression tests. The method for applying hydrostatic stress is also identical to that employed for triaxial testing. However, the process that differs from triaxial testing is when the actuator is inserted into the pressure vessel and begins to apply axial differential stress, confining pressure is increased to maintain a zero lateral strain condition. The control for the zero lateral strain condition is the radial LVDT mounted at sample mid-height. Another radial LVDT is mounted 25% from the top of the sample (same mounting arrangement as for the triaxial compression test when sample barreling was investigated).

The frame actuator was displaced at a rate that allowed the test to be conducted over approximately 8 hours. The slow rate was desired because of the anticipated large increases in confining pressure to maintain the zero lateral strain condition and to allow proper drainage of brine from the sample. Another change from the triaxial tests was the measurement of brine expelled from the test just before each unload/reload loop was performed. This allowed the density to be calculated and plotted as a function of Young's modulus and Poisson's ratio.

3.5 Data Reduction

Data obtained from the data acquisition system (DAS) during each test included axial force, confining pressure, pore pressure, axial and radial displacements (or volume strain from dilatometry), and elapsed time. All data except for time were collected in voltage form. These data were transferred to individual Microsoft® Excel spreadsheets where they were converted to engineering units of stress and strain which were subsequently plotted in graphical form for visual display and analysis.

During this data reduction, the traditional rock mechanics sign convention was used in which compressive stresses and strains were taken as positive quantities and tensile stresses and strains were taken as negative quantities.

3.5.1 Hydrostatic Compression

Data was collected from all hydrostatic compression tests to facilitate creation of a pressure versus volumetric strain plot. Pressure is collected directly from the DAS in voltage form and converted to pressure units (MPa) using calibration sensitivity values. Volume was determined by measuring (in voltage) the I/D's movement and converting to units of milliliters using calibration sensitivity values. As discussed in Section 3.4.1, the volume measured included sample deformation and system deformation. A system response test that was performed identically to the sample test created a pressure versus volume curve on the system minus the sample. The test sample for the system response test was an aluminum billet of identical volume as a triaxial test specimen. The pressure/volume response of the system was then subtracted from the pressure/volume response of the system plus the sample, therefore isolating the volumetric response of the sample as a function of pressure.

Subtracting out the system deformation was accomplished using two methods. The first method used a look up table to factor out system deformation. A look up table is best used when the response of the system cannot be easily represented by a polynomial best fit curve. Pressure/volume data from the system response test was divided into different groups representing periods of uninterrupted pressure increase. Sample pressure data was then matched to pressure from the system response. That pressure then correlated to a volumetric strain of the system that was subtracted from the sample volume data. The system deformation was typically less than 12% of the sample deformation. The look up table method was used to subtract out system deformation for the entire pressure versus volume curve with the exception of the unload/reload loops.

The second method was used to correct the unload/reload data and took advantage of the accuracy of the fit that a polynomial or linear trendline gave. Figure 13 shows a plot of volume versus pressure data from the system response after the valve on the 0.1 MN I/D was closed (indicating 400 ml of fluid has already been pushed into the pressure vessel).

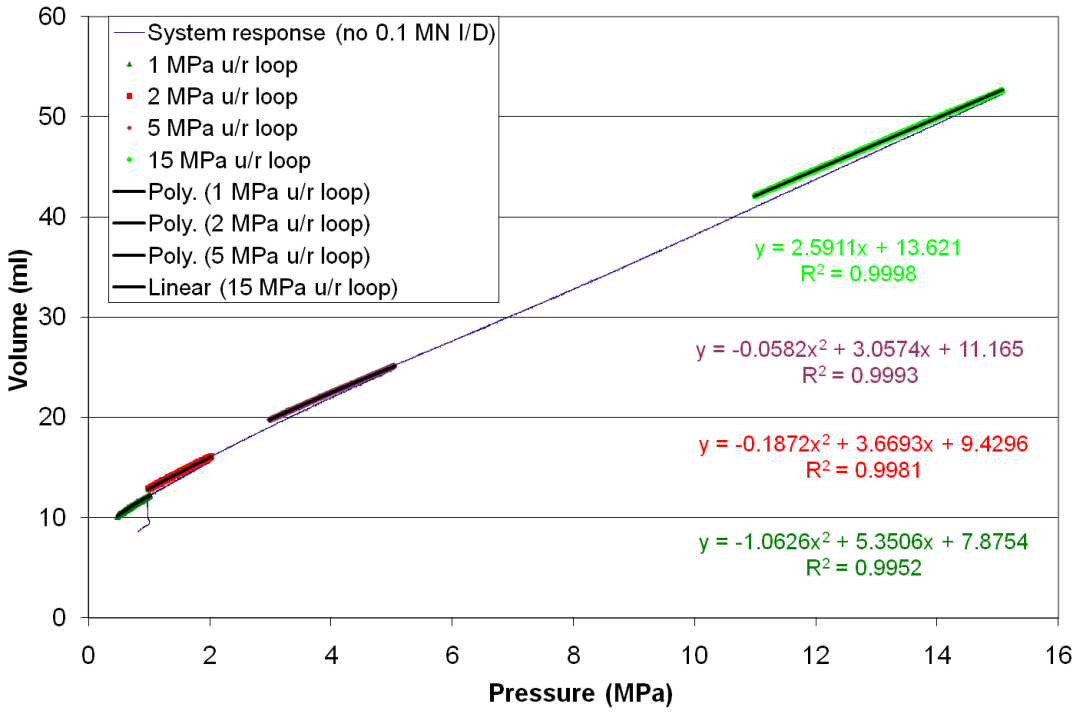

Figure 13. Volume versus pressure for a system response test. Equations of best fit lines from unload/reload (u/r) data were used to determine bulk modulus data as a function of pressure.

This plot shows unload/reload loops performed at the same pressures where sample unload/reload loops were performed. All equations of the best fit lines show R^2 values at least 0.995 indicating a very good fit. These equations were used to calculate the volume to subtract from the equivalent test pressure.

Both methods described above (look up table and best fit equation) were combined to create a complete pressure versus volumetric strain plot of the sample. This plot and elastic properties derived from it will be presented and discussed in Section 4.1. Bulk modulus values as a function of confining pressure were determined for both 50% and 100% material. Bulk modulus was calculated from,

$$K = \frac{\sigma_c}{\epsilon_v} \qquad \text{Eq. 1}$$

where:

σ_c = confining pressure
ϵ_v = volumetric strain

3.5.2 Triaxial Compression

Data was collected from all triaxial compression tests to facilitate creation of a differential stress versus axial, lateral and volume strain plot and allow calculation of bulk modulus prior to starting the triaxial portion of the test. Specifically, the data collected were time, confining pressure, internal force, external force, axial sample displacement, and lateral sample displacements. The bulk modulus was calculated using Equation 1 where $\boldsymbol{\epsilon_v}$ was calculated from,

$$\boldsymbol{\varepsilon_v = \varepsilon_a + 2\varepsilon_l} \qquad \text{Eq. 2}$$

where:

$\boldsymbol{\varepsilon_a}$ = axial strain
$\boldsymbol{\varepsilon_l}$ = lateral strain

Also, true or Cauchy stress and true or logarithm strain were calculated from the acquired data rather than engineering stresses and strains because of the relatively large deformations measured in the tests. Cauchy stress (σ_a = axial specimen stress and σ_r = radial specimen stress) and true strain (ε_a = axial strain and ε_l = lateral strain) are calculated from,

$$\sigma_a = \frac{F_{sp}^a}{\frac{\pi}{4}\left(D_{sp}^i\right)^2} = \frac{F_{sp}^a}{\frac{\pi}{4}\left(D_{sp}^0 - \Delta D_{sp}\right)^2} \qquad \text{Eq. 3}$$

$$\sigma_r = \sigma_c \qquad \text{Eq. 4}$$

$$\varepsilon_a = -\ln\left(\frac{L_{sp}^i}{L_{sp}^o}\right) = -\ln\left(1 - \frac{\Delta L_{sp}}{L_{sp}^o}\right) \qquad \text{Eq. 5}$$

$$\varepsilon_l = -\ln\left(\frac{D_{sp}^i}{D_{sp}^o}\right) = -\ln\left(1 - \frac{\Delta D_{sp}}{D_{sp}^o}\right) \qquad \text{Eq. 6}$$

where:

F_{sp}^a	=	Axial specimen force
D_{sp}^o, D_{sp}^i	=	Original and current specimen diameters, respectively
ΔD_{sp}	=	Change in specimen diameter
L_{sp}^o, L_{sp}^i	=	Original and current specimen lengths, respectively
ΔL_{sp}	=	Change in specimen length
σ_c	=	Confining pressure

Other quantities useful in plotting the data and interpreting the results include:

$$\sigma_m = \frac{(\sigma_a + 2\sigma_r)}{3} \quad \text{Eq. 7}$$

$$\Delta\sigma = \sigma_a - \sigma_r \quad \text{Eq. 8}$$

where σ_m is the mean normal stress and $\Delta\sigma$ is the principal stress difference.

3.5.3 Uniaxial Strain

Data was reduced from the uniaxial strain tests in the same manner as the triaxial compression tests with the exception of calculating axial stress. Axial stress was determined by adding differential stress to confining pressure. This data facilitated plots of confining pressure versus axial stress and differential stress versus axial strain. From these plots, Young's modulus and ν can be determined from the following formulae:

From Fung (1993),

$$\boldsymbol{\varepsilon_{11} = \frac{1}{E}\left(\sigma_{11} - \nu(\sigma_{22} + \sigma_{33})\right)} \quad \text{Eq 9}$$

$$\boldsymbol{\varepsilon_{22} = \frac{1}{E}\left(\sigma_{22} - \nu(\sigma_{11} + \sigma_{33})\right)} \quad \text{Eq 10}$$

$$\boldsymbol{\varepsilon_{33} = \frac{1}{E}\left(\sigma_{33} - \nu(\sigma_{11} + \sigma_{22})\right)} \quad \text{Eq 11}$$

For a uniaxial strain tests conducted under triaxial compression

$$\boldsymbol{\sigma_{11} = \sigma_a} \quad \text{Eq 12}$$

$$\boldsymbol{\sigma_{22} = \sigma_{33} = \sigma_r} \quad \text{Eq 13}$$

$$\boldsymbol{\varepsilon_{22} = \varepsilon_{33} = 0} \quad \text{Eq 14}$$

From either Eq 10 or 11 above, with substitution of Eqs 12 – 14,

$$\boldsymbol{0 = \frac{1}{E}\left(\sigma_r - \nu(\sigma_a + \sigma_r)\right)} \quad \text{Eq 15}$$

Re-arranging

$$\boldsymbol{\sigma_r = \left(\frac{\nu}{1-\nu}\right)\sigma_a} \quad \text{Eq 16}$$

For a uniaxial strain test with unload/reload loops, Eq 16 suggests the slopes of the σ_r versus σ_a plots for the unload/reload curves will equal [ν/(1-ν)] from which ν can be calculated directly. If Eq 10 is subtracted from Eq 9 and the substitutions of Eqs 12-14 are made, then

$$\varepsilon_a - \varepsilon_r = \varepsilon_a - 0 = \frac{1}{E}(\sigma_a - 2\nu\sigma_r) - \frac{1}{E}\left(\sigma_r - \nu(\sigma_r + \sigma_a)\right) \quad \text{Eq 17}$$

$$\varepsilon_a = \frac{1}{E}(\sigma_a - 2\nu\sigma_r - \sigma_r + \nu\sigma_r + \nu\sigma_a) \quad \text{Eq 18}$$

$$\varepsilon_a = \frac{1}{E}\left((\sigma_a + \nu\sigma_a) - (\sigma_r + \nu\sigma_r)\right) \quad \text{Eq 19}$$

$$\sigma_a - \sigma_r = \left(\frac{E}{1+\nu}\right)\varepsilon_a \quad \text{Eq 20}$$

Again for a uniaxial strain test with unload/reload loops, Eq 20 suggests the slopes of the ($\sigma_a - \sigma_r$) versus ε_a plots for the unload/reload curves will equal [E/(1+ν)]. Since ν is determined directly from Eq 16, then E can be determined from Eq 20. Note: ($\sigma_a - \sigma_r$) is simply the measured stress difference during the test.

4. RESULTS AND ANALYSIS

4.1 Hydrostatic Compression

Four hydrostatic tests were performed on the 50% degraded material and five tests were performed on the 100% degraded material. That the results were consistent from sample to sample was apparent by both post test observation and from the pressure versus volume response. Figure 14 shows all post test hydrostatic samples of both 50% and 100% degraded recipes.

Table 4 summarizes the results of all hydrostatic tests. Bulk modulus values in Table 4 are calculated from two points; the upper point is where the reload data intersects the unload data and the lower point is the lowest pressure measured during unloading. Using these two points effectively averages the slope of the unload/reload loop. Bulk modulus values labeled with an "N" indicate that value was not measured either because of a jacket leak or in the case of sample WC-HC-50-04, the pressure was ramped directly to 5 MPa without unload/reload loops performed at 1 MPa and 2 MPa. Pore pressure measurements were made on the last two and last three 50% and 100% degraded specimens, respectively. These measurements will be discussed in further detail later in this section.

Figure 14. Post test 50% (a) and 100% (b) degraded hydrostatic compression samples.

Table 4. Summary of results from hydrostatic tests.

		Bulk modulus (MPa)				
Sample	Material	K @ 1MPa	K @ 2MPa	K @ 5MPa	K @ 15MPa	Comments
WC-HC-50-01	50%	274	577	1931	11350	
WC-HC-50-02	50%	239	680	2146	4703	
WC-HC-50-03	50%	283	749	2510	N	Jacket leak at 15MPa
WC-HC-50-04	50%	N	N	2194	4690	Pressure ramped directly to 5MPa
WC-HC-100-01	100%	460	1083	2186	32640	
WC-HC-100-02	100%	482	1134	2174	N	Pressure vessel leaked above 5MPa
WC-HC-100-03	100%	509	1427	2786	18720	Pore pressure tube pinched off above 5MPa
WC-HC-100-04	100%	463	1399	3490	N	Pressure vessel leaked
WC-HC-100-05	100%	653	1396	3130	5982	

Combined pressure versus engineering volume strain responses of 50% and 100% degraded samples are shown in Figures 15 and 16, respectively, and illustrates the consistency of samples with like material types. Represented in Table 4 by bulk modulus values and Figures 15 and 16 by engineering volume strain, 100% degraded specimens are stiffer than 50% degraded specimens. A large percentage of sample deformation occurs during initial pressurization up to 1 MPa. Above 1 MPa, the material begins to stiffen and after 5 MPa confining pressure, little compaction is observed up to the maximum confining pressure of 15 MPa.

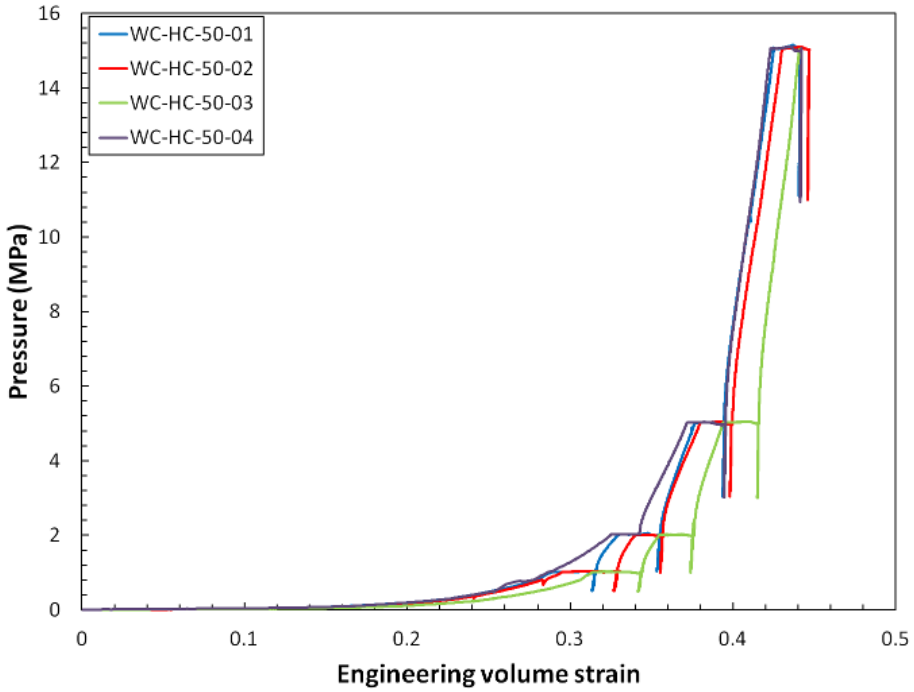

Figure 15. Pressure versus engineering volume strain for all 50% degraded samples.

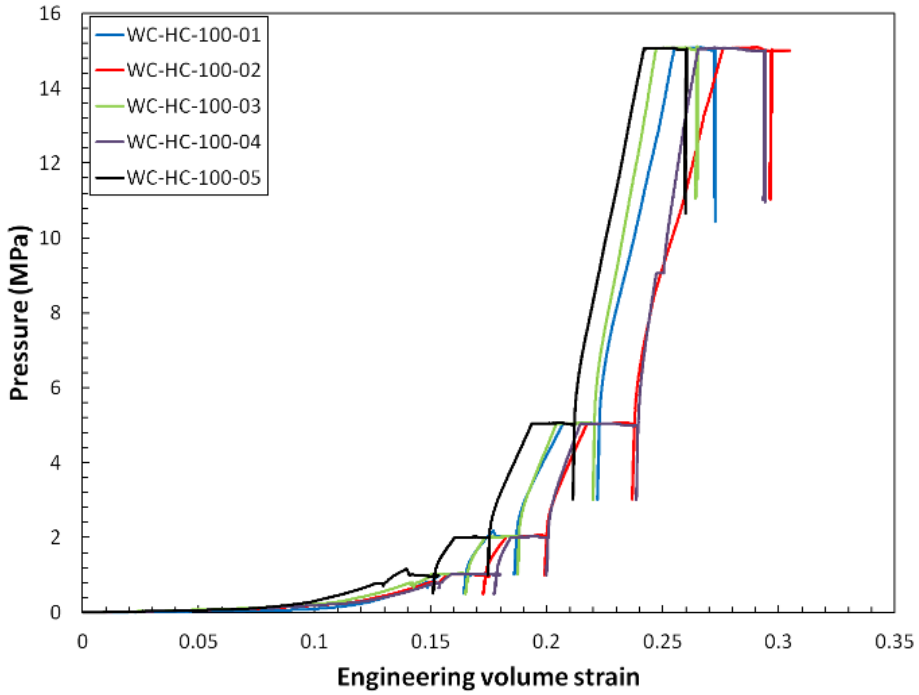

Figure 16. Pressure versus engineering volume strain for all 100% degraded samples.

A typical response of pore pressure to an increase in sample confining pressure is shown in Figure 17. Pore pressure is multiplied by 100 so it can be represented on the same vertical axis as confining pressure. Additional plots similar to Figure 17 are presented in Appendix A.

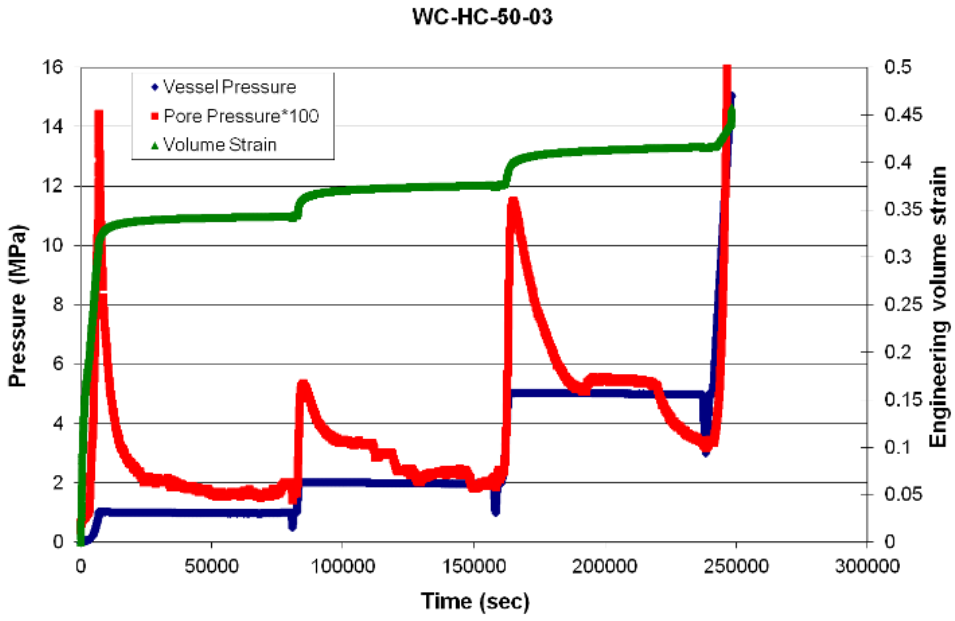

Figure 17. Pressure, pore pressure and engineering volume strain versus time for sample WC-HC-50-03. Sample jacket leaked at 15 MPa resulting in spike in pore pressure.

Interest in measuring pore pressure arose from the concern of sample creep. Sample creep can either be from creep of the material itself, continued compaction of the material due to a buildup of pore pressure within the sample, or a combination of both. Because pore pressure measurements indicate an overall small but measureable decay in pore pressure with time after an increase in confining pressure, pore pressure is likely a contributing factor to sample creep. Figure 18 shows a plot where pore pressure is subtracted from confining pressure and compared against confining pressure versus volume strain response of sample WC-HC-50-03.

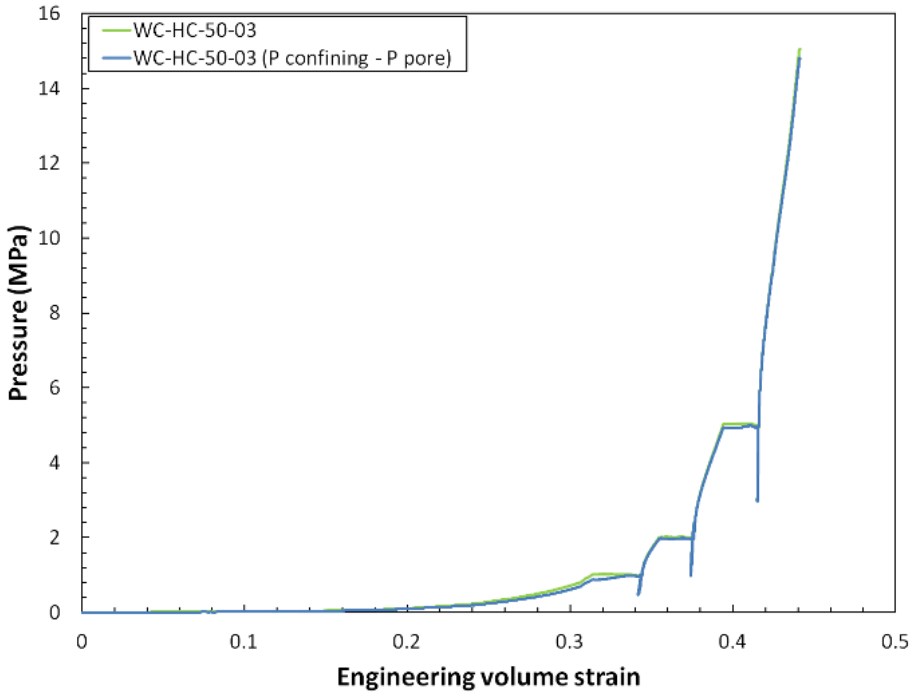

Figure 18. $P_{confining}$ and $P_{confining}$-P_{pore} versus engineering volume strain for sample WC-HC-50-03. Sample jacket leaked at 15 MPa resulting in no overnight hold data at this pressure.

As the sample is held overnight at 1, 2, and 5 MPa (15 MPa overnight hold was not achieved on this sample due to a jacket leak), $P_{confining}$-P_{pore} is lower than $P_{confining}$ initially. After a few hours, $P_{confining}$-P_{pore} reaches nearly the same value as $P_{confining}$ indicating a reduction of pore pressure as seen in Figure 18. Only one measurement of pore pressure was made and the sample was vented from the other end (pore pressure = 0 at the vented end). The measured values of pore pressure are nearly two orders of magnitude smaller than confining pressure and it remains unclear of the extent that sample creep is influenced by pore pressure.

As shown in Figure 3, the volume and weight of starting material for each sample is known. By subtracting the volume reduction measured during testing and weighing the sample post test, both pre- and post test sample densities are known. In the case of sample WC-HC-50-03, the post test density is high likely due to a jacket leak that added confining fluid to the sample mass. Samples WC-HC-100-02 and WC-HC-100-04 also have higher than average post test density values and are likely a result of the small pressure vessel leak detected during both of these tests.

A pressure vessel leak would give a false volume measurement yielding an inaccurate post test density measurement. Table 5 lists pre- and post test density values for all hydrostatic samples.

Table 5. Density values for all hydrostatic samples.

		Density (g/cc)		
Sample	Material	Pretest	Post test	Comments
WC-HC-50-01	50%	1.88	2.48	
WC-HC-50-02	50%	1.89	2.55	
WC-HC-50-03	50%	1.9	2.75*	Jacket leak at 15MPa
WC-HC-50-04	50%	1.93	2.62	Pressure ramped directly to 5MPa
(asterisk values not included in average)		1.9	2.55	Average 50%
WC-HC-100-01	100%	2.08	2.52	
WC-HC-100-02	100%	2.12	2.66**	Pressure vessel leaked above 5MPa
WC-HC-100-03	100%	2.13	2.52	Pore pressure tube pinched off above 5MPa
WC-HC-100-04	100%	2.12	2.68**	Pressure vessel leaked
WC-HC-100-05	100%	2.14	2.53	
(asterisk values not included in average)		2.12	2.52	Average 100%
* Note: Post test density from sample WC-HC-50-03 is likely inaccurate due to jacket leak and resulting in a heavier post test sample weight.				
** Note: Post test density is likely inaccurate due to a leak in the pressure vessel resulting in an inaccurate post compaction volume measurement				

4.2 Triaxial Compression

Ten triaxial tests were performed on 50% degraded material and nine triaxial tests were performed on 100% degraded material. Confining pressures were 1, 2, 5, and 15 MPa.

Based on initial hand measurements of each sample after die compaction to 80% of target confining pressure, Table 6 lists the density for each triaxial sample at three different stages during the test; 1) post die compaction, 2) post overnight hydrostatic hold, and 3) post triaxial test. To compute sample density after the overnight hydrostatic hold, fluid was captured and weighed and volume strain was determined from axial and radial displacement transducers mounted directly on the sample.

Two samples, WC-TX-50-02-02 and WC-TX-50-02-04, were die compacted to 1.8 MPa or 90% of target hydrostatic confining pressure as opposed to 80% for all other samples. While these samples exhibit overall higher Young's modulus values throughout the test, the data appear

within the expected scatter based on other tests at different confining pressures. Thus these samples are included in the analyses.

A typical plot of true differential stress versus true strain is shown in Figure 19 and represents a test on 100% degraded material. Note that a peak stress is observed; a feature most commonly seen on the 100% degraded material. All 50% degraded tests except for tests at 15 MPa confining pressure did not reach a peak stress value. All true differential stress versus true strain plots are presented in Appendix B. Peak stress values for the 100% degraded material are shown in Figure 20 and plotted versus confining pressure. This plot presents the data in a Mohr-Coulomb manner and gives an idea of the failure surface for the material.

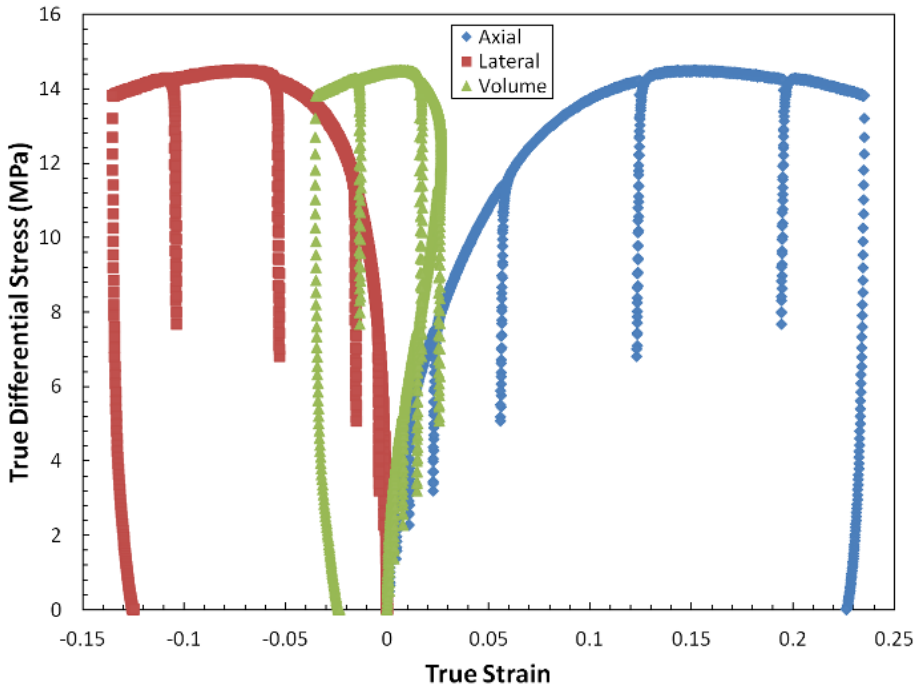

Figure 19. Typical plot (specimen WC-TX-100-05-02) of true differential stress versus true strain from a 100% degraded material triaxial test.

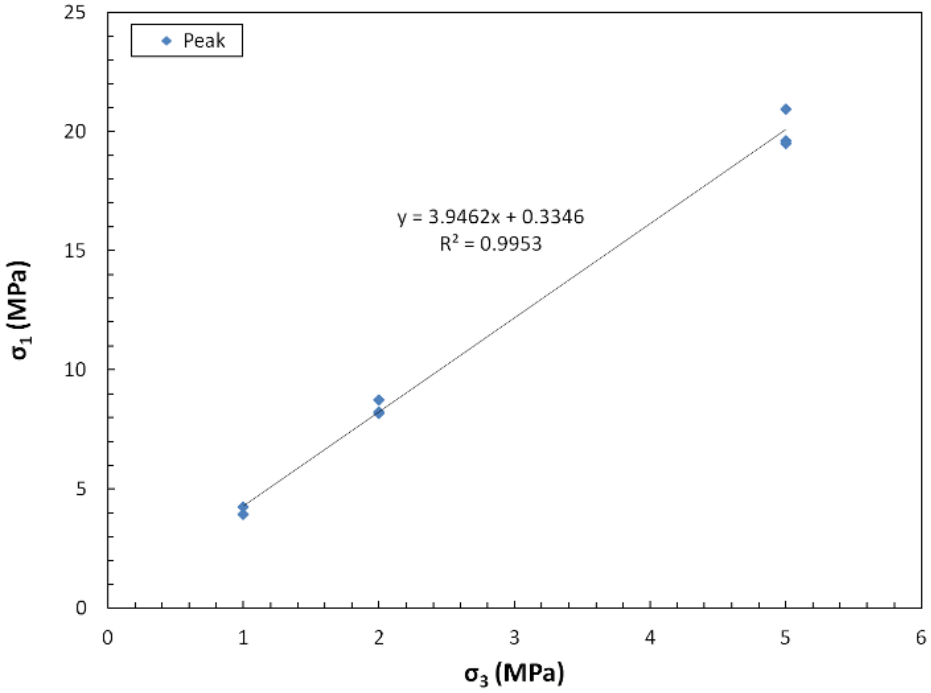

Figure 20. Plot of σ_1 versus σ_3 (peak strength values) for all 100% degraded material tests.

Table 6. Density values all triaxial samples.

Sample	Density post die compaction (g/cc)	Density post overnight hydrostatic hold (g/cc)	Density post triaxial test (g/cc)
WC-TX-50-01-01	2.02	2.2	2.29
WC-TX-50-01-02	2.09	2.26	2.27
WC-TX-50-02-01	1.99	No Test	
WC-TX-50-02-02	2.07	2.35	2.43
WC-TX-50-02-03	2	No Test	
WC-TX-50-02-04	2.07	2.35	2.38
WC-TX-50-02-05	2.08	No Test	
WC-TX-50-02-06	2.05	2.31	2.31
WC-TX-50-05-01	2.2	2.49	2.52
WC-TX-50-05-02	2.11	2.42	2.43
WC-TX-50-05-03*	2.07	2.41	2.37
WC-TX-50-15-01	2.14	No Test	
WC-TX-50-15-02	2.18	2.61	2.61
WC-TX-50-15-03	2.15	2.62	2.56
WC-TX-100-01-01	2.28	2.36	2.25
WC-TX-100-01-02	2.28	2.35	2.22
WC-TX-100-02-01	2.32	2.46	2.39
WC-TX-100-02-02	2.29	2.39	2.37
WC-TX-100-02-03**	2.34	N/A	2.39
WC-TX-100-05-01	2.33	2.48	2.48
WC-TX-100-05-02	2.31	2.49	2.4
WC-TX-100-05-04*	2.26	2.23	N/A
WC-TX-100-05-05*	2.36	2.51	2.58
* Slow test (20 times slower than other tests)			
** Sample barreling investigated (Lateral LVDT's mounted at midheight and 25% from one end)			

From the internal sample mounted LVDT's, Young's modulus and Poisson's ratio were determined as a function of axial strain. Young's modulus results are presented graphically in Figure 21 and Figure 22 for 50% and 100% degraded materials respectively. The same results are presented in Table D 1 in Appendix D. Poisson ratio values are not shown for triaxial tests due to erroneous high values. An investigation was conducted that included running tests on each material type at pressurization and axial strain rates 20 times slower than used in the other tests. This change in rates did not give a change in Poisson ratio values. It was decided that sample barreling was occurring from the results of changing the location of the lateral LVDT's (one gage mounted at sample midheight and one 25% from one end). The LVDT mounted 25% from one end gave significantly smaller lateral strains than the LVDT mounted at sample midheight. It was concluded that lateral strain was a function of location along the length of the sample. Tests with asterisk markers next to them in Table 6, Figure 21, and Figure 22 are tests run with different rates and transducer configuration as described in the aforementioned sample

barreling investigation. These erroneous Poisson ratio values from the triaxial test series was the motivator for conducting the uniaxial strain tests discussed in Section 6.3.

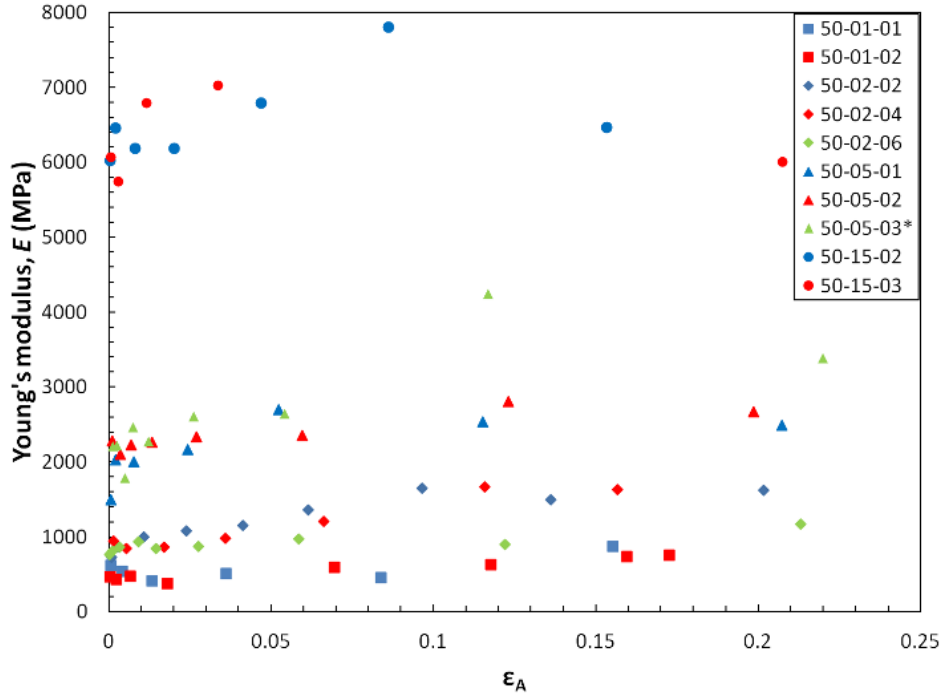

Figure 21. Young's modulus versus axial strain for all 50% degraded material triaxial tests. The "*" in the legend is the same note as in Table 6.

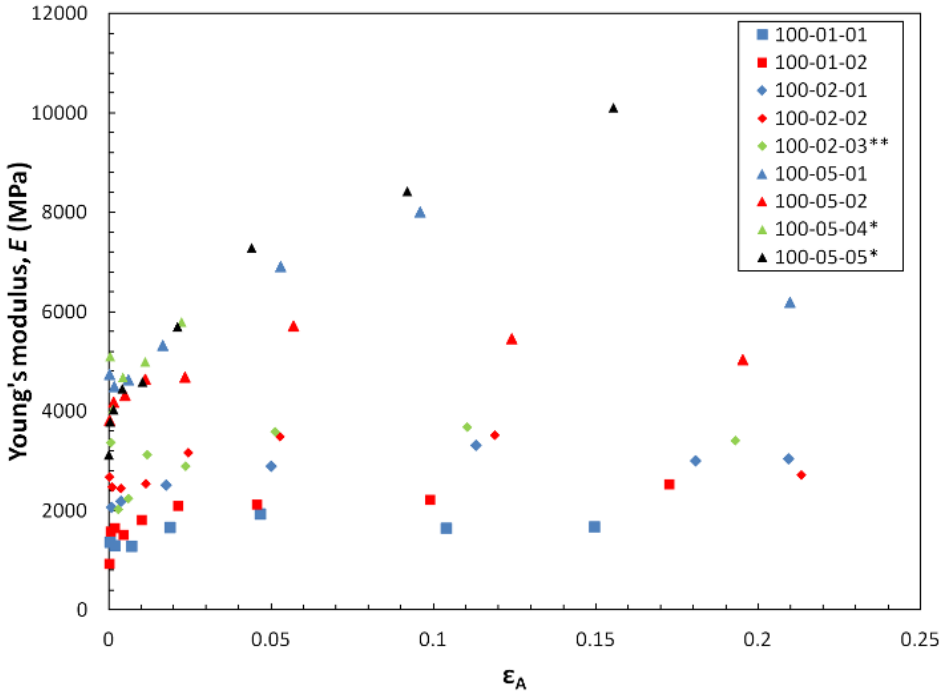

Figure 22. Young's modulus versus axial strain for all 100% degraded material triaxial tests. The "*" and "" in the legend are the same notes as in Table 6.**

Bulk modulus values were determined after the overnight hydrostatic hold prior to the application of differential stress. Volumetric strain was calculated from Equation (2) using the sample mounted LVDT's. These values are compared to the average bulk modulus values from the hydrostatic test series and compare reasonably well at lower confining pressures. At higher confining pressures (5 and 15 MPa) bulk modulus values determined using sample mounted LVDT's are lower than bulk modulus values determined using dilatometry (hydrostatic test series). This discrepancy could be a result of two factors: 1) lateral strain measurement taken at two discreet points along the length of the sample (see sample barreling investigation presented earlier in this section) and 2) the limitation of resolution of dilatometry measurements at higher confining pressures.

4.3 Uniaxial Strain

Figure 23 shows a typical plot of radial stress versus axial stress. Axial stress was increased and subsequently radial stress increased to enforce a zero lateral strain condition. After the test loading was finished, axial and radial stress were decreased following a stress path similar to when the specimen was loaded. Final specimen unloading is represented by the upper line in Figure 23.

During application of axial and radial stress, unload/reload loops were performed. Poisson's ratio and Young's modulus were determined from the slope of the unload portion of the unload/reload loop following Equation 16 (arrows pointing to typical unload/reload loops are shown in Figures 23 and 24). Once Poisson's ratio is known, Young's modulus can be calculated from Equation 20. The slope of the line in Equation 20 is represented by a plot of true differential stress versus true axial strain (Figure 24). Unload/reload loops are shown in Figure 24 from which Young's modulus is calculated from the slope of the unload portion of the unload/reload loops. These are the same loops shown in Figure 23 but plotted in true differential stress versus true axial strain space. Plots similar to Figures 23 and 24 for all other uniaxial strain specimens are listed in Appendix C.

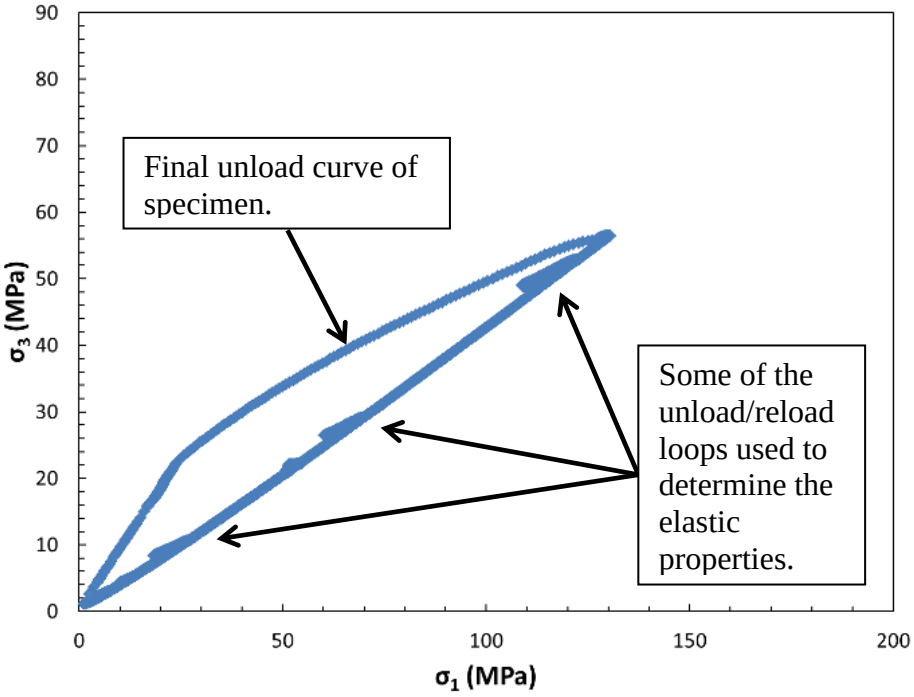

Figure 23. Typical plot (specimen WC-TX-100-01-03) of confining pressure versus axial stress used to determine Poisson's ratio from unload/reload loops.

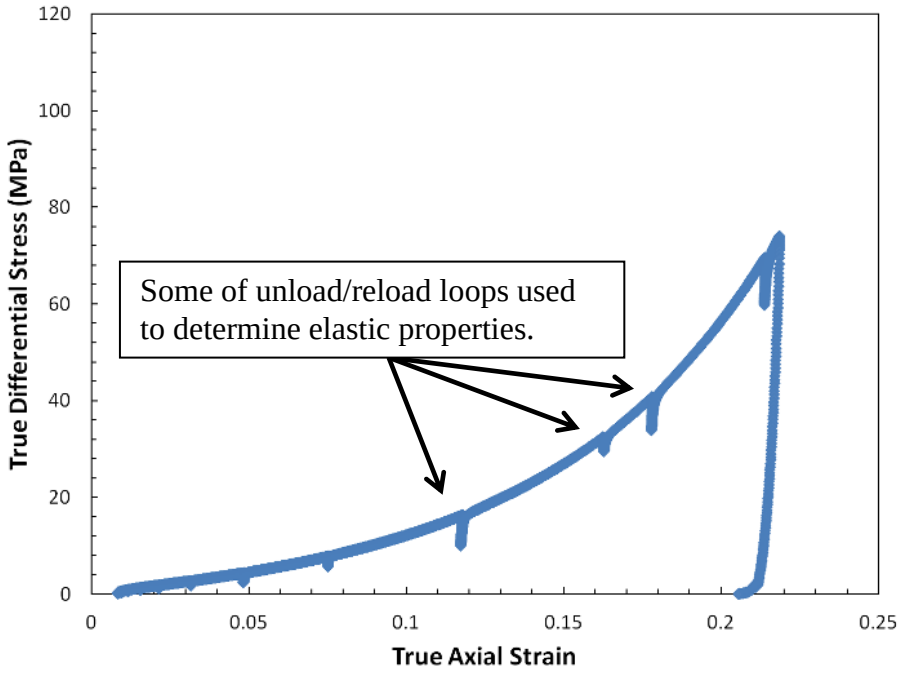

Figure 24. Typical plot (specimen WC-TX-100-01-03) of true differential stress versus true axial strain. Once Poisson's ratio is known, a plot such as this is used to calculate Young's modulus from unload/reload loops.

With lateral strain held at zero, sample volume for uniaxial strain tests was calculated directly from axial strain measurements. Weight of the sample at each unload/reload loop was determined by weighing brine expelled from the sample. These measurements allow determination of Young's modulus and Poisson's ratio as a function of density. These relationships are shown for both 50% and 100% degraded materials in Figures 25 and 26 respectively and in Table D 2 in Appendix D. Densities for both materials range between 2.2 g/cc to 2.9 g/cc. Young's modulus increases gradually up to a density of ~2.5g/cc after which the samples stiffen at a faster rate. Poisson's ratio also increases with increasing density, but the increase is more subtle than with Young's modulus. At the highest density measured, Poisson's ratio is ~0.35 and ~0.25 for 50% and 100% degraded materials, respectively. Young's modulus values and densities obtained from uniaxial strain testing more than cover the range of values obtained during triaxial testing. Young's modulus is much higher for all densities measured for the 100% degraded material.

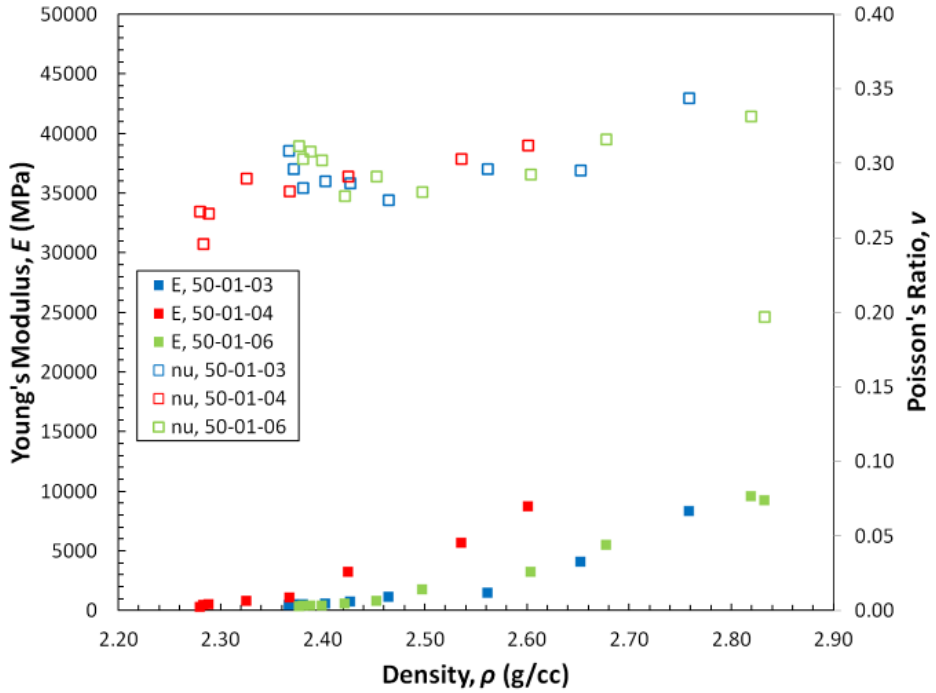

Figure 25. Young's modulus and Poisson's ratio versus density for 50% degraded material uniaxial strain tests.

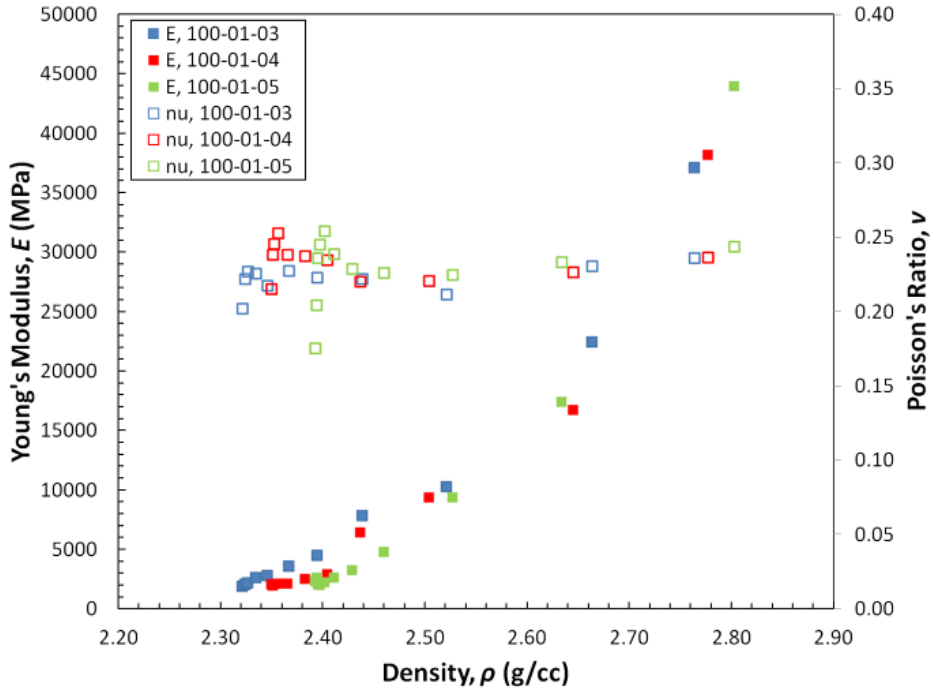

Figure 26. Young's modulus and Poisson's ratio versus density for 100% degraded material uniaxial strain tests.

5. CONCLUSIONS

A test suite was conducted that established the following for two surrogate material recipes representing 50% and 100% degraded waste states at the WIPP:

- Bulk modulus was determined as a function of confining pressure
- Young's modulus and Poisson's ratio were determined as a function of density
- The effect of pore pressure was investigated
- A Mohr-Coulomb failure envelope was developed from 100% degraded triaxial tests

In some cases, novel test methods and equipment were developed to handle the unique material composition. Included was the following: 1) use of a dual piston dilatometer system capable of handling large volumetric strains while still giving the precision necessary for reliable bulk modulus measurements, 2) dual LVDT radial displacement rings to allow for measurement of large radial sample displacements within the limited confines of a pressure vessel and 3) uniaxial strain condition using confining pressure to maintain zero lateral strain allowing determination of Young's modulus and Poisson's ratio as a function of sample density.

The specific objective of this report is to document hydrostatic, triaxial, and uniaxial strain loading tests conducted on surrogate degraded waste as data required to develop an improved constitutive model for WIPP waste behavior. The test plan (Broome and Costin, 2010) governing the experimental program calls for testing both surrogate fresh and degraded waste forms to capture the full evolutionary behavior of the waste as it is expected to degrade with time. Testing was terminated after completion of the surrogate degraded waste experiments as part of programmatic cuts enacted by the DOE/CBFO. Further testing on surrogate fresh waste is required to capture the full range of WIPP waste compaction behavior before a new model can be implemented in WIPP Performance Assessment. The compaction behavior of surrogate fresh waste is needed to describe the anticipated behavior of WIPP waste during early times of the repository when room closure, waste compaction, and chemical changes are occurring at their fastest rates. Hydrostatic, triaxial, and uniaxial compaction tests on surrogate fresh waste are planned to begin in calendar year 2014.

6. REFERENCES

1. ASTM D2664-04, 2004, *Standard Test Method for Triaxial Compressive Strength of Undrained Rock Core Specimens Without Pore Pressure Measurements*, American Society for Testing and Materials, ASTM International, West Conshohocken, PA.

2. ASTM D4543-07, 2007, *Standard Practices for Preparing Rock Core as Cylindrical Test Specimens and Verifying Conformance to Dimensional and Shape Tolerances*, American Society for Testing and Materials, ASTM International, West Conshohocken, PA.

3. ASTM D7012-07, 2007, *Standard Test Method for Compressive Strength and Elastic Moduli of Intact Rock Core Specimens under Varying States of Stress and Temperatures*, American Society for Testing and Materials, ASTM International, West Conshohocken, PA.

4. Broome, S.T. and Costin, L.S., 2010. Compaction Behavior of Emplaced Waste, Rev. 1, Test Plan 08-01, Sandia National Laboratories, Carlsbad, NM.

5. Fung, Y.C., 1993, *A First Course in Continuum Mechanics*, 3rd ed., Prentice-Hall, Inc.

6. Hansen, F.D., Knowles, M.K., Thompson, T.W., Gross, M., McLennan, J.D., Schatz, J.F., 1997, *Description and Evaluation of a Mechanistically Based Conceptual Model for Spall*, SAND97-1369, Sandia National Laboratories, Albuquerque, NM.

7. SNL 2010. *Scientific Notebook WIPP-DWT-1 WIPP Waste Compaction Program*. Sandia National Laboratories, Carlsbad, NM. ERMS 558033.

8. SNL 2012. *Supplemental Binder #1 to Scientific Notebook WIPP-DWT-1; WIPP-DWT-1-SB1 WIPP Waste Compaction Program*. Sandia National Laboratories, Carlsbad, NM. ERMS 558034

APPENDIX A
HYDROSTATIC COMPRESSION TEST RESULTS FOR 50% AND 100% DEGRADED MATERIAL

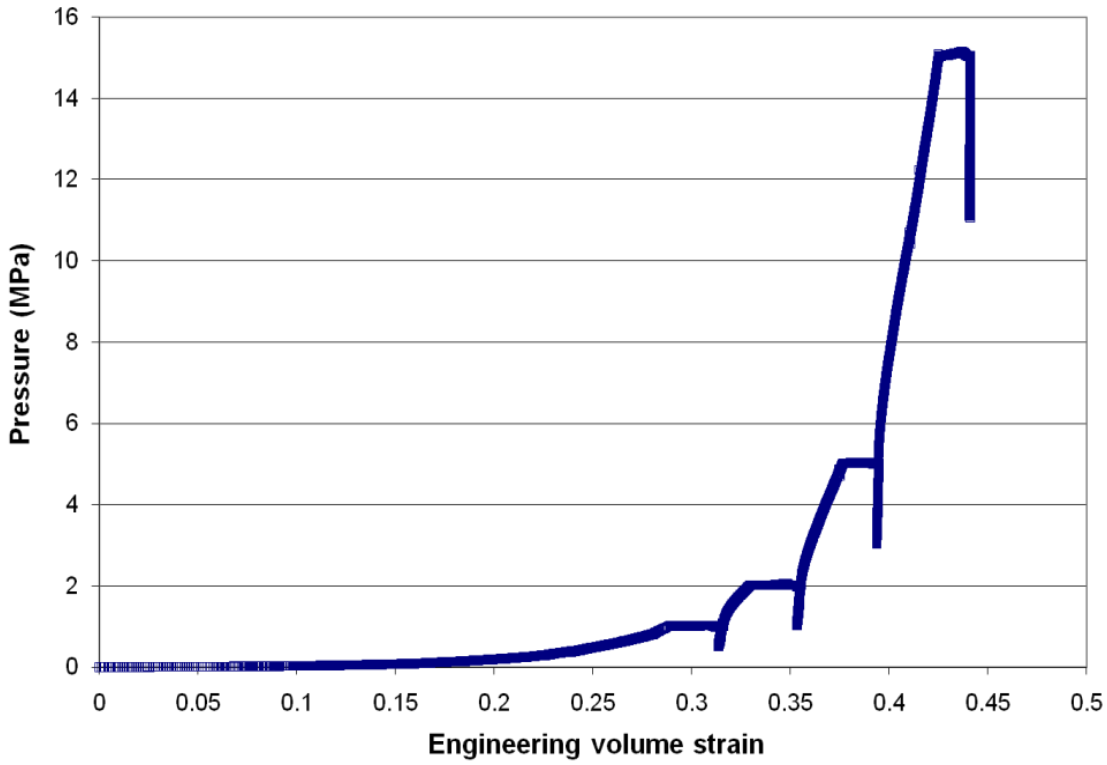

Figure A 1. WC-HC-50-01 Pressure versus engineering volume strain.

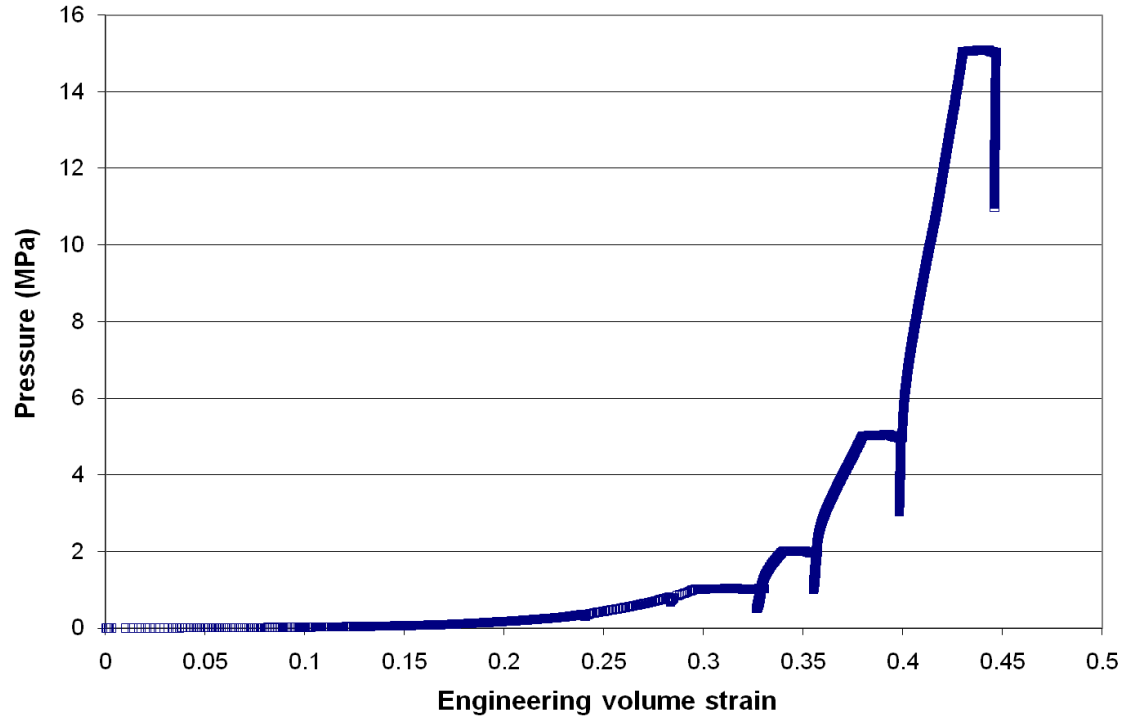

Figure A 2. WC-HC-50-02 Pressure versus engineering volume strain.

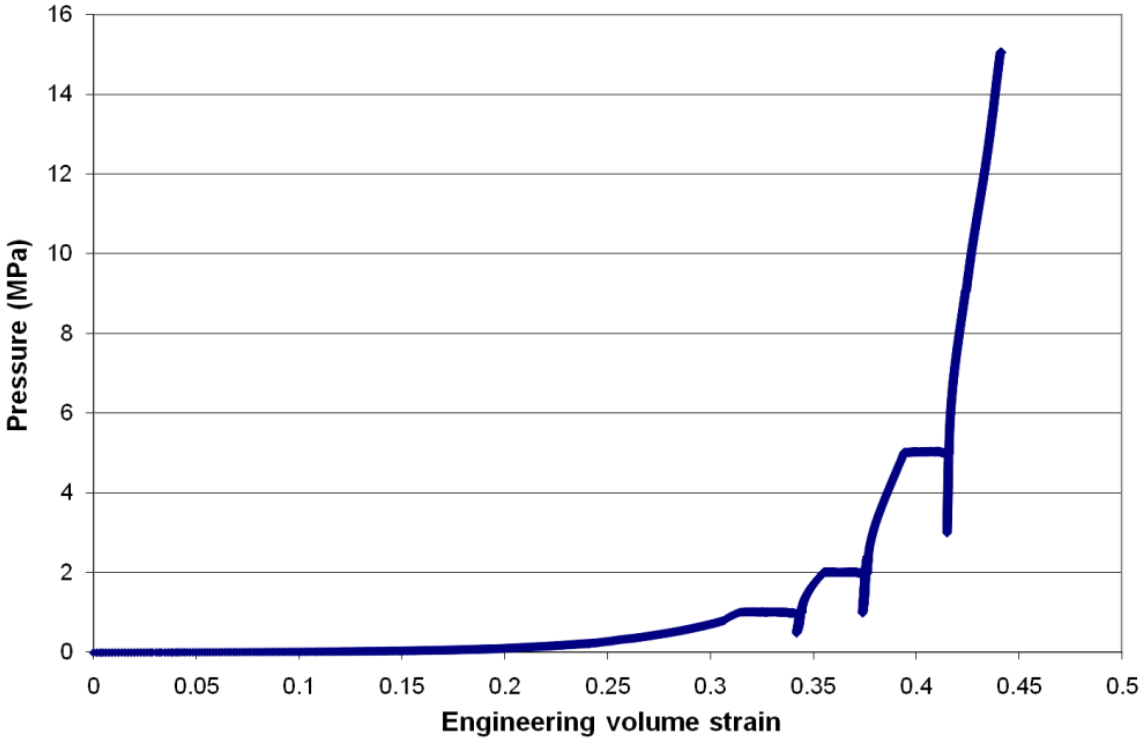

Figure A 3. WC-HC-50-03 Pressure versus engineering volume strain. Jacket leak at 15 MPa.

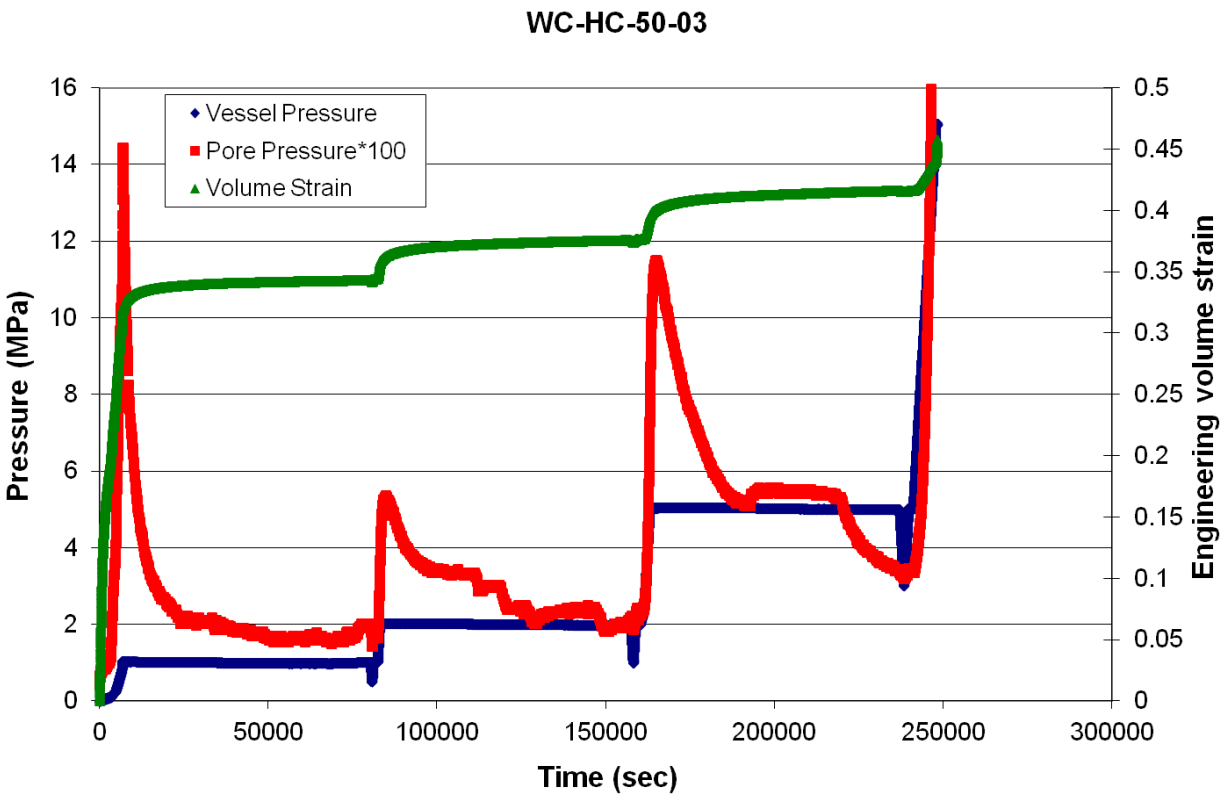

Figure A 4. WC-HC-50-03 Confining pressure, pore pressure, and engineering volume strain versus time. Jacket leak at 15 MPa.

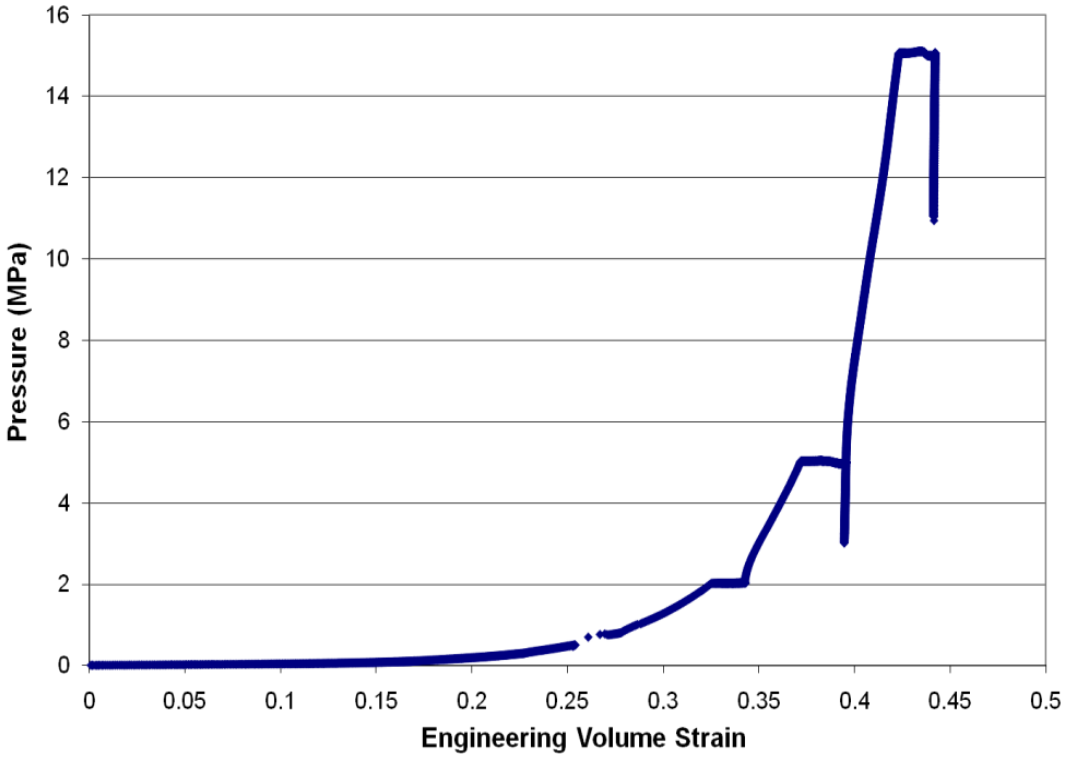

Figure A 5. WC-HC-50-04 Pressure versus engineering volume strain. Loops at 5 and 15 MPa.

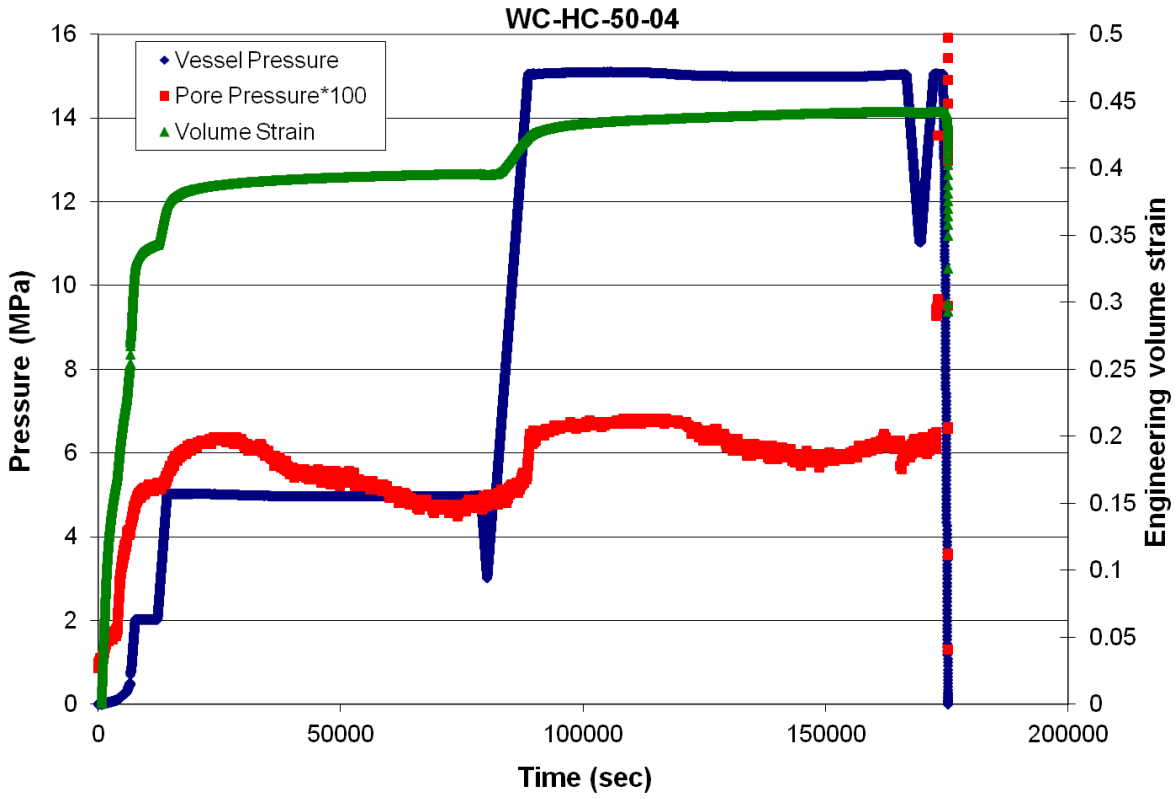

Figure A 6. WC-HC-50-04 Confining pressure, pore pressure, and engineering volume strain versus time. Loops at 5 and 15 MPa.

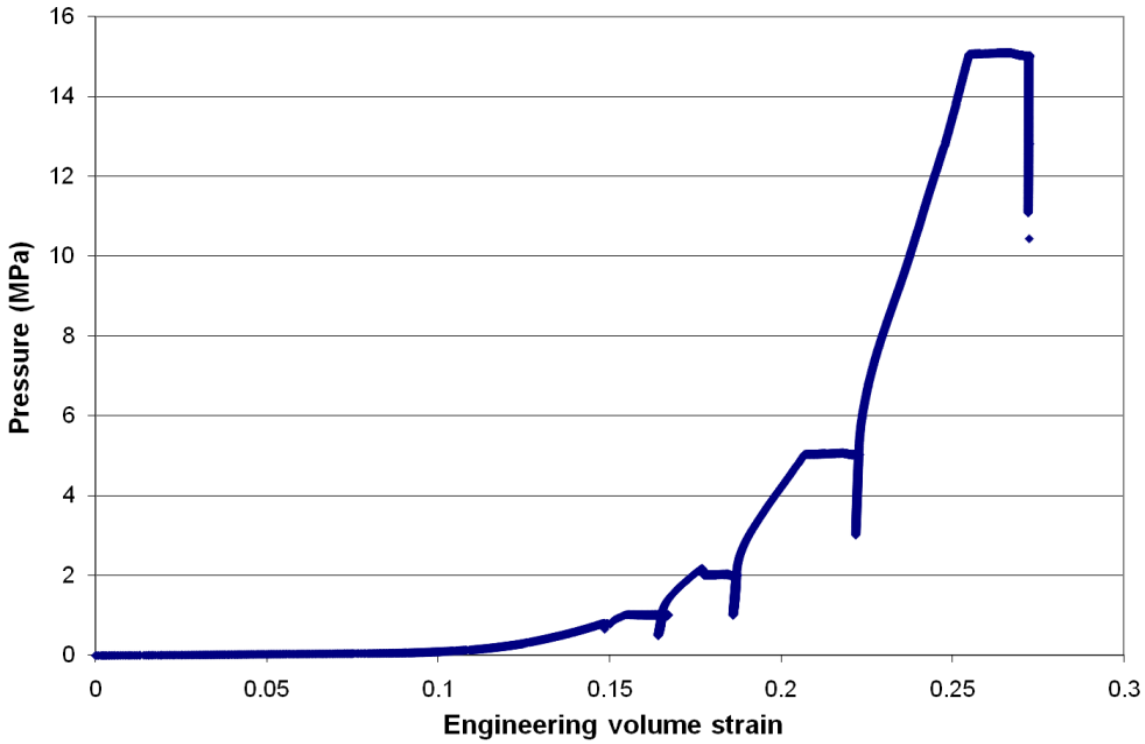

Figure A 7. WC-HC-100-01 Pressure versus engineering volume strain

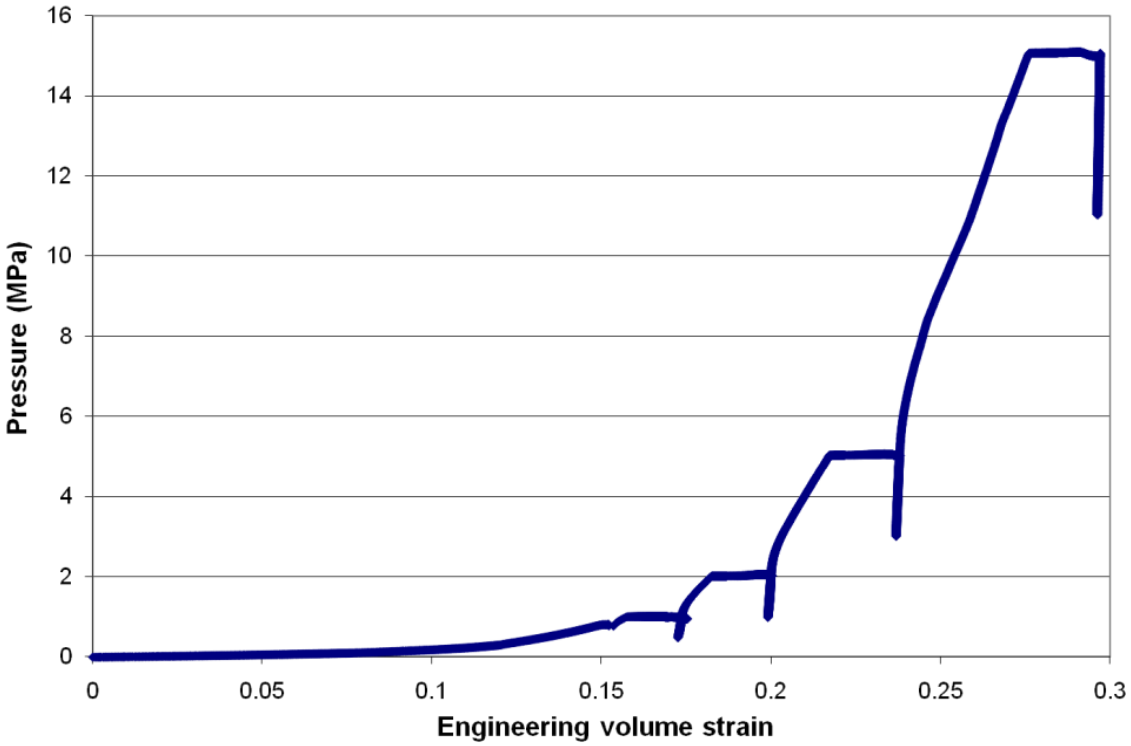

Figure A 8. WC-HC-100-02 Pressure versus engineering volume strain. Pressure vessel leaked above 5 MPa.

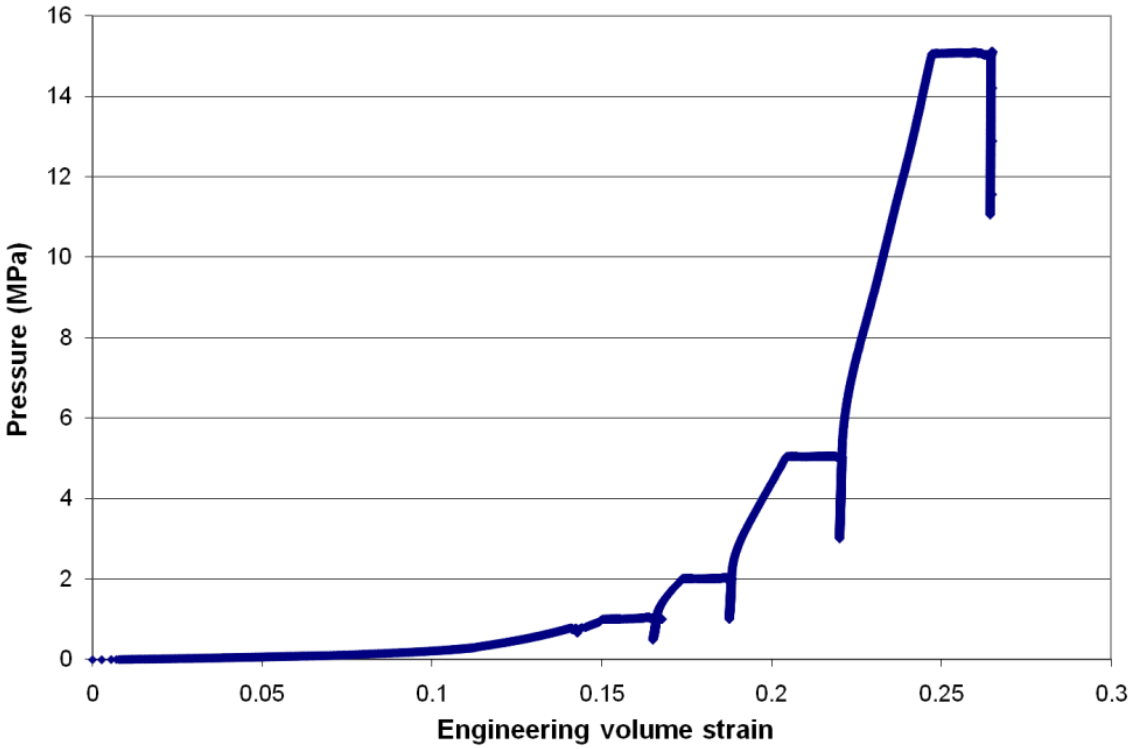

Figure A 9. WC-HC-100-03 Pressure versus engineering volume strain.

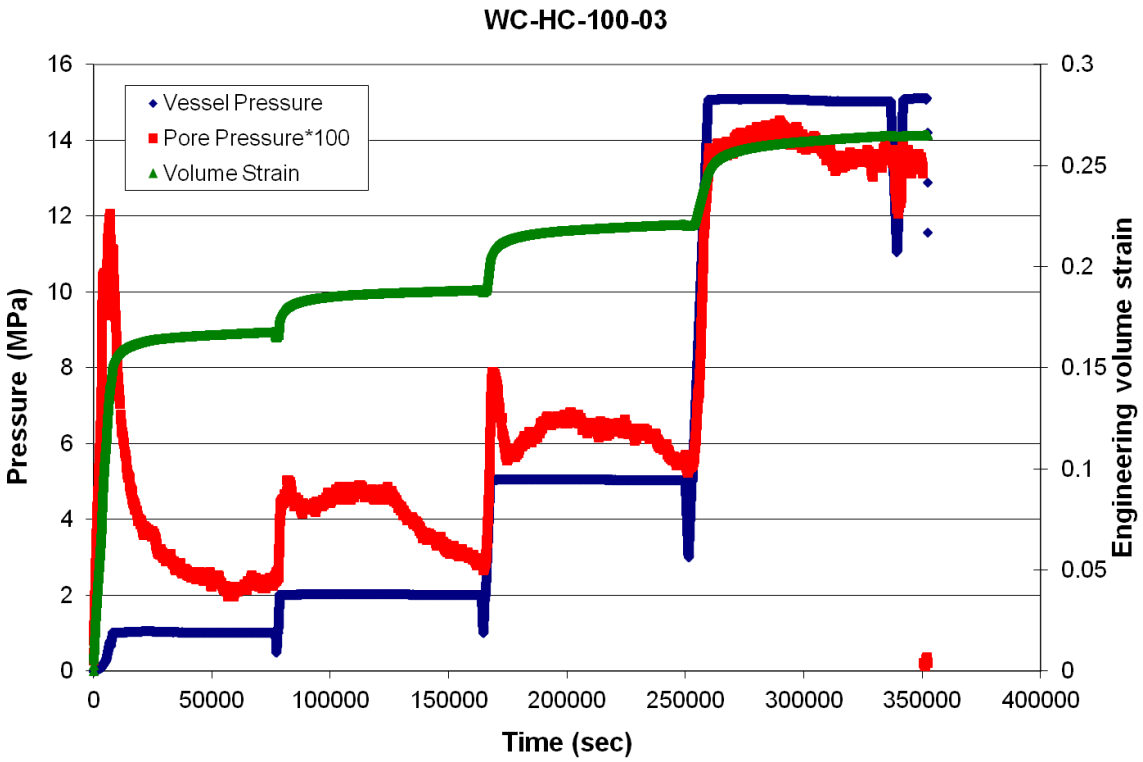

Figure A 10. WC-HC-100-03 Confining pressure, pore pressure, and engineering volume strain versus time.

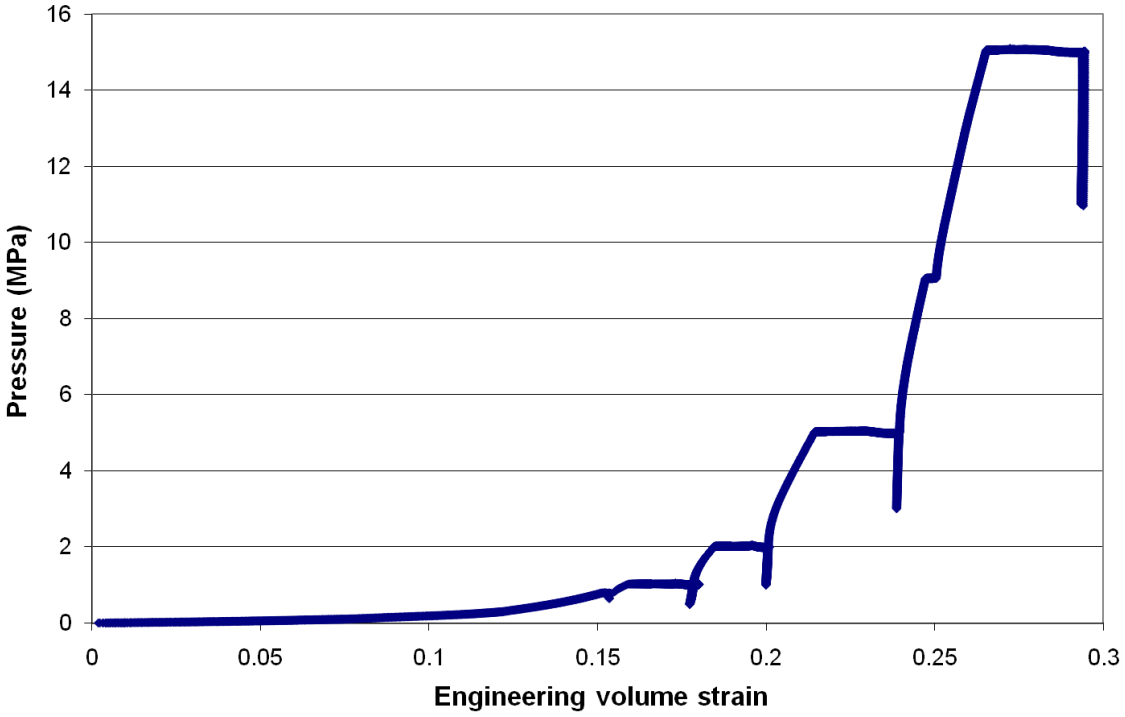

Figure A 11. WC-HC-100-04 Pressure versus engineering volume strain. Pressure vessel leaked.

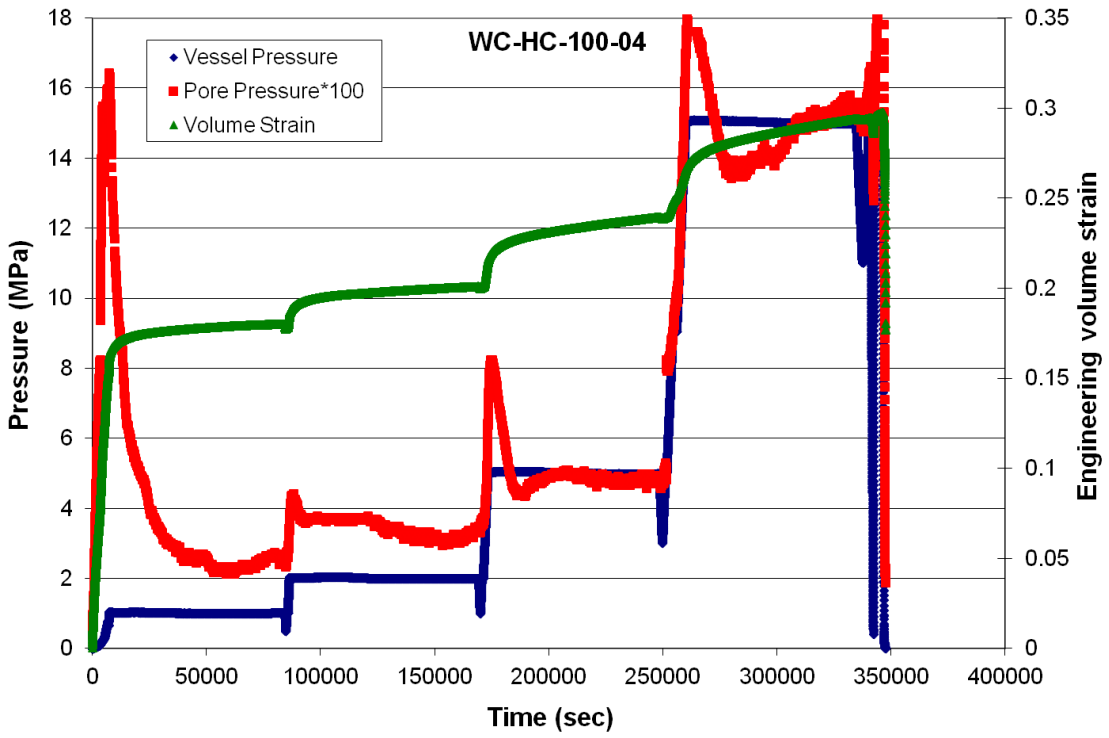

Figure A 12. WC-HC-100-04 Confining pressure, pore pressure, and engineering volume strain versus time. Pressure vessel leaked.

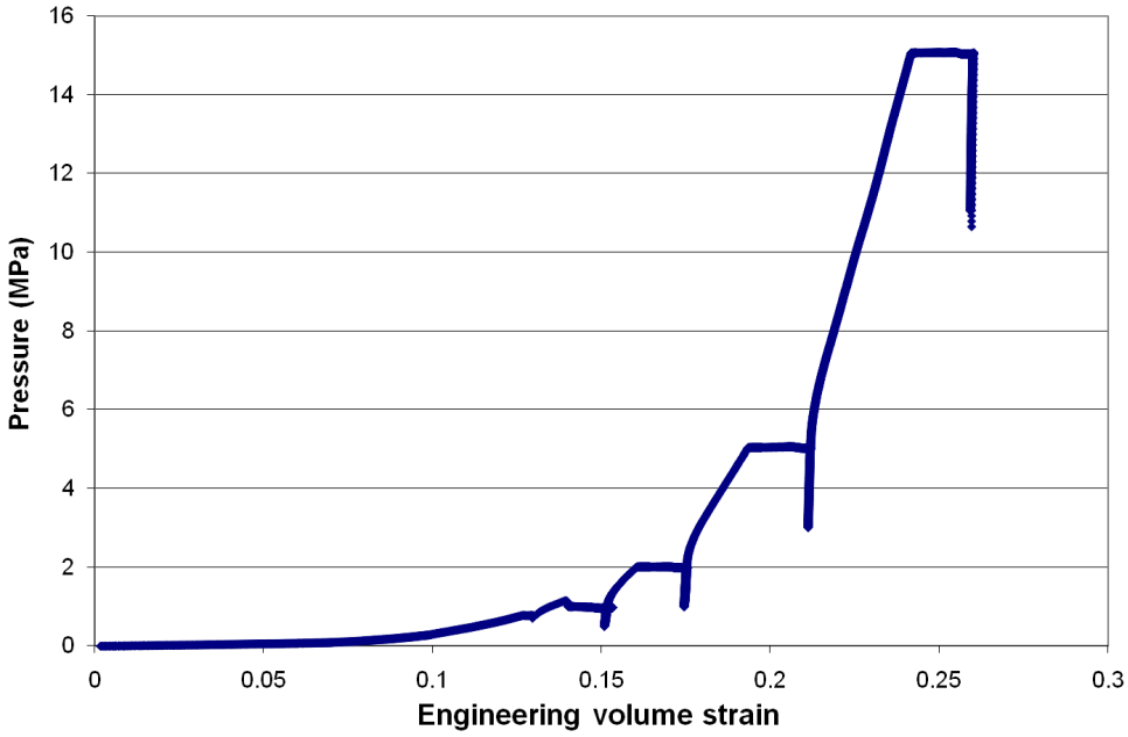

Figure A 13. WC-HC-100-05 Pressure versus engineering volume strain.

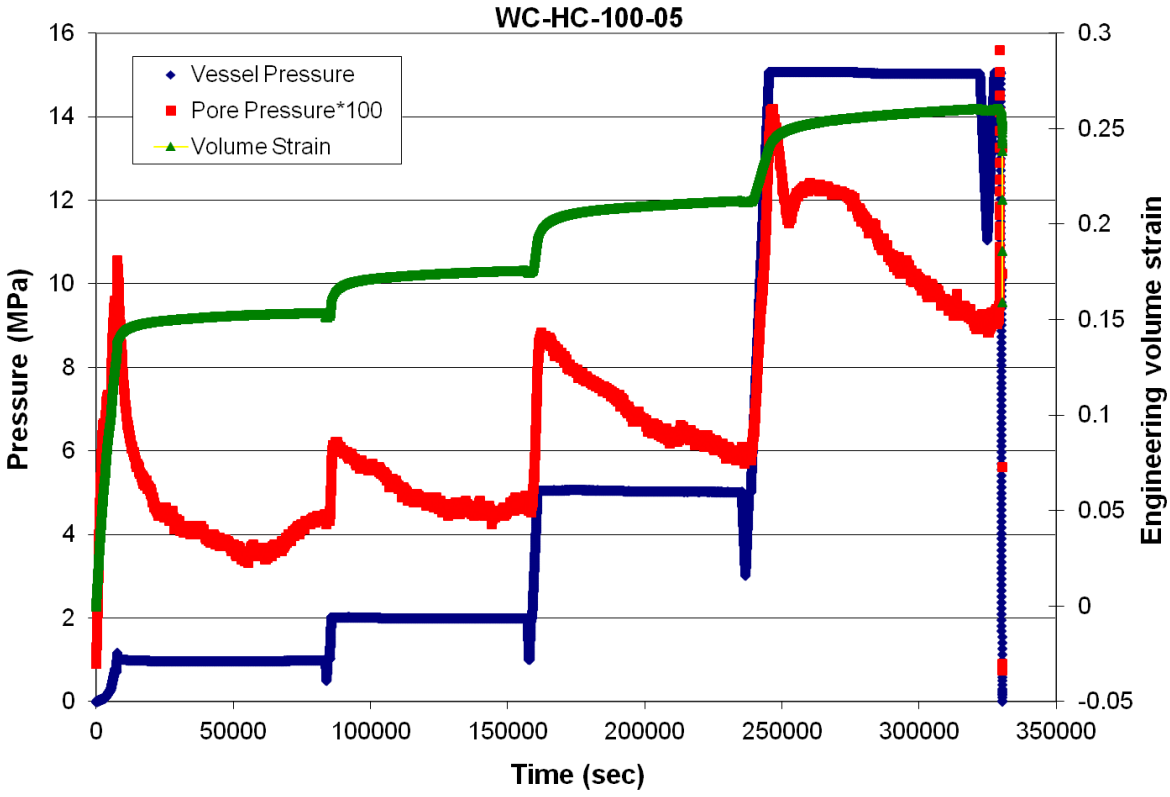

Figure A 14. WC-HC-100-05 Confining pressure, pore pressure, and engineering volume strain versus time.

APPENDIX B
TRIAXIAL COMPRESSION TEST RESULTS FOR 50% AND 100% DEGRADED MATERIAL

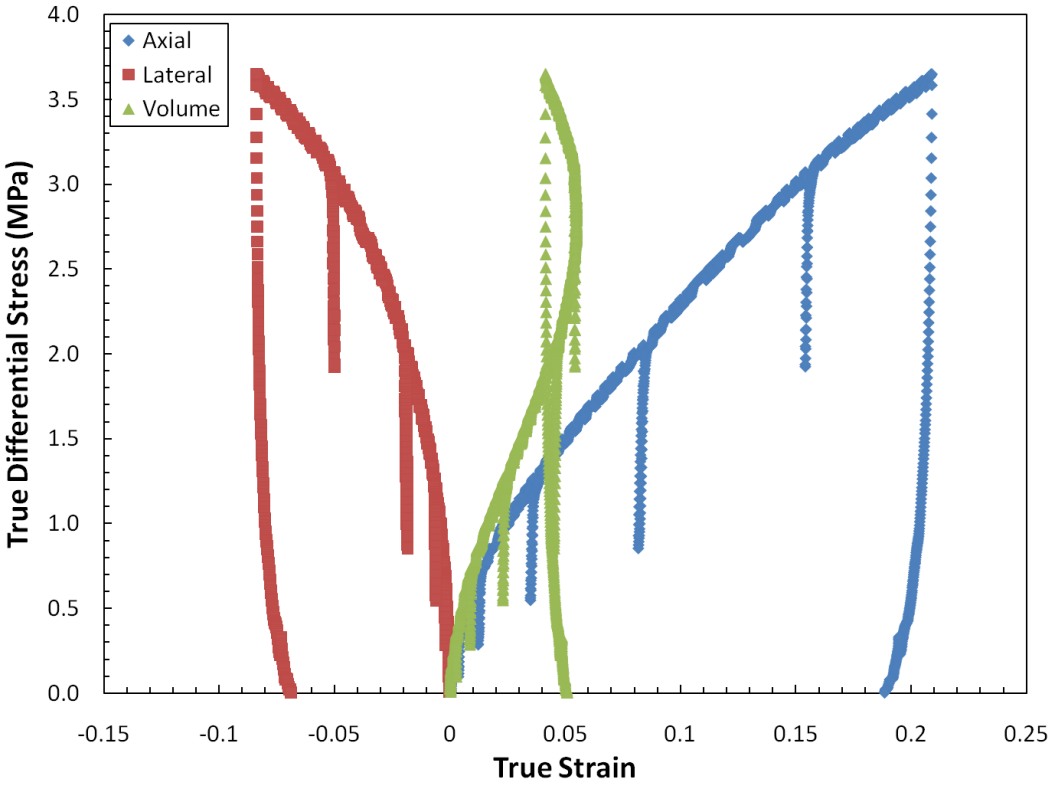

Figure B 1. WC-TX-50-01-01 True differential stress versus true strain.

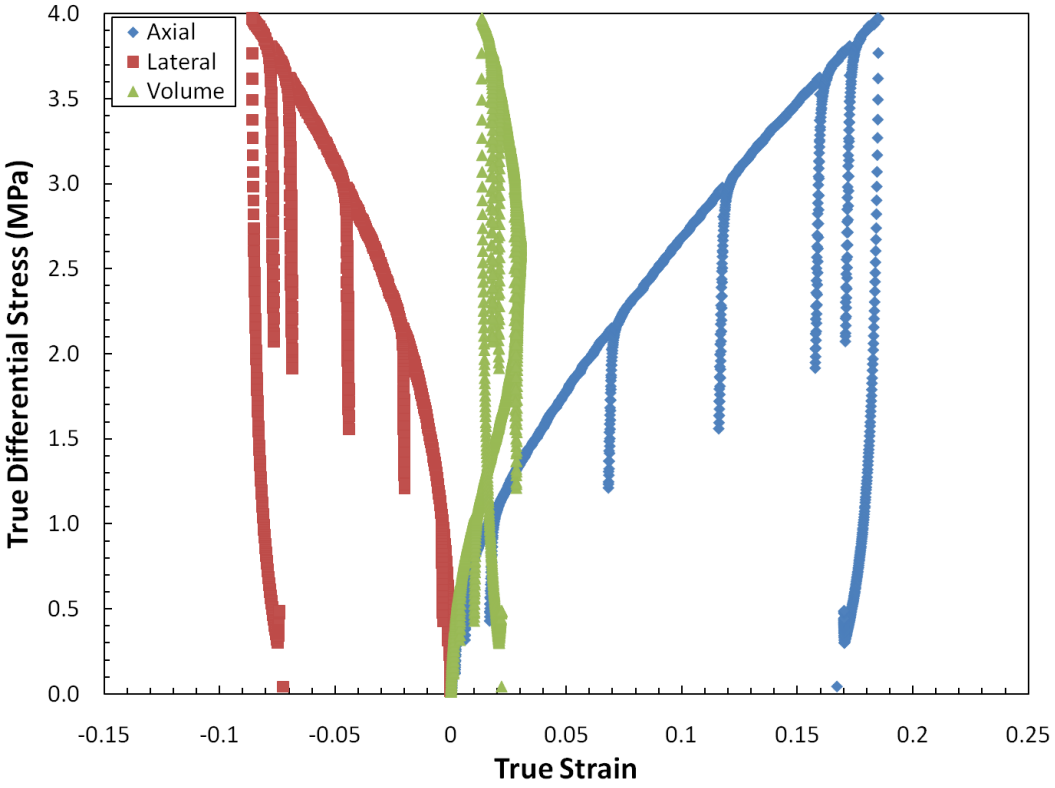

Figure B 2. WC-TX-50-01-02 True differential stress versus true strain.

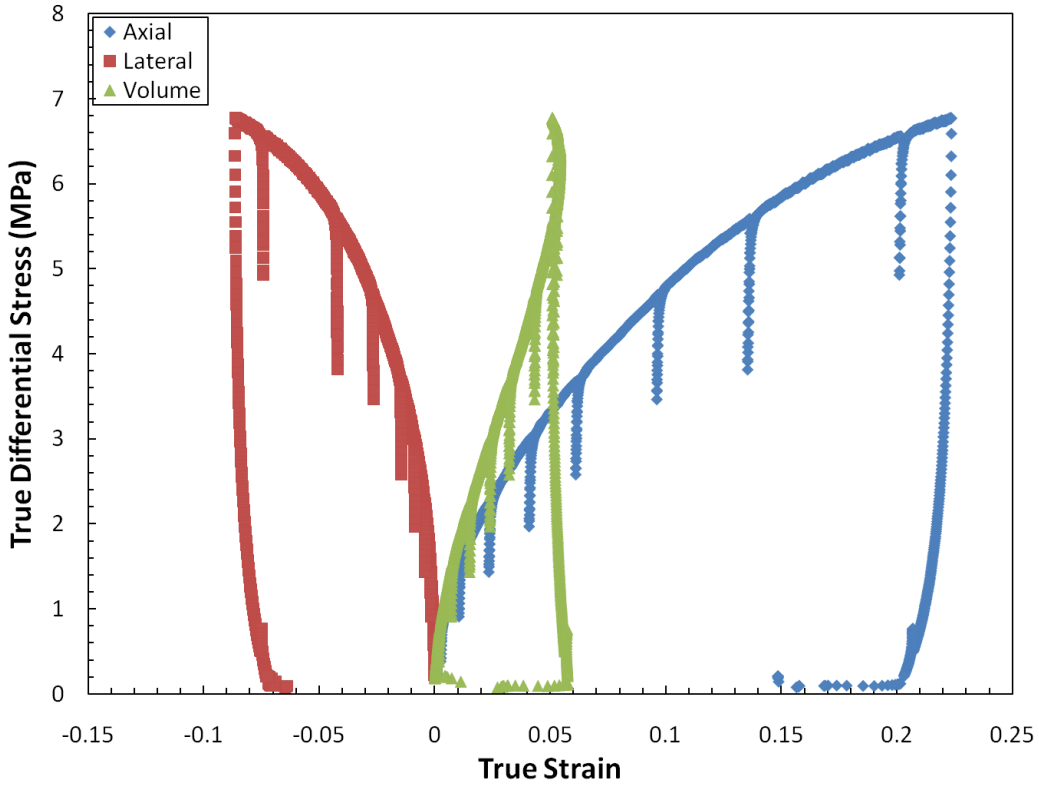

Figure B 3. WC-TX-50-02-02 True differential stress versus true strain.

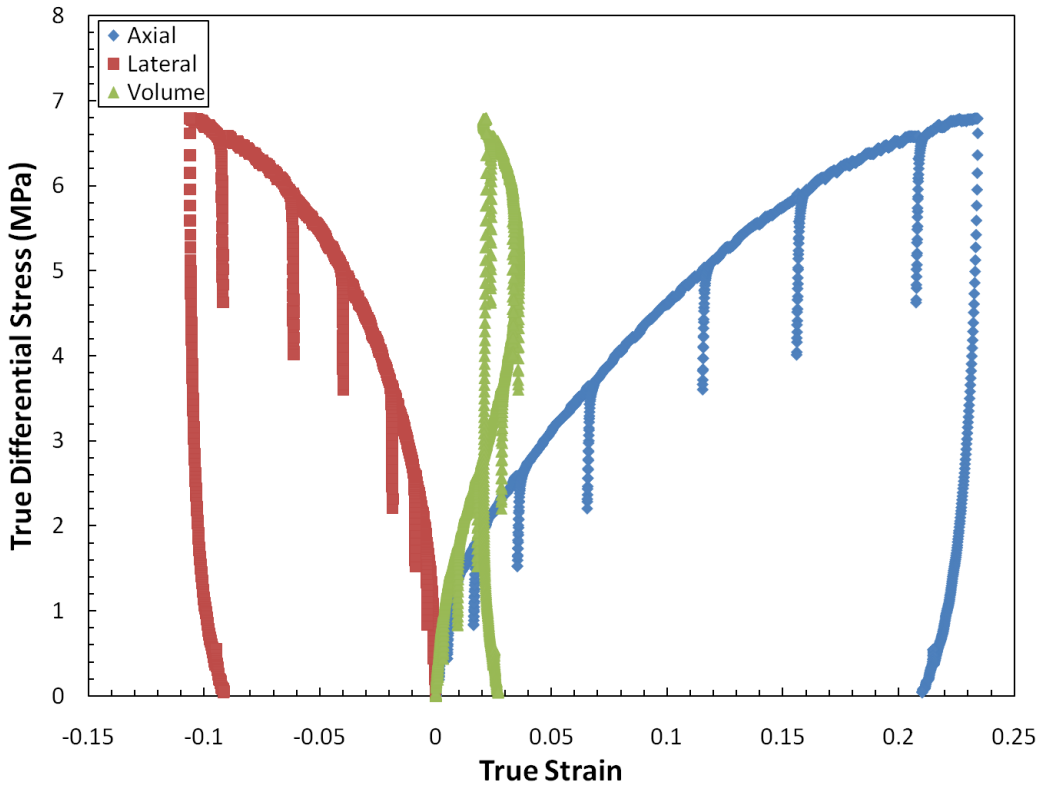

Figure B 4. WC-TX-50-02-04 True differential stress versus true strain.

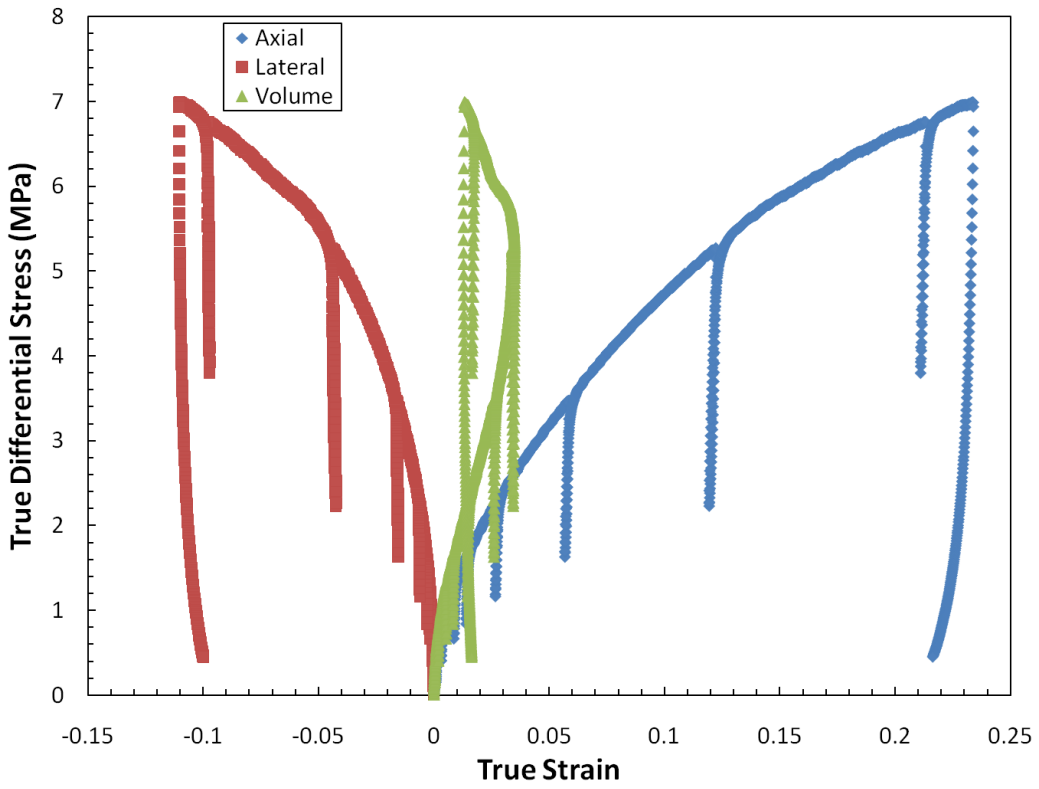

Figure B 5. WC-TX-50-02-06 True differential stress versus true strain.

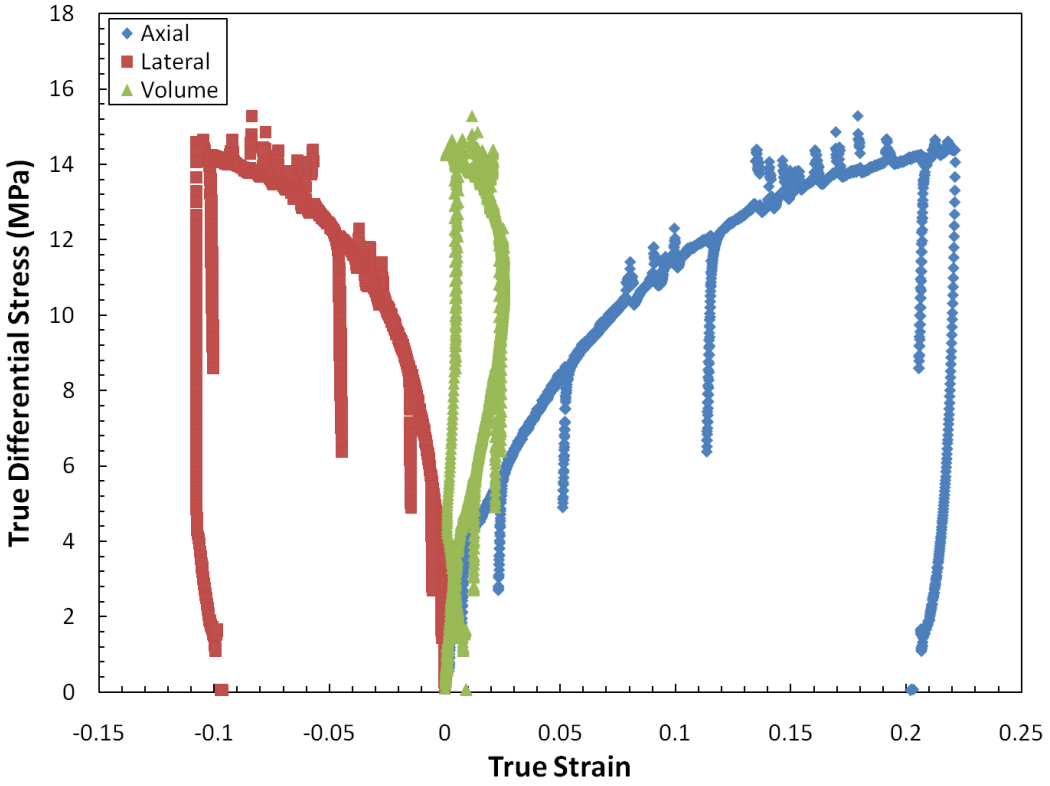

Figure B 6. WC-TX-50-05-01 True differential stress versus true strain.

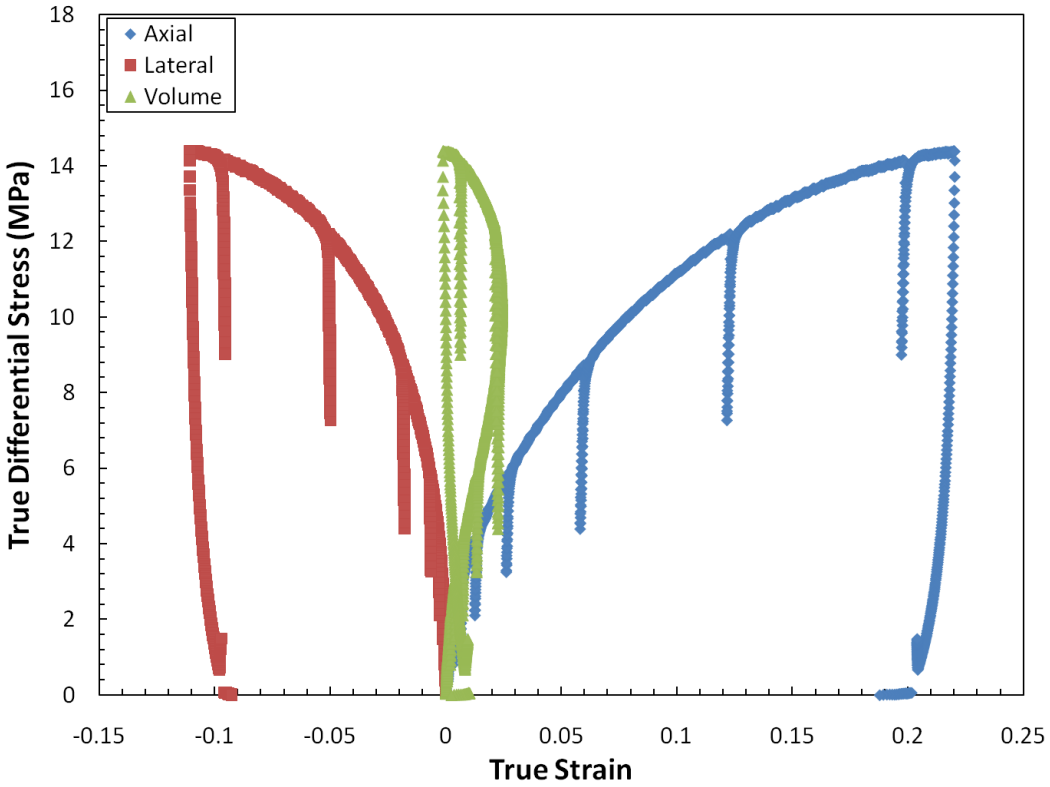

Figure B 7. WC-TX-50-05-02 True differential stress versus true strain.

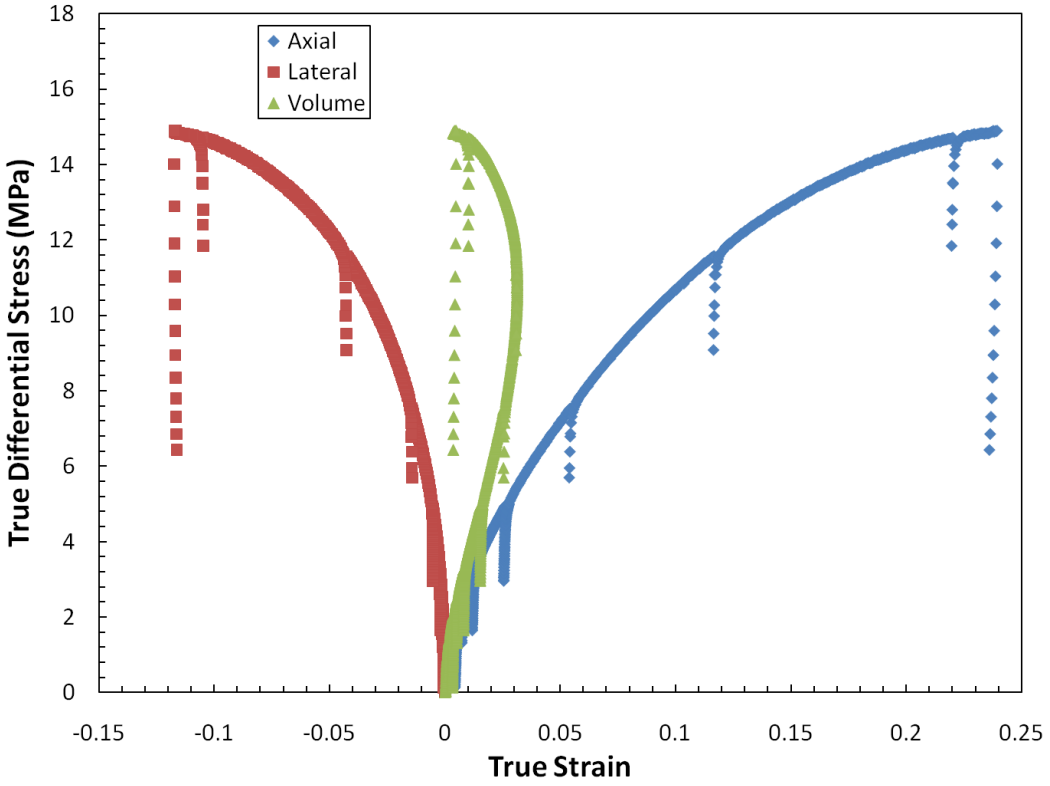

Figure B 8. WC-TX-50-05-03 True differential stress versus true strain. Test ran 20 times slower than other triaxial compression tests to evaluate pore pressure effects on radial measurements.

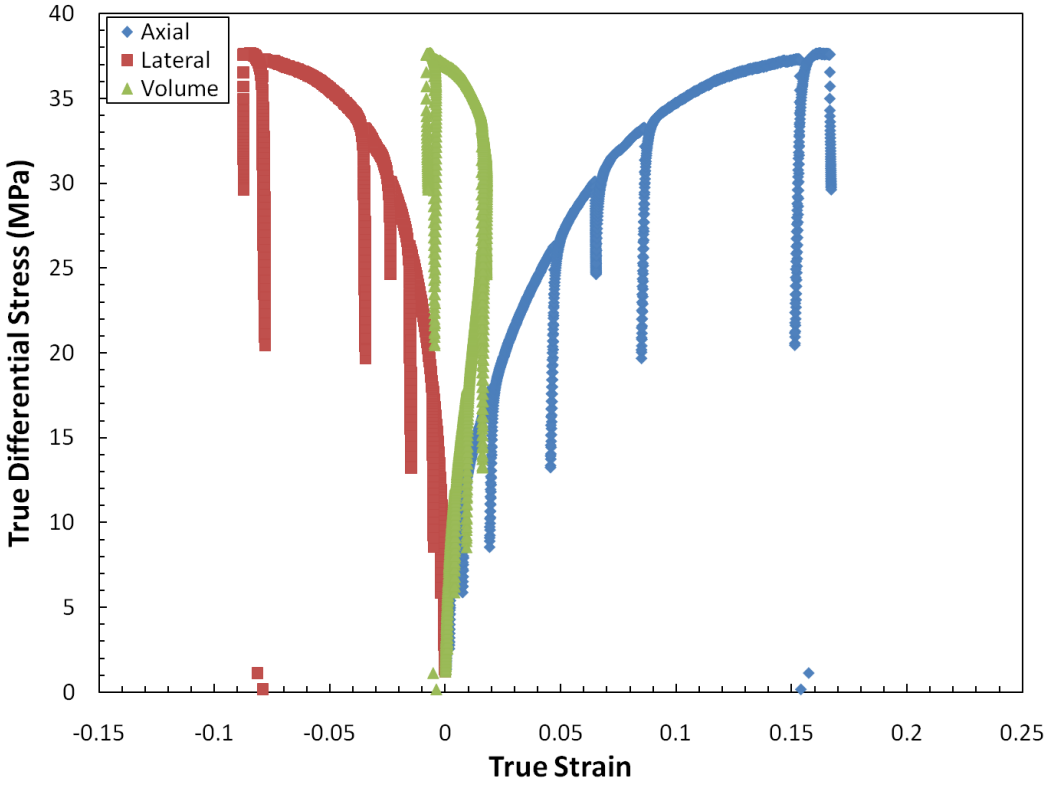

Figure B 9. WC-TX-50-15-02 True differential stress versus true strain.

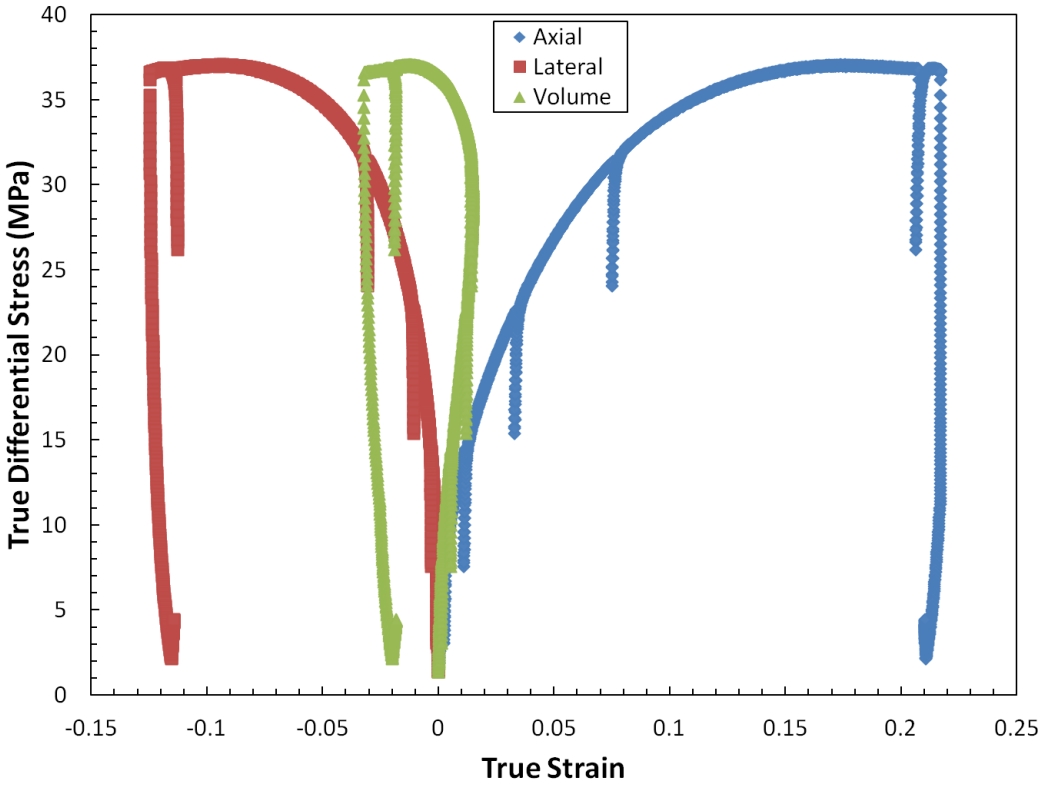

Figure B 10. WC-TX-50-15-03 True differential stress versus true strain.

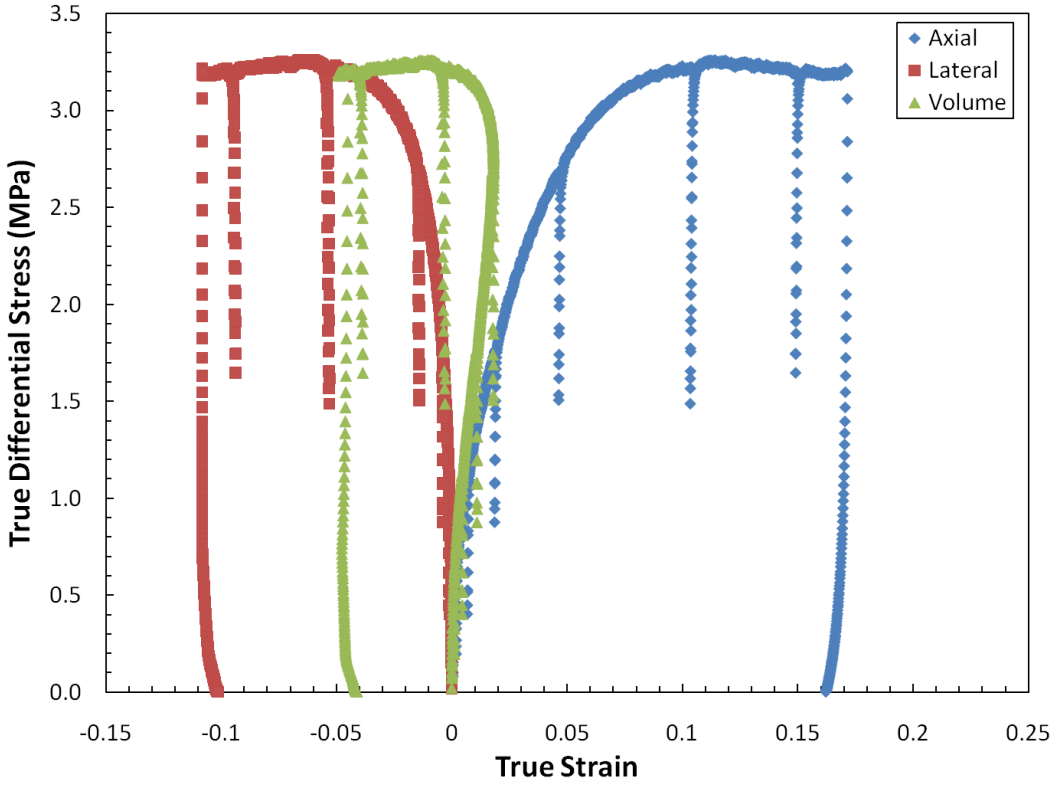

Figure B 11. WC-TX-100-01-01 True differential stress versus true strain.

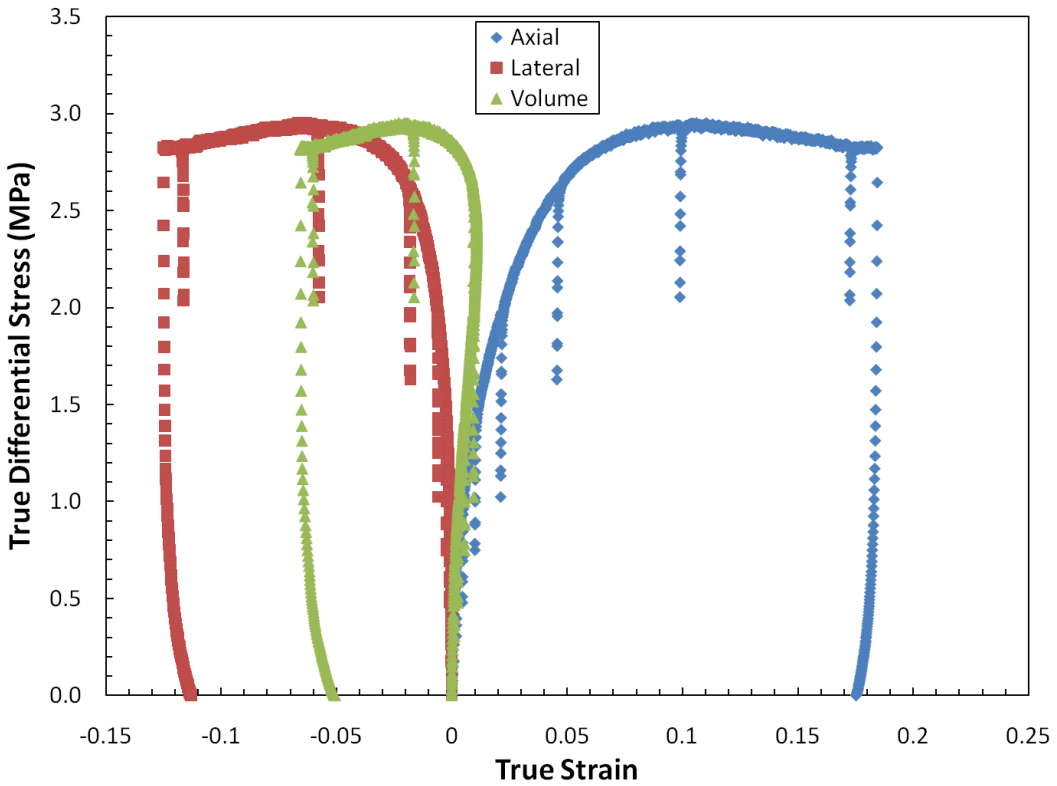

Figure B 12. WC-TX-100-01-02 True differential stress versus true strain.

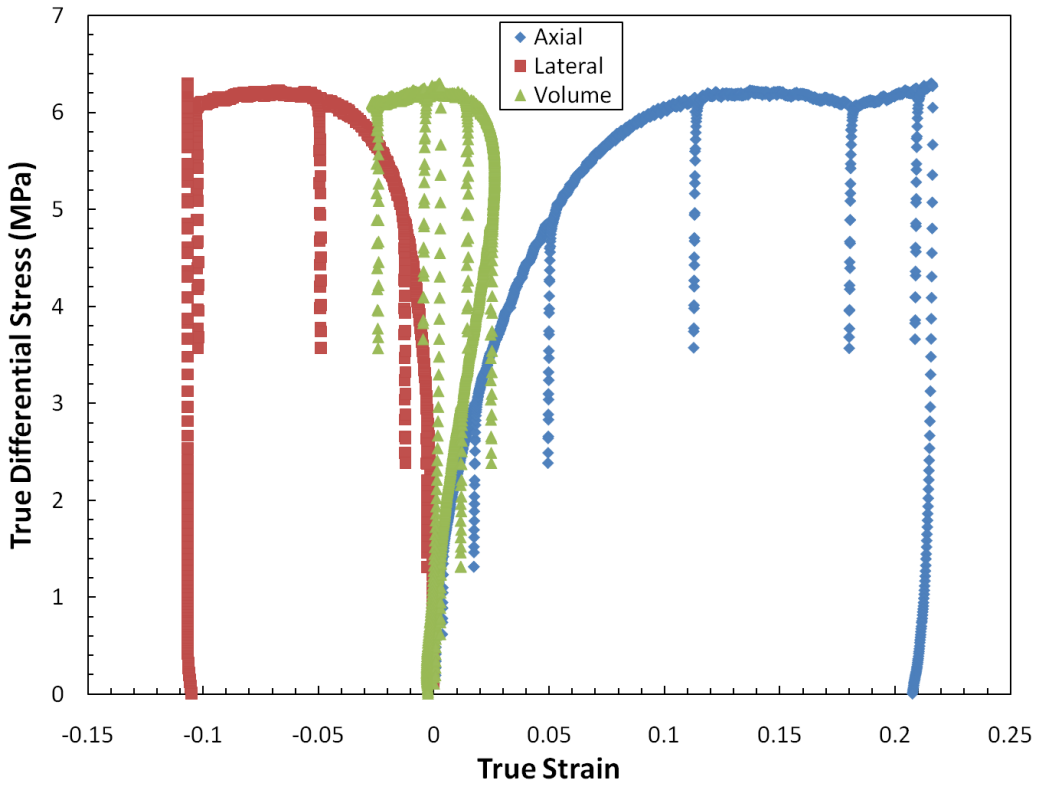

Figure B 13. WC-TX-100-02-01 True differential stress versus true strain.

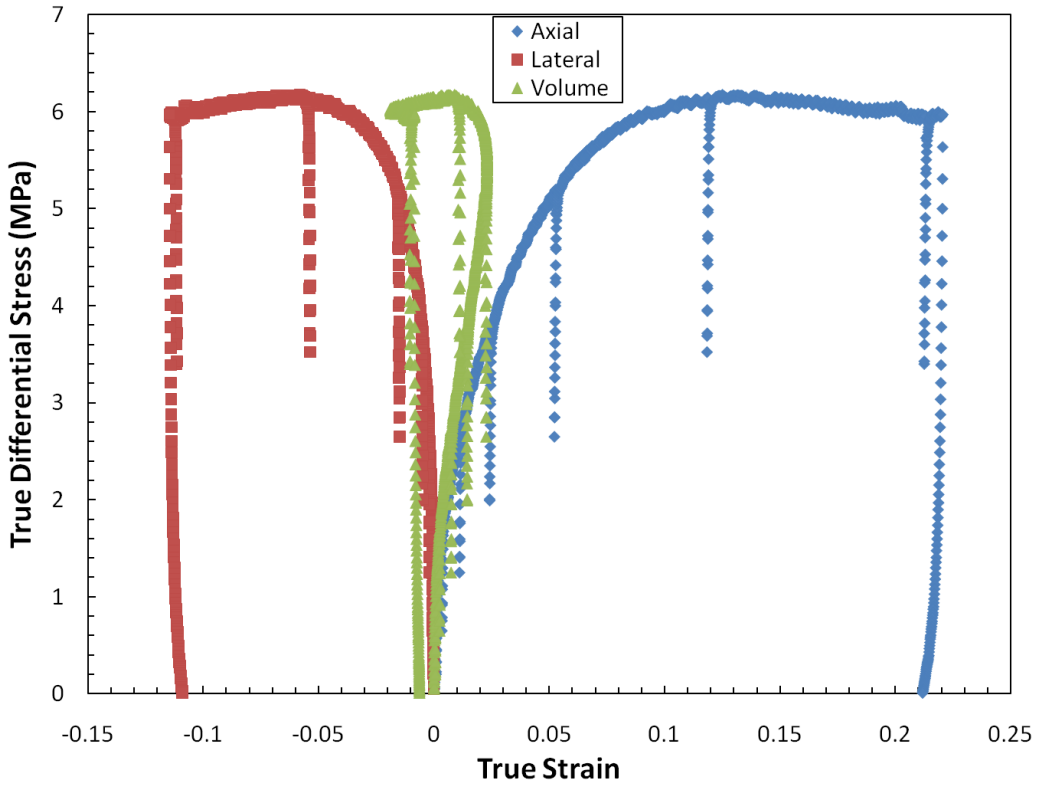

Figure B 14. WC-TX-100-02-02 True differential stress versus true strain.

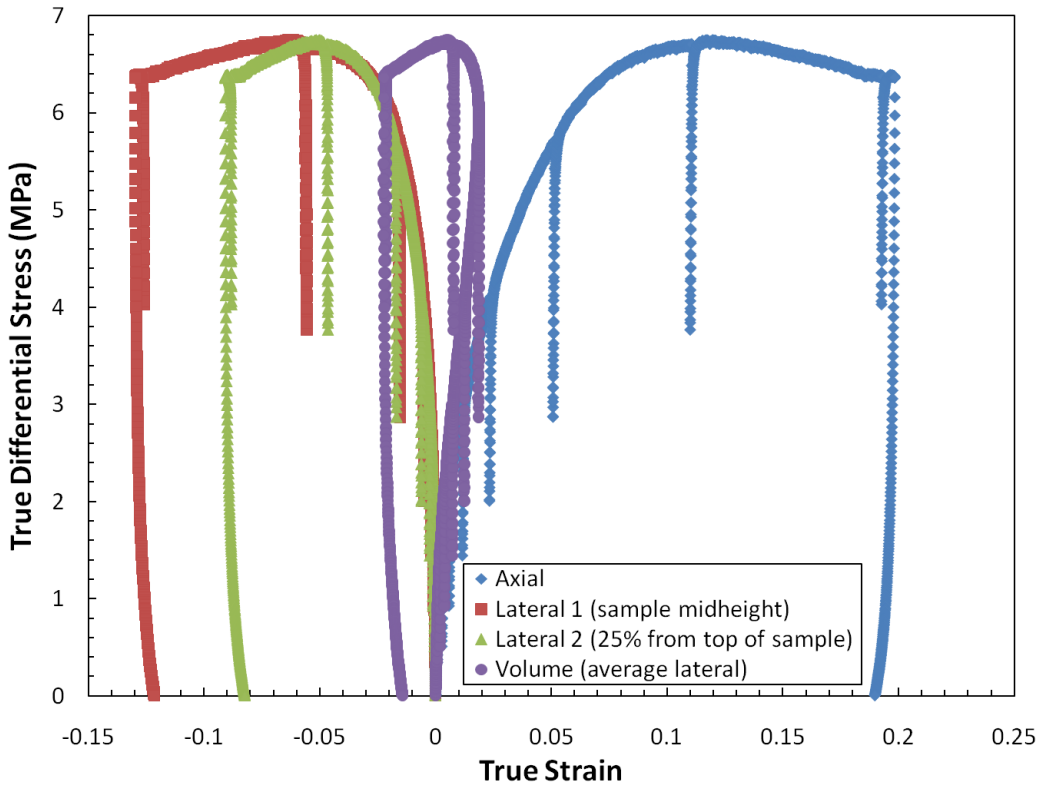

Figure B 15. WC-TX-100-02-03 True differential stress versus true strain. Lateral gages separated to determine degree of sample "barreling".

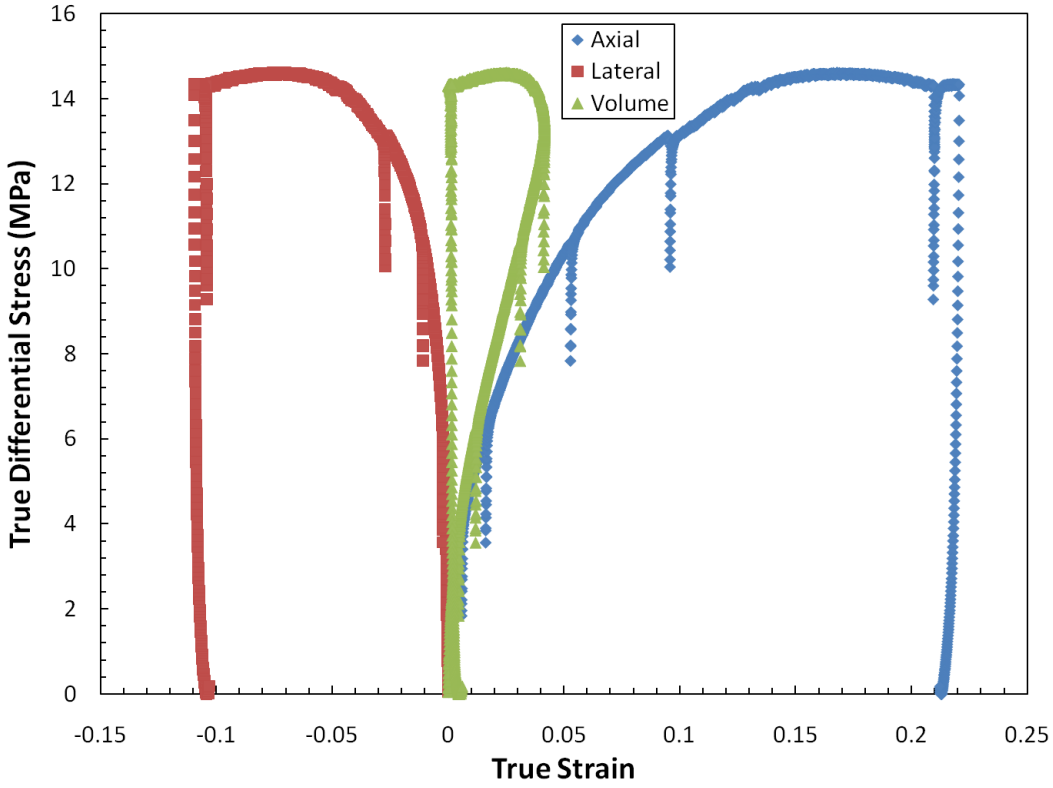

Figure B 16. WC-TX-100-05-01 True differential stress versus true strain.

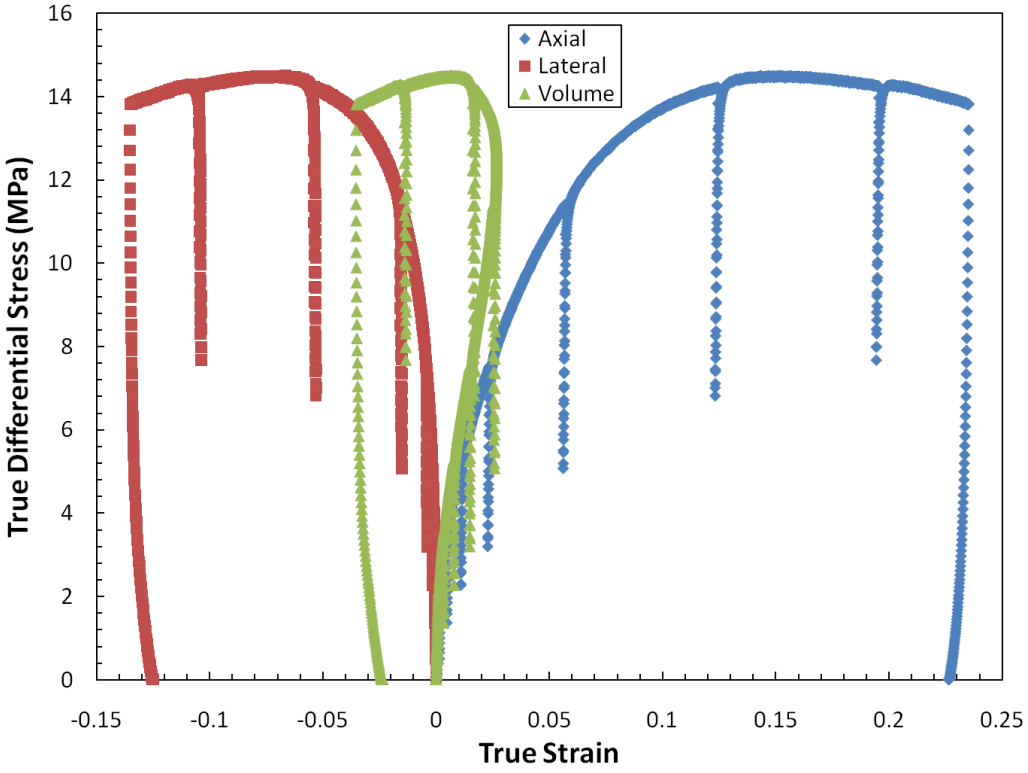

Figure B 17. WC-TX-100-05-02 True differential stress versus true strain.

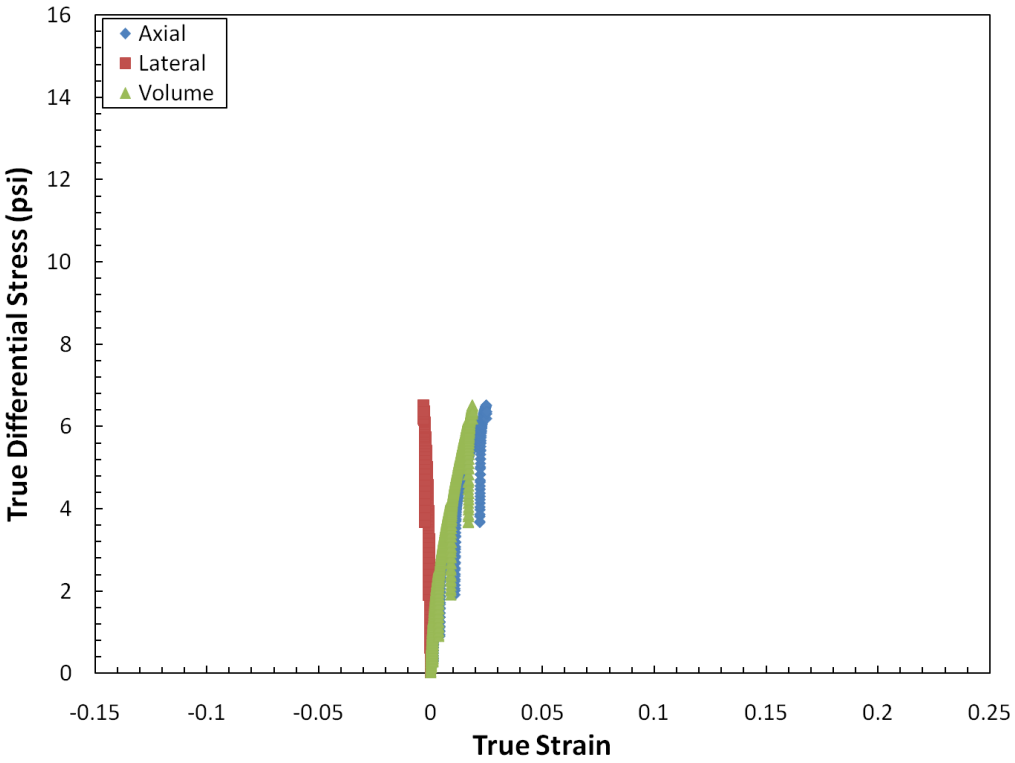

Figure B 18. WC-TX-100-05-04 True differential stress versus true strain. Test ran 20 times slower than other triaxial compression tests to evaluate pore pressure effects on radial measurements. Data shown is before test loss control of confining pressure.

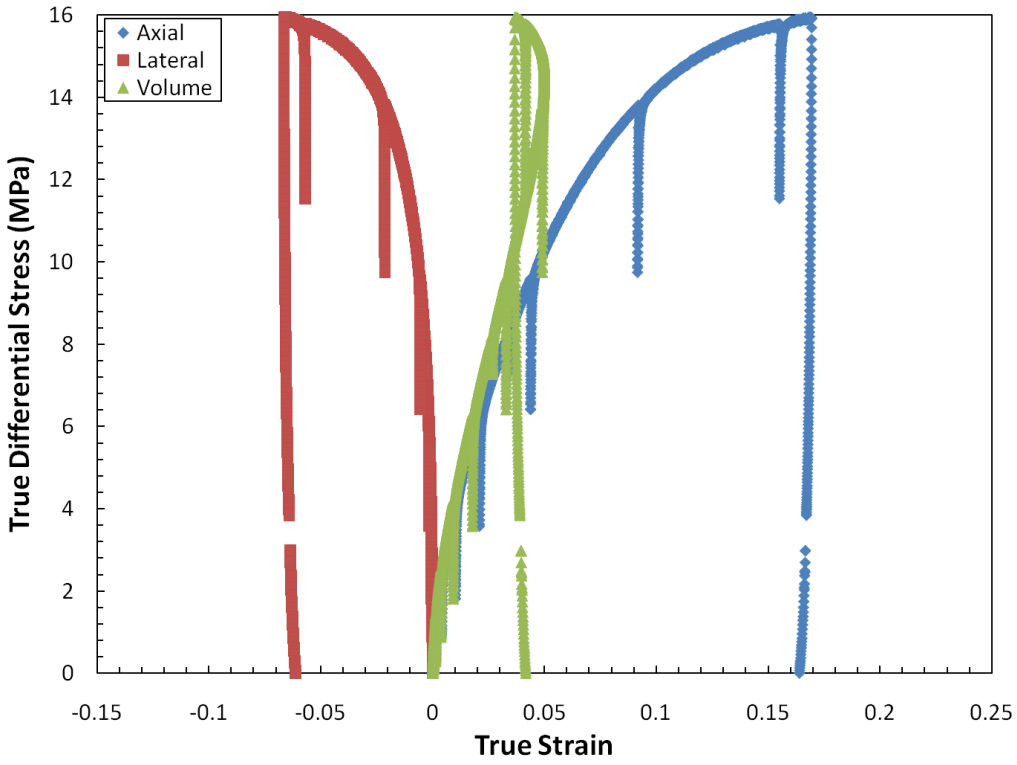

Figure B 19. WC-TX-100-05-05 True differential stress versus true strain. Test ran 20 times slower than other triaxial compression tests to evaluate pore pressure effects on radial measurements.

APPENDIX C
UNIAXIAL STRAIN TEST RESULTS FOR 50% AND 100% DEGRADED MATERIAL

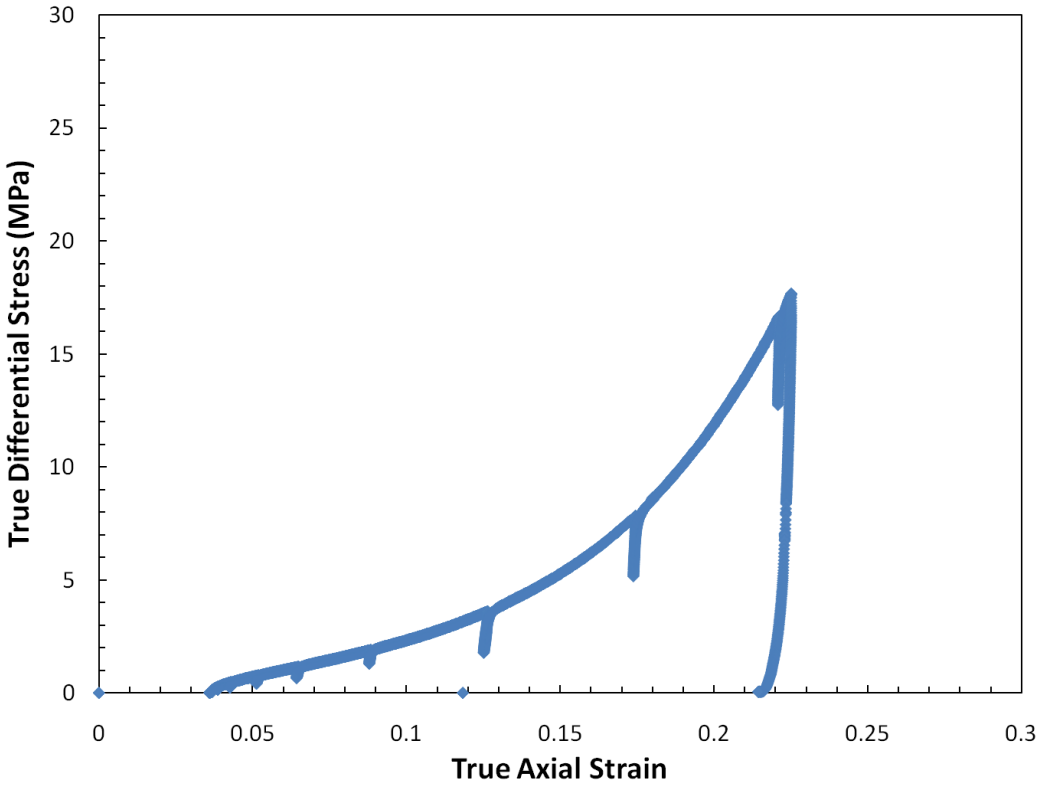

Figure C 1. WC-TX-50-01-03 True differential stress versus true axial strain.

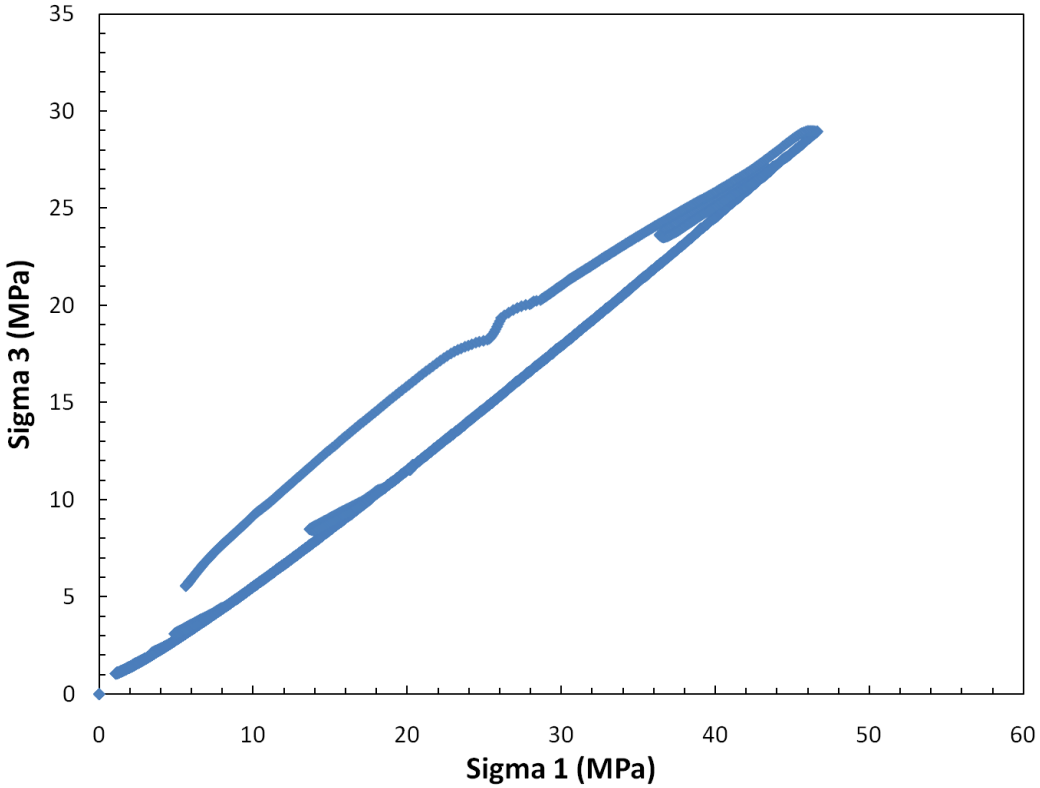

Figure C 2. WC-TX-50-01-03 Sigma 3 versus sigma 1.

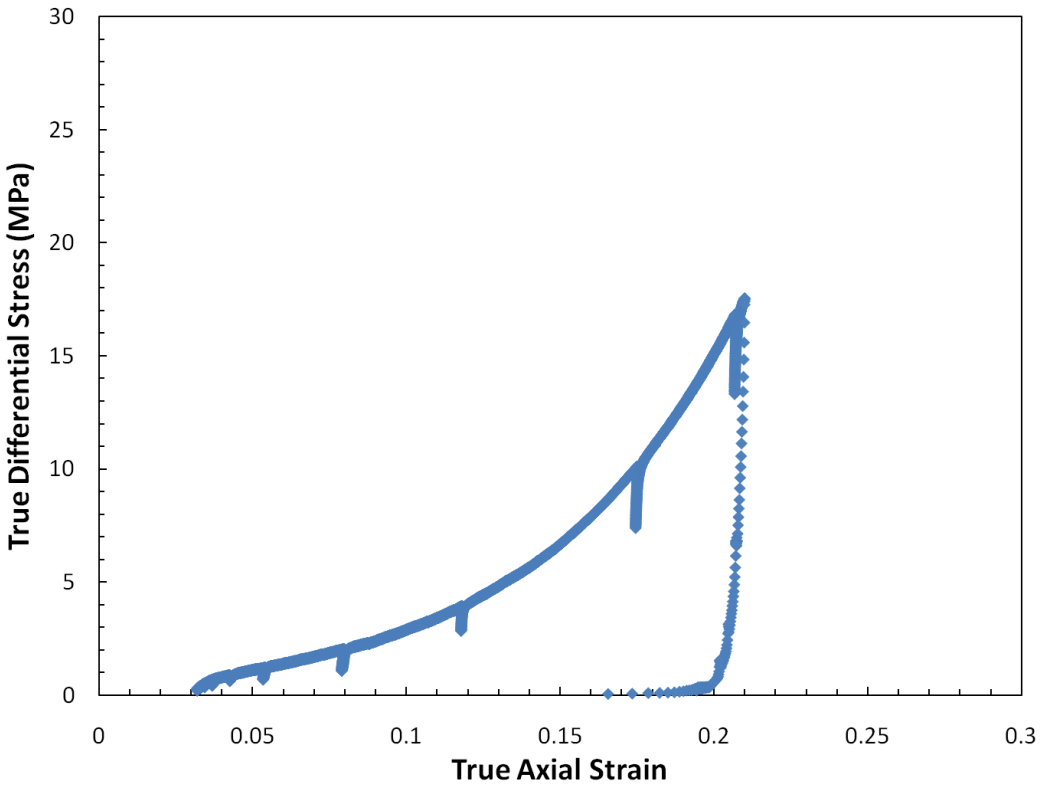

Figure C 3. WC-TX-50-01-04 True differential stress versus true axial strain.

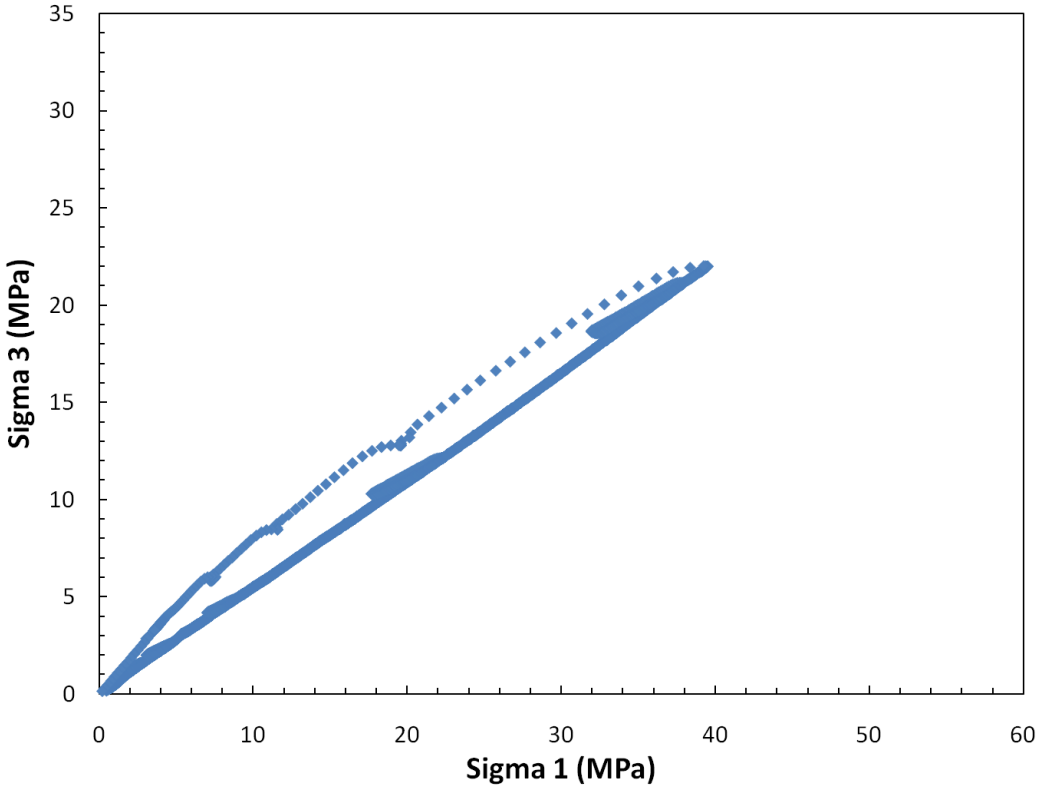

Figure C 4. WC-TX-50-01-04 Sigma 3 versus sigma 1.

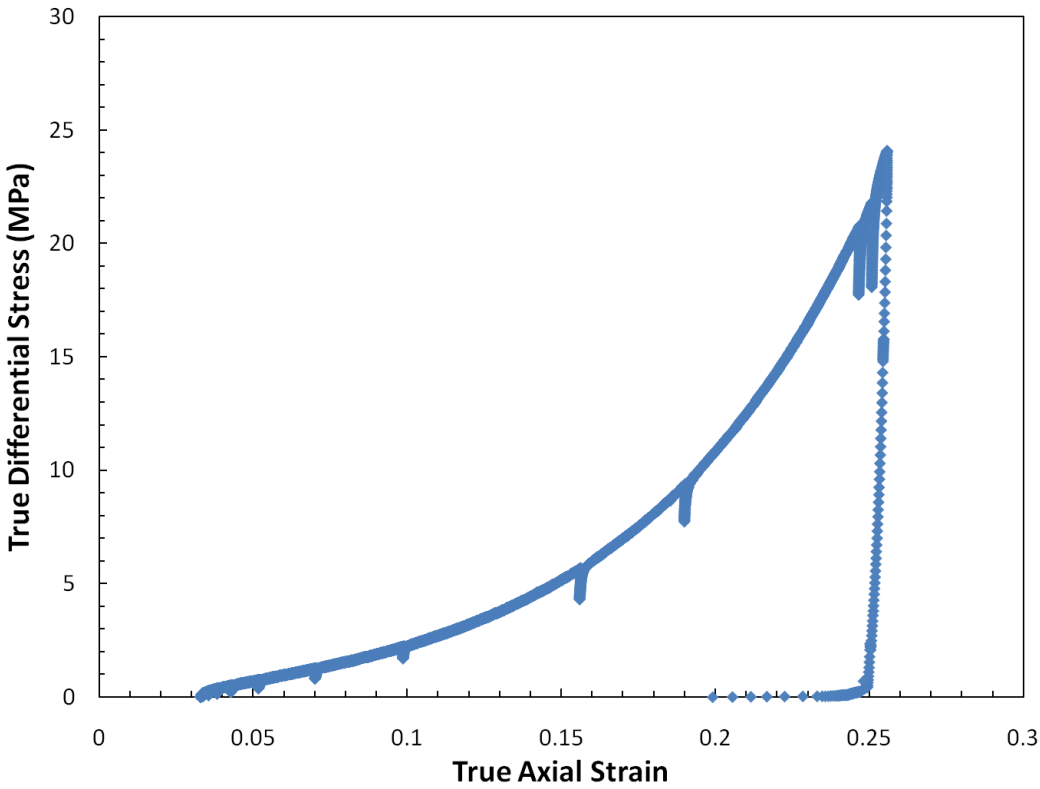

Figure C 5. WC-TX-50-01-06 True differential stress versus true axial strain.

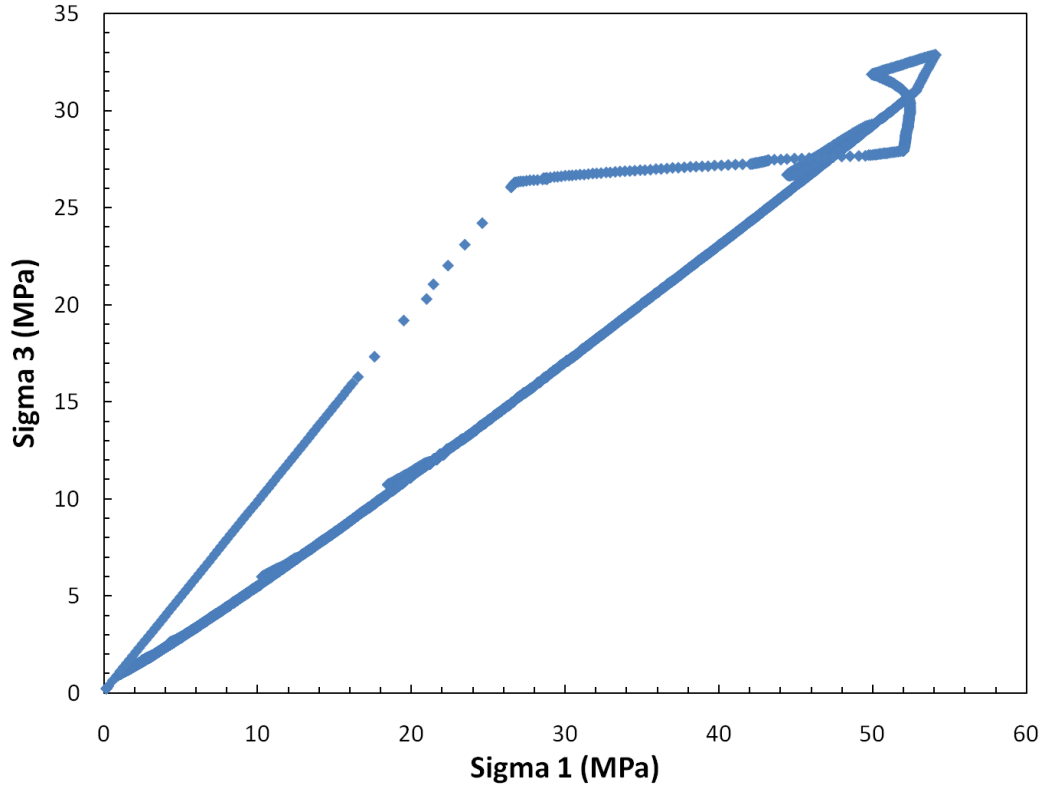

Figure C 6. WC-TX-50-01-06 Sigma 3 versus sigma 1.

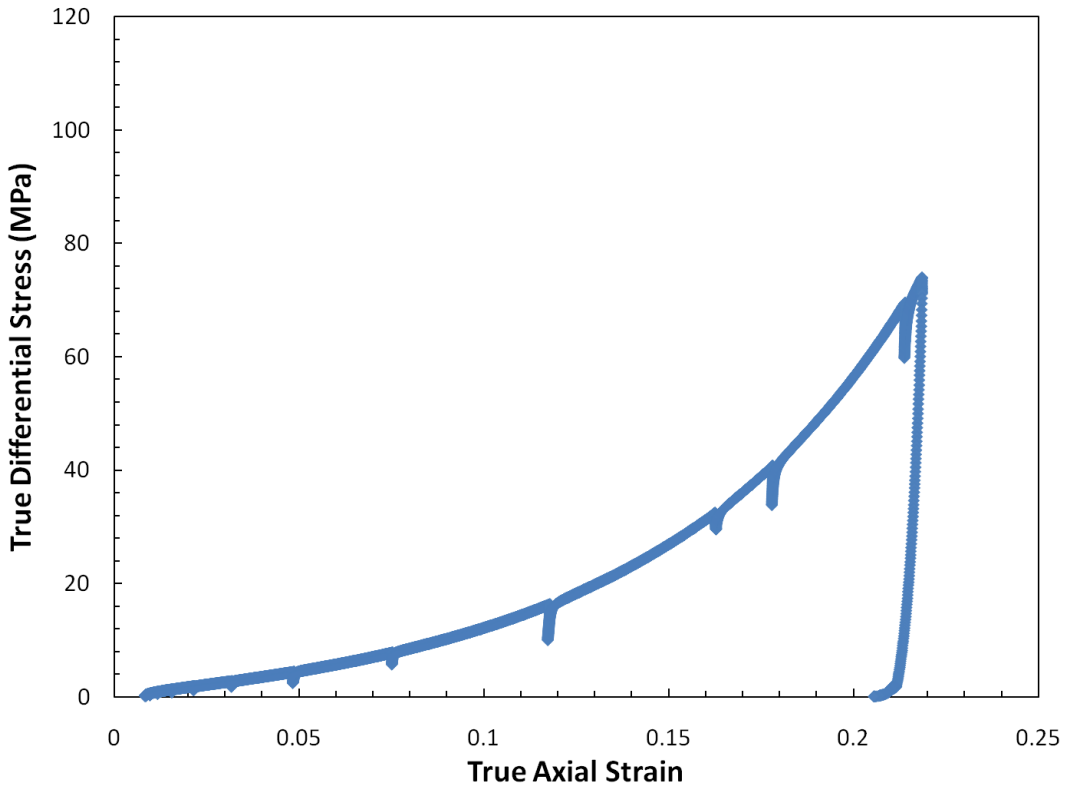

Figure C 7. WC-TX-100-01-03 True differential stress versus true axial strain.

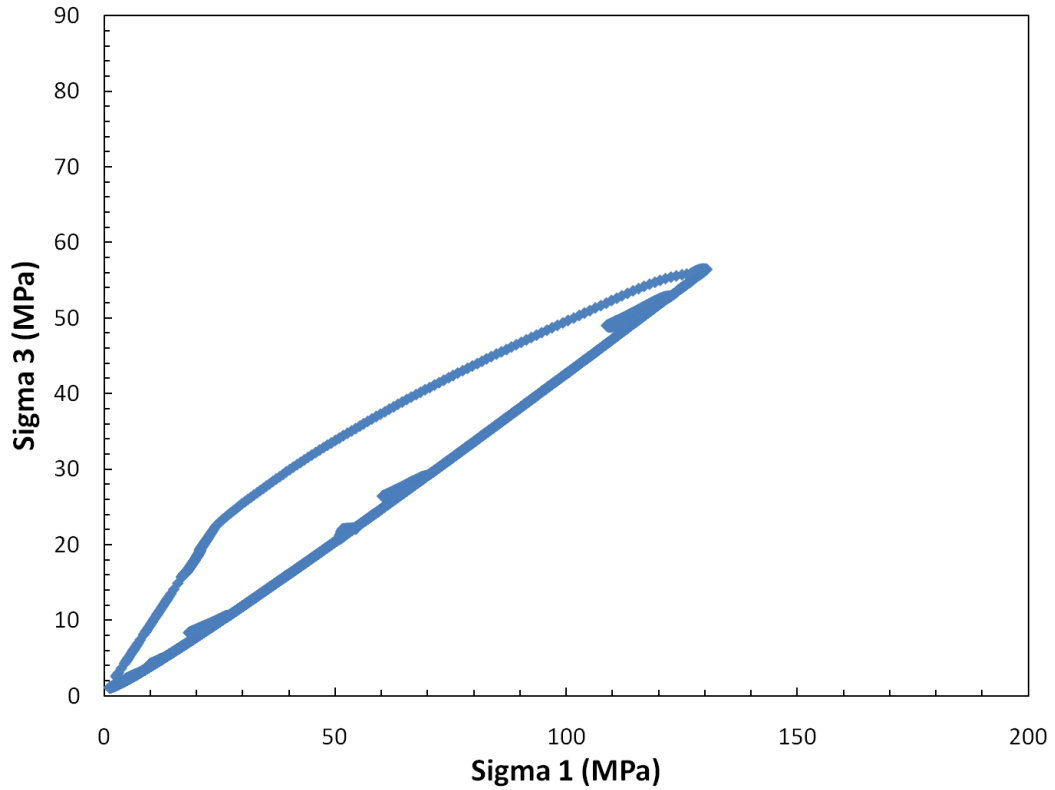

Figure C 8. WC-TX-100-01-03 Sigma 3 versus sigma 1.

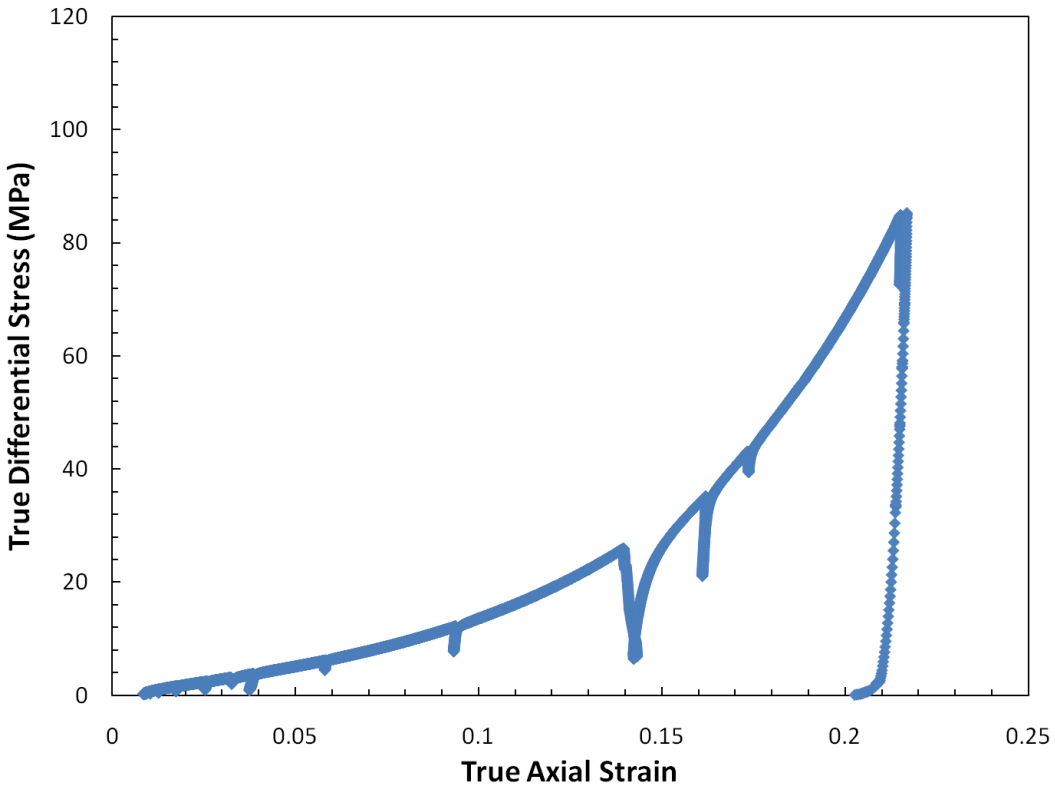

Figure C 9. WC-TX-100-01-04 True differential stress versus true axial strain.

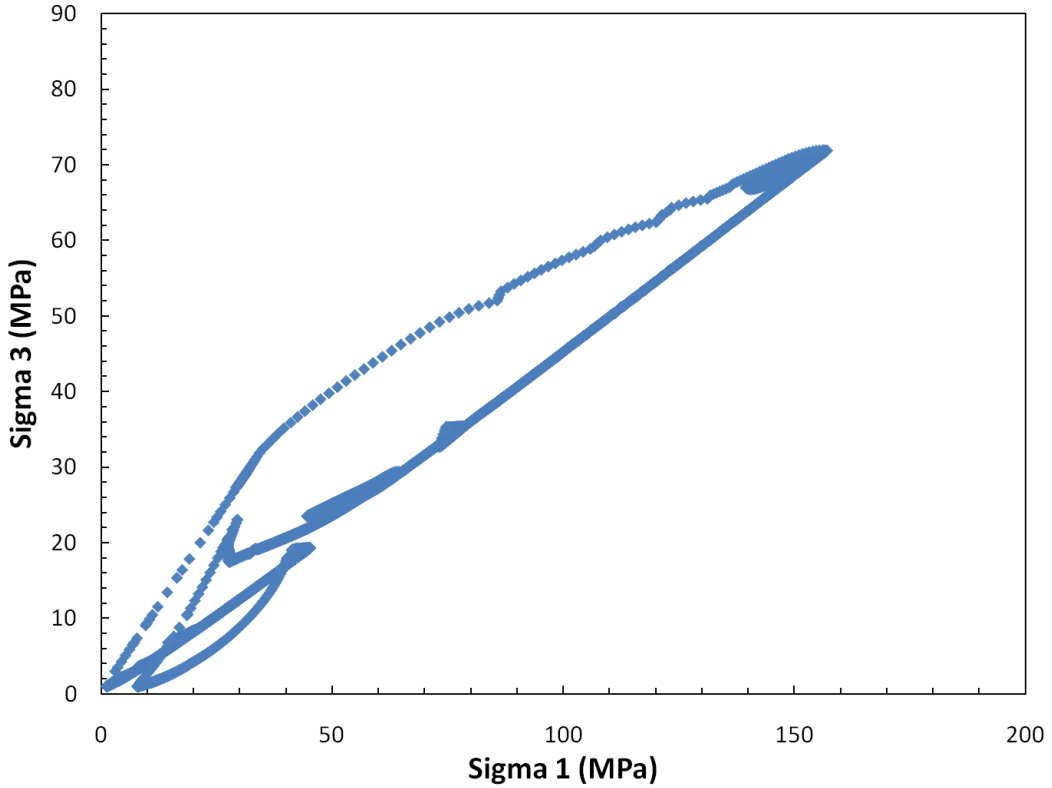

Figure C 10. WC-TX-100-01-04 Sigma 3 versus sigma 1.

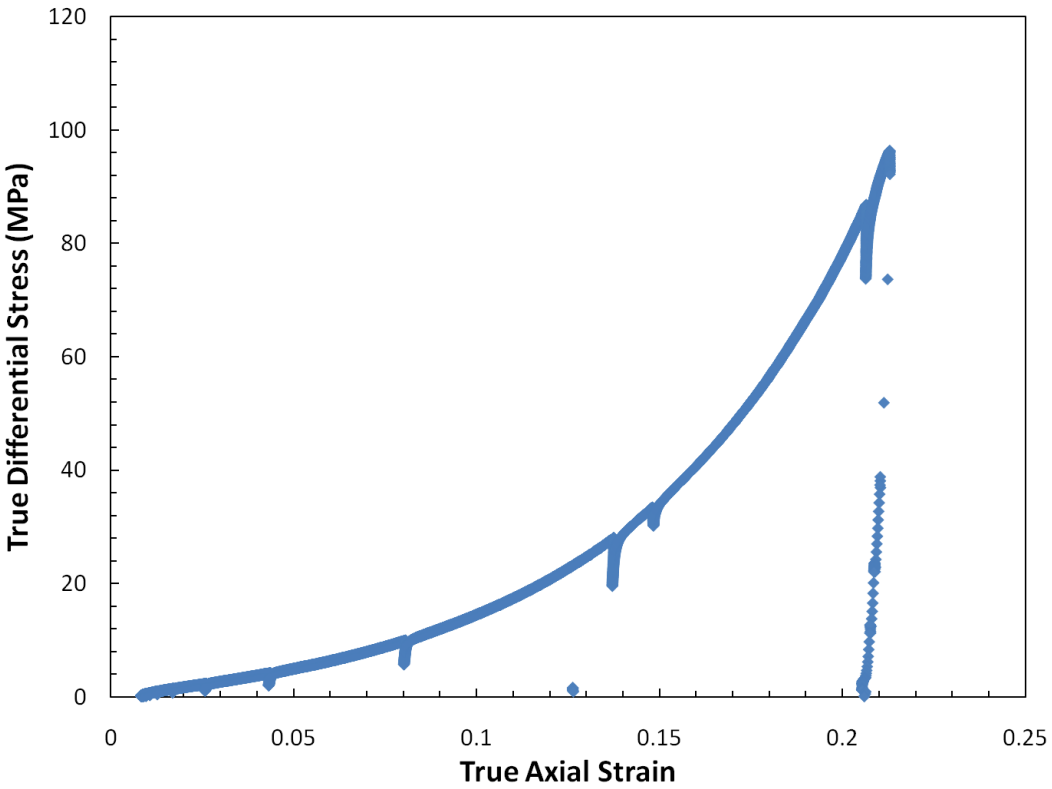

Figure C 11. WC-TX-100-01-05 True differential stress versus true axial strain.

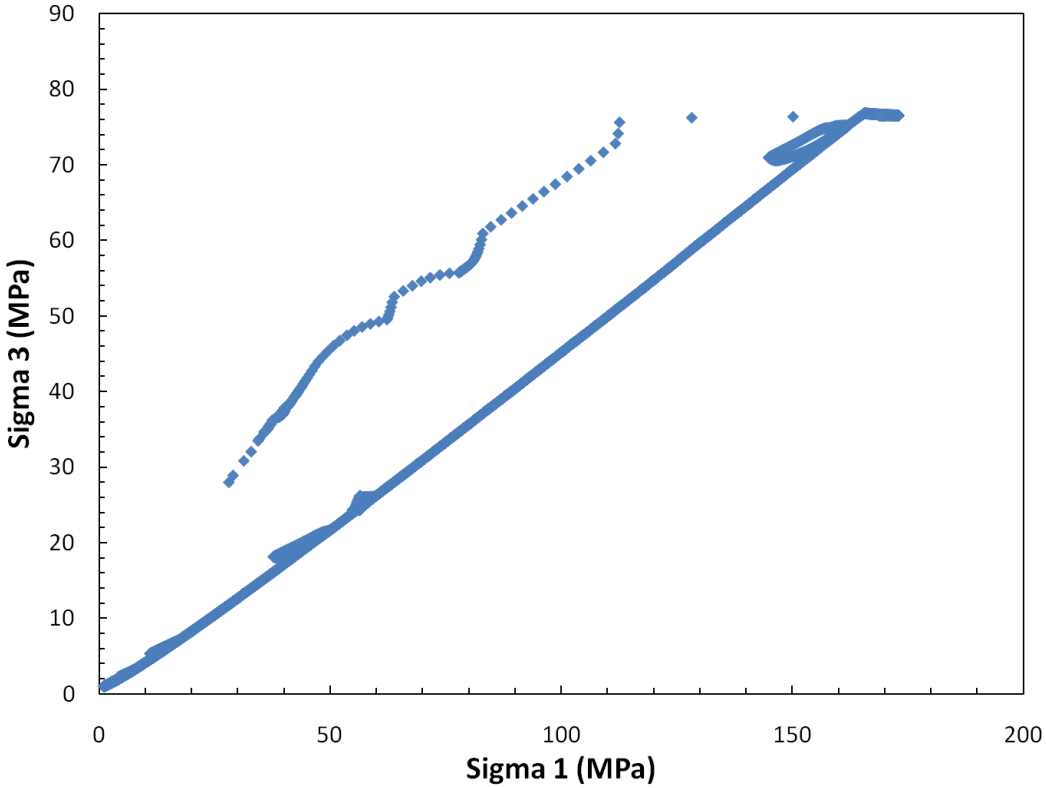

Figure C 12. WC-TX-100-01-05 Sigma 3 versus sigma 1.

APPENDIX D
TRIAXIAL AND UNIAXIAL STRAIN ELASTIC PROPERTY AND DENSITY RESULTS FOR 50% AND 100% DEGRADED MATERIAL

Table D 1. Young's modulus and axial strain values from triaxial compression tests on 50% and 100% degraded materials.

Specimen	50-01-01		50-01-02		50-02-02		50-02-04		50-02-06	
	E (MPa)	ε_A	*E* (MPa)	ε_A	*E* (MPa)	ε_A	*E* (MPa)	ε_A	*E* (MPa)	ε_A
	614	0.0008094	466	0.0005733	725	0.000912	944	0.001638	767	0.00024
	540	0.0042427	426	0.0023387	862	0.002887	845	0.005527	806	0.001057
	412	0.0132809	472	0.0068145	1001	0.010824	866	0.017129	859	0.0034
	514	0.0362523	375	0.0180407	1075	0.023879	977	0.03604	936	0.009241
	458	0.0838713	588	0.0695903	1156	0.041435	1207	0.066283	845	0.014603
	871	0.1552141	626	0.1177464	1357	0.061488	1666	0.11585	870	0.027637
			735	0.1596963	1647	0.096616	1632	0.156641	970	0.058524
			751	0.1726517	1496	0.136201			900	0.122134
					1622	0.201796			1173	0.213141
Specimen	50-05-01		50-05-02		50-05-03		50-15-02		50-15-03	
	E (MPa)	ε_A	*E* (MPa)	ε_A	*E* (MPa)	ε_A	*E* (MPa)	ε_A	*E* (MPa)	ε_A
	1493	0.0007421	2284	0.0010915	2213	0.001387	6022	0.000521	6064	0.000667
	2028	0.0020662	2104	0.0035478	2221	0.002669	6456	0.002071	5742	0.003011
	1998	0.007853	2223	0.0069498	1780	0.005092	6188	0.008203	6791	0.011763
	2168	0.0243462	2266	0.0132899	2458	0.007585	6186	0.020245	7025	0.033703
	2692	0.0523052	2339	0.0271392	2272	0.012418	6794	0.046951	8560	0.075685
	2532	0.1152773	2353	0.0595812	2610	0.026128	7801	0.086251	6007	0.207563
	2487	0.2072014	2803	0.123059	2642	0.054261	6469	0.153432		
			2666	0.198602	4239	0.116843				
					3388	0.220051				
Specimen	100-01-01		100-01-02		100-02-01		100-02-02		100-02-03	
	E (MPa)	ε_A	*E* (MPa)	ε_A	*E* (MPa)	ε_A	*E* (MPa)	ε_A	*E* (MPa)	ε_A
	1355	0.0004835	926	0.0002396	2060	0.000934	2673	0.000295	3374	0.0008
	1287	0.0020446	1572	0.0007989	2182	0.003905	2470	0.001121	2025	0.002977
	1279	0.0070433	1642	0.0020503	2510	0.017778	2442	0.00373	2245	0.006112
	1660	0.0188967	1513	0.0046852	2898	0.0501	2547	0.011499	3125	0.011921
	1936	0.0467658	1803	0.0101515	3314	0.113221	3166	0.024634	2887	0.023758
	1652	0.104075	2090	0.021448	3007	0.180714	3490	0.052791	3582	0.051238
	1676	0.1496124	2122	0.0457975	3046	0.209297	3513	0.119009	3683	0.110519
			2216	0.0990963			2721	0.213362	3408	0.193048
			2532	0.1727551						
Specimen	100-05-01		100-05-02		100-05-04		100-05-05			
	E (MPa)	ε_A	*E* (MPa)	ε_A	*E* (MPa)	ε_A	*E* (MPa)	ε_A		
	4738	0.0003309	3815	0.0003251	5096	0.000402	3127	0.000172		
	4492	0.0018001	4175	0.0016108	4048	0.001369	3787	0.000594		
	4625	0.0060896	4317	0.0050062	4684	0.004408	4031	0.001548		
	5317	0.0165793	4642	0.0113308	4996	0.011264	4453	0.004257		
	6907	0.0530692	4688	0.0234303	5789	0.022438	4590	0.010529		
	8005	0.0959699	5716	0.0569615			5700	0.021293		
	6189	0.2097972	5454	0.1241869			7281	0.044121		
			5038	0.1953747			8419	0.092035		
							10103	0.155458		

Table D 2. Young's modulus, Poisson's ratio and density values from uniaxial strain tests on 50% and 100% degraded materials.

WC-TX-50-01-03			WC-TX-50-01-04			WC-TX-50-01-06		
E (MPa)	ν	Density (g/cc)	*E* (MPa)	ν	Density (g/cc)	*E* (MPa)	ν	Density (g/cc)
449	0.31	2.37	302	0.27	2.28	364	0.31	2.38
507	0.30	2.37	458	0.25	2.28	404	0.30	2.38
555	0.28	2.38	537	0.27	2.29	398	0.31	2.39
589	0.29	2.40	799	0.29	2.33	417	0.30	2.40
739	0.29	2.43	1099	0.28	2.37	579	0.28	2.42
1179	0.28	2.46	3249	0.29	2.42	790	0.29	2.45
1500	0.30	2.56	5661	0.30	2.54	1782	0.28	2.50
4104	0.30	2.65	8739	0.31	2.60	3262	0.29	2.60
8344	0.34	2.76				5511	0.32	2.68
						9602	0.33	2.82
						9228	0.20	2.83
WC-TX-100-01-03			WC-TX-100-01-04			WC-TX-100-01-05		
E (MPa)	ν	Density (g/cc)	*E* (MPa)	ν	Density (g/cc)	*E* (MPa)	ν	Density (g/cc)
1891	0.20	2.32	2032	0.22	2.35	2336	0.18	2.39
2031	0.22	2.32	1931	0.24	2.35	2624	0.20	2.39
2153	0.23	2.33	2043	0.25	2.35	2084	0.24	2.40
2634	0.23	2.33	2117	0.25	2.36	2018	0.24	2.40
2794	0.22	2.35	2132	0.24	2.37	2222	0.25	2.40
3582	0.23	2.37	2516	0.24	2.38	2614	0.24	2.41
4517	0.22	2.39	2908	0.23	2.40	3240	0.23	2.43
7841	0.22	2.44	6422	0.22	2.44	4783	0.23	2.46
10257	0.21	2.52	9333	0.22	2.50	9384	0.22	2.53
22417	0.23	2.66	16746	0.23	2.64	17395	0.23	2.63
37088	0.24	2.76	38148	0.24	2.78	43972	0.24	2.80

DISTRIBUTION

4 Lawrence Livermore National Laboratory
Attn: N. Dunipace (1)
P.O. Box 808, MS L-795
Livermore, CA 94551-0808

3 Waste Isolation Pilot Plant
Attn: Roger Nelson
Abe van Luik
Russ Patterson
U.S. Department of Energy
4021 National Parks Highway
Carlsbad, NM 88220

2 WIPP Technical Library GSA-214
P.O. Box 2078
Carlsbad, NM 88221

1 Dr. Michael Gross
415 Riviera Drive
San Rafael, CA 94901-1530

1 Golder Associates Inc.
Attn: Dr. Bill Thompson
44 Union Boulevard, Suite 300
Lakewood, CO 80228

1	MS0721	Peter B. Davies	06200
1	MS0735	Moo Lee	06910
1	MS0747	Robert J. MacKinnon	06224
1	MS0751	Francis D. Hansen	06910
1	MS0751	Byoung Yoon Park	06914
1	MS0840	James Bean	01525
1	MS1033	Steve Bauer	06914
1	MS1395	Paul Shoemaker	06210
1	MS1395	Sean Dunagan	06211
1	MS1395	Christie D. Leigh	06212
2	MS1395	WIPP Library	06210
1	MS0899	Technical Library	9536 (electronic copy)


Sandia National Laboratories